

**NUMERICAL MODELING OF EROSION AND
RECOVERY OF REHOBOTH AND DEWEY
BEACHES IN DELAWARE**

BY

HOORYOUNG JUNG AND NOBUHISA KOBAYASHI

RESEARCH REPORT NO. CACR-11-01
JULY 2011



CENTER FOR APPLIED COASTAL RESEARCH

Ocean Engineering Laboratory
University of Delaware
Newark, Delaware 19716

ACKNOWLEDGMENTS

This study was supported by the U.S. Army Corps of Engineers, Coastal and Hydraulics Laboratory under Contract Nos. W912HZ-10-P-0234 and W912BU-09-C-0023 as well as by the EU THESEUS Project (Innovative Technologies for Safer European Coasts in a Changing Climate). The beach profile data used in this study have been provided by Randy Wise.

TABLE OF CONTENTS

LIST OF TABLES.....	iv
LIST OF FIGURES.....	v
ABSTRACT	xi
Chapter	
1 INTRODUCTION	12
2 FIELD DATA.....	14
2.1 Field Site	14
2.2 Water Level and Wave Data.....	17
2.3 Beach Profile Data	27
3 NUMERICAL MODEL CSHORE.....	38
3.1 Hydrodynamic Model	38
3.2 Sediment Transport Model	39
3.3 Profile Evolution Model	40
3.4 CSHORE Input	43
4 COMPARISON OF NUMERICAL MODEL WITH FIELD DATA.....	44
4.1 Erosion Period	44
4.2 Accretion Period	63
4.3 Sensitivity to Bed Load Parameter B.....	81
4.4 Erosion and Accretion Volumes.....	107
4.5 Longshore Sediment Transport.....	109
5 CONCLUSION.....	111
REFERENCES	112

LIST OF TABLES

Table 2. 1	Average Water Level and Wave Conditions during Erosion Period and Accretion Period.....	16
Table 2. 2	Alongshore Distance y , Increment Δy , and Cross-Shore Distance x_m Used for Computation	29
Table 2. 3	Sediment Volume above MSL on 29 October 1992, Erosion Volume above MSL during Erosion Period, Accretion Volume above MSL during Accretion Period, and Net Erosion Volume above MSL for Entire Duration.....	36

LIST OF FIGURES

Figure 2.1	Rehoboth beach, Dewey beach, Lewes tide gauge, and wave gauge DE001 in water depth of 9m offshore of Dewey beach(Google™).....	15
Figure 2.2	Water level, root-mean-square wave height, spectral peak period, and peak spectral wave direction for erosion period.....	18
Figure 2.3	Storm of 10 December 1992 during erosion period	19
Figure 2.4	Water level, root-mean-square wave height, spectral peak period, and peak spectral wave direction during 0 to 55 days of accretion period	20
Figure 2.5	Water level, root-mean-square wave height, spectral peak period, and peak spectral wave direction during 55 to 110 days of accretion period	21
Figure 2.6	Water level, root-mean-square wave height, spectral peak period, and peak spectral wave direction during 110 to 165 days of accretion period	22
Figure 2.7	Water level, root-mean-square wave height, spectral peak period, and peak spectral wave direction during 165 to 220.8 days of accretion period	23
Figure 2.8	Storm of 8 January 1993 during accretion period	24
Figure 2.9	Storms of 3 March and 12 March 1993during accretion period	25
Figure 2.10	Storm of 5 April 1993 during accretion period	26
Figure 2.11	Eight cross-shore lines (RN38 to RS36) for Rehoboth beach and eight cross-shore lines (DN40 to DS40) for Dewey beach	28
Figure 2.12	Profile survey data(top) and survey lines(bottom)	31
Figure 2.13	Measured profiles along lines RN38, RN31, RN22, and RN17 on 29 October 1992, 18 December 1992, and 27 July 1993	32

Figure 2.14	Measured profiles along lines RS0, RS14, RS24, and RS36 on 29 October 1992, 18 December 1992, and 27 July 1993	33
Figure 2.15	Measured profiles along lines DN40, DN25, DN15, and DN0 on 29 October 1992, 18 December 1992, and 27 July 1993	34
Figure 2.16	Measured profiles along lines DS10, DS20, DS30, and DS40 on 29 October 1992, 18 December 1992, and 27 July 1993	35
Figure 2.17	Measured initial sediment volume, erosion volume, and accretion volume per unit longshore length.....	37
Figure 4.1	Measured and computed beach profiles (top), cumulative cross-shore (middle) and longshore (bottom) sand transport volume per unit width during erosion period for RN38 and RN31.....	47
Figure 4.2	Measured and computed beach profiles (top), cumulative cross-shore (middle) and longshore (bottom) sand transport volume per unit width during erosion period for RN22 and RN17.....	48
Figure 4.3	Measured and computed beach profiles (top), cumulative cross-shore (middle) and longshore (bottom) sand transport volume per unit width during erosion period for RS0 and RS14.	49
Figure 4.4	Measured and computed beach profiles (top), cumulative cross-shore (middle) and longshore (bottom) sand transport volume per unit width during erosion period for RS24 and RS36.	50
Figure 4.5	Measured and computed beach profiles (top), cumulative cross-shore (middle) and longshore (bottom) sand transport volume per unit width during erosion period for DN40 and DN25.....	51
Figure 4.6	Measured and computed beach profiles (top), cumulative cross-shore (middle) and longshore (bottom) sand transport volume per unit width during erosion period for DN15 and DN0.....	52
Figure 4.7	Measured and computed beach profiles (top), cumulative cross-shore (middle) and longshore (bottom) sand transport volume per unit width during erosion period for DS10 and DS20.....	53
Figure 4.8	Measured and computed beach profiles (top), cumulative cross-shore (middle) and longshore (bottom) sand transport volume per unit width during erosion period for DS30 and DS40.....	54

Figure 4.9	Cumulative total cross-shore sand transport volume per unit width during erosion period for RN38, RN31, RN22, and RN17.	55
Figure 4.10	Cumulative total cross-shore sand transport volume per unit width during erosion period for RS0, RS14, RS24, and RS36.	56
Figure 4.11	Cumulative total cross-shore sand transport volume per unit width during erosion period for DN40, DN25, DN15, and DN0.	57
Figure 4.12	Cumulative total cross-shore sand transport volume per unit width during erosion period for DS10, DS20, DS30, and DS40.	58
Figure 4.13	Bottom elevation difference on 18 December 1992 caused by alongshore gradient of longshore sediment transport rate for RN38, RN31, RN22, and RN17.....	59
Figure 4.14	Bottom elevation difference on 18 December 1992 caused by alongshore gradient of longshore sediment transport rate for RS0, RS14, RS24, and RS36.	60
Figure 4.15	Bottom elevation difference on 18 December 1992 caused by alongshore gradient of longshore sediment transport rate for DN40, DN25, DN15, and DN0.	61
Figure 4.16	Bottom elevation difference on 18 December 1992 caused by alongshore gradient of longshore sediment transport rate for DS10, DS20, DS30, and DS40.	62
Figure 4.17	Measured and computed beach profiles (top), cumulative cross-shore (middle) and longshore (bottom) sand transport volume per unit width during accretion period for RN38 and RN31.	65
Figure 4.18	Measured and computed beach profiles (top), cumulative cross-shore (middle) and longshore (bottom) sand transport volume per unit width during accretion period for RN22 and RN17.	66
Figure 4.19	Measured and computed beach profiles (top), cumulative cross-shore (middle) and longshore (bottom) sand transport volume per unit width during accretion period for RS0 and RS14.	67
Figure 4.20	Measured and computed beach profiles (top), cumulative cross-shore (middle) and longshore (bottom) sand transport volume per unit width during accretion period for RS24 and RS36.	68

Figure 4.21	Measured and computed beach profiles (top), cumulative cross-shore (middle) and longshore (bottom) sand transport volume per unit width during accretion period for DN40 and DN25.....	69
Figure 4.22	Measured and computed beach profiles (top), cumulative cross-shore (middle) and longshore (bottom) sand transport volume per unit width during accretion period for DN15 and DN0.....	70
Figure 4.23	Measured and computed beach profiles (top), cumulative cross-shore (middle) and longshore (bottom) sand transport volume per unit width during accretion period for DS10 and DS20.....	71
Figure 4.24	Measured and computed beach profiles (top), cumulative cross-shore (middle) and longshore (bottom) sand transport volume per unit width during accretion period for DS30 and DS40.....	72
Figure 4.25	Cumulative total cross-shore sand transport volume per unit width during accretion period for RN38, RN31, RN22, and RN17.....	73
Figure 4.26	Cumulative total cross-shore sand transport volume per unit width during accretion period for RS0, RS14, RS24, and RS36.....	74
Figure 4.27	Cumulative total cross-shore sand transport volume per unit width during accretion period for DN40, DN25, DN15, and DN0.....	75
Figure 4.28	Cumulative total cross-shore sand transport volume per unit width during accretion period for DS10, DS20, DS30, and DS40.....	76
Figure 4.29	Bottom elevation difference on 27 July 1993 caused by alongshore gradient of longshore sediment transport rate for RN38, RN31, RN22, and RN17.....	77
Figure 4.30	Bottom elevation difference on 27 July 1993 caused by alongshore gradient of longshore sediment transport rate for RS0, RS14, RS24, and RS36.....	78
Figure 4.31	Bottom elevation difference on 27 July 1993 caused by alongshore gradient of longshore sediment transport rate for DN40, DN25, DN15, and DN0.....	79

Figure 4.32	Bottom elevation difference on 27 July 1993 caused by alongshore gradient of longshore sediment transport rate for DS10, DS20, DS30, and DS40.....	80
Figure 4.33	Effects of reduced bed load parameter $B = 0.001$ in Figure 4.1 based on $B = 0.002$	83
Figure 4.34	Effects of reduced bed load parameter $B = 0.001$ in Figure 4.2 based on $B = 0.002$	84
Figure 4.35	Effects of reduced bed load parameter $B = 0.001$ in Figure 4.3 based on $B = 0.002$	85
Figure 4.36	Effects of reduced bed load parameter $B = 0.001$ in Figure 4.4 based on $B = 0.002$	86
Figure 4.37	Effects of reduced bed load parameter $B = 0.001$ in Figure 4.5 based on $B = 0.002$	87
Figure 4.38	Effects of reduced bed load parameter $B = 0.001$ in Figure 4.6 based on $B = 0.002$	88
Figure 4.39	Effects of reduced bed load parameter $B = 0.001$ in Figure 4.7 based on $B = 0.002$	89
Figure 4.40	Effects of reduced bed load parameter $B = 0.001$ in Figure 4.8 based on $B = 0.002$	90
Figure 4.41	Cumulative total cross-shore sand transport volume per unit width during erosion period for RN38, RN31, RN22, and RN17.	91
Figure 4.42	Cumulative total cross-shore sand transport volume per unit width during erosion period for RS0, RS14, RS24, and RS36.	92
Figure 4.43	Cumulative total cross-shore sand transport volume per unit width during erosion period for DN40, DN25, DN15, and DN0.	93
Figure 4.44	Cumulative total cross-shore sand transport volume per unit width during erosion period for DS10, DS20, DS30, and DS40.	94
Figure 4.45	Effects of increased bed load parameter $B = 0.003$ in Figure 4.17 based on $B = 0.002$	95

Figure 4.46	Effects of increased bed load parameter $B = 0.003$ in Figure 4.18 based on $B = 0.002$	96
Figure 4.47	Effects of increased bed load parameter $B = 0.003$ in Figure 4.19 based on $B = 0.002$	97
Figure 4.48	Effects of increased bed load parameter $B = 0.003$ in Figure 4.20 based on $B = 0.002$	98
Figure 4.49	Effects of increased bed load parameter $B = 0.003$ in Figure 4.21 based on $B = 0.002$	99
Figure 4.50	Effects of increased bed load parameter $B = 0.003$ in Figure 4.22 based on $B = 0.002$	100
Figure 4.51	Effects of increased bed load parameter $B = 0.003$ in Figure 4.23 based on $B = 0.002$	101
Figure 4.52	Effects of increased bed load parameter $B = 0.003$ in Figure 4.24 based on $B = 0.002$	102
Figure 4.53	Cumulative total cross-shore sand transport volume per unit width during accretion period for RN38, RN31, RN22, and RN17.	103
Figure 4.54	Cumulative total cross-shore sand transport volume per unit width during accretion period for RS0, RS14, RS24, and RS36.	104
Figure 4.55	Cumulative total cross-shore sand transport volume per unit width during accretion period for DN40, DN25, DN15, and DN0.....	105
Figure 4.56	Cumulative total cross-shore sand transport volume per unit width during accretion period for DS10, DS20, DS30, and DS40.	106
Figure 4.57	Measured and computed erosion (top) and accretion (bottom) volumes above MSL per unit alongshore length	108
Figure 4.58	Computed sand (no void) volumes transported alongshore for $B = 0.001$, 0.002 , and 0.003 during erosion period (top 3 lines) and accretion period (bottom 3 lines)	110

ABSTRACT

Our capability for predicting beach and dune erosion has improved for the last three decades but the recovery of an eroded beach cannot be predicted at present. The cycle of beach erosion and recovery will need to be predicted for the long-term maintenance of a sand beach with a dune for coastal flooding reduction. The cross-shore numerical model CSHORE is extended and evaluated using natural beach erosion and recovery data along 16 cross-shore lines spanning 5 km alongshore for the duration of 272 days. CSHORE predicts beach and dune erosion fairly well as has been shown in the previous comparisons. The bed load formula used in CSHORE is adjusted to predict the accreted beach profile with a berm. The computed beach profile evolutions are shown to be affected little by the alongshore gradient of the longshore sediment transport rate along the straight beach. The extended CSHORE predicts both erosion and accretion above the mean sea level within a factor of about 2.

Chapter 1

INTRODUCTION

Beach nourishment has been widely adopted in the U.S. in order to maintain a wide beach with a high dune and provide coastal storm protection and flooding damage reduction. Numerical models such as SBEACH (e.g., Wise et al. 1996) and Xbeach (Roelvink et al. 2009) have been developed to predict storm-induced beach and dune erosion and design the beach and dune profile required for storm protection. The amount and frequency of the periodic beach nourishment may increase due to the combined effects of sea level rise and storm intensification due to global warming. A process-based numerical model is required to predict the cycle of beach erosion and recovery and assess the long-term performance of a nourished beach in a changing climate. Presently, the long-term shoreline change is predicted using one-line models such as GENESIS (e.g., Hanson 1989) and equilibrium shoreline response models (e.g., Yates et al. 2009) without regard to beach profile evolution.

The cross-shore numerical model CSHORE developed by Kobayashi et al. (2010) consists of the combined wave and current model based on the time-averaged continuity, momentum and wave energy equations coupled with the transparent formulas for suspended sand and bed load transport rates which have been shown to synthesize available sediment transport data and formulas. CSHORE includes a probabilistic model for the wet and dry zone above the shoreline to predict dune erosion and overwash as well as longshore sediment transport in the swash zone.

CSHORE has been compared with a number of small-scale and large-scale laboratory data as well as field data. However, these comparisons do not include the recovery of eroded beaches after storms. In this study, CSHORE is compared with beach erosion and recovery data from the Atlantic coast in Delaware. In addition, CSHORE is extended to multiple cross-shore lines so as to include the alongshore gradient of the longshore sediment transport rate in the beach profile evolution prediction.

In the following, field data are presented in chapter 2. The existing model CSHORE is described concisely and the modifications of CSHORE are presented in chapter 3. The modified CSHORE is compared with the field data and the sensitivities of the computed profiles to the modifications are assessed in chapter 4. Finally, the findings of this study are summarized in chapter 5.

Chapter 2

FIELD DATA

In this chapter, field data from surveyed Delaware beaches are presented first. The corresponding wave and water level time series are discussed. Then, the measured erosion and accretion are analyzed.

2.1 Field Site

The Atlantic sandy coast of 40 km length in Delaware is suffering from chronic beach erosion and has been maintained by periodic beach nourishment for the last two decades (Figlus and Kobayashi 2008). This study is limited to 16 beach profiles at Rehoboth and Dewey beaches as depicted in Figure 2.1. These 16 profiles were measured on 29 October 1992, 18 December 1992 and 27 July 1993 before the major nourishment of these beaches in 1994 (Garriga and Dalrymple 2002). These profile data indicate the cycle of erosion and recovery of the natural beaches. The beach sand was fairly well sorted and its median diameter was 0.33 mm. Data from the tide gauge at Lewes, Delaware in Figure 2.1 is used to specify the hourly variation of the water level. A wave gauge (DE001 in Figure.2.1) was located at a depth of about 9 m off the coast of Dewey Beach.



Figure 2.1 Rehoboth beach, Dewey beach, Lewes tide gauge, and wave gauge DE001 in water depth of 9m offshore of Dewey beach(Google™)

The Google Earth satellite map was utilized to present the coast line including the locations of surveyed lines and gauges (<http://www.google.com/earth/index.html>) in Figure 2.1. The map has geographic coordinates (latitude/longitude) for most of the whole world. The time series of the root-mean-square wave height H_{rms} , spectral peak period T_p , and peak spectral wave direction θ are available every four hours (http://sandbar.wes.army.mil/public_html/pmab2web/htdocs/de001.html). The available time series are interpolated to obtain the hourly time series corresponding to the hourly water level data (<http://tidesandcurrents.noaa.gov/gmap3/>).

A storm attacked Rehoboth and Dewey beaches on 10 December 1992. The comparison of the beach profiles measured on 29 October 1992 and 18 December 1992 indicated considerable erosion above the mean sea level (MSL) for the 16 profiles. The datum of the water level and beach profiles is taken as MSL in this study. The eroded beaches recovered almost completely when the 16 profiles were measured on 27 July 1993. The erosion and accretion periods analyzed in this study

Table 2.1 Average Water Level and Wave Conditions during Erosion Period and Accretion Period

Period	Erosion	Accretion
Start Date	29 Oct 1992	18 Dec 1992
End Date	18 Dec 1992	27 Jul 1993
Number of Days	50.8	220.8
Average Water Level(m)	0.171	0.125
Average H_{rms}(m)	0.812	0.586
Average T_p(s)	9.42	8.26
Average Wave Angle(θ)	8.54°	8.45°

are summarized in Table 2.1 which lists the average values of the water level above MSL, H_{rms} , T_p and θ during each period. The wave angle is taken to be positive clockwise from the normal to the straight shoreline inclined at an angle of 8.86° counterclockwise from the north. The net longshore sediment transport along these beaches is northward.

2.2 Water Level and Wave Data

Figure 2.2 and 2.3 show the measured time series of the water level, H_{rms} , T_p and θ during the erosion period where the abscissa is the number of days since 29 October 1992. The horizontal line in each panel is the average value listed in Table 2.1. The storm of 10 December 1992, which is shown separately in Figure 2.3, lasted about 4 days with a peak water level of almost 2 m, a peak wave height of almost 3 m, wave periods of about 15 s, and wave directions of about 20° . Figures 2.4 through 2.7 show the measured time series of the water level, H_{rms} , T_p and θ for the accretion period.

Several minor storms with a peak water level of about 1 m, a peak wave height of about 2 m, and storm duration of 1 to 2 days occurred during the accretion period as shown in Figures 2.8 to 2.10. The water level, wave height and duration of these minor storms were clearly less than those of the major storm during the erosion period. The entire time series of the water level, H_{rms} , T_p and θ are specified as input at the seaward boundary of CSHORE in the water depth of about 9 m in order to simulate the beach profile evolution during the erosion and accretion periods. The alongshore variation of the wave conditions is assumed to be negligible.

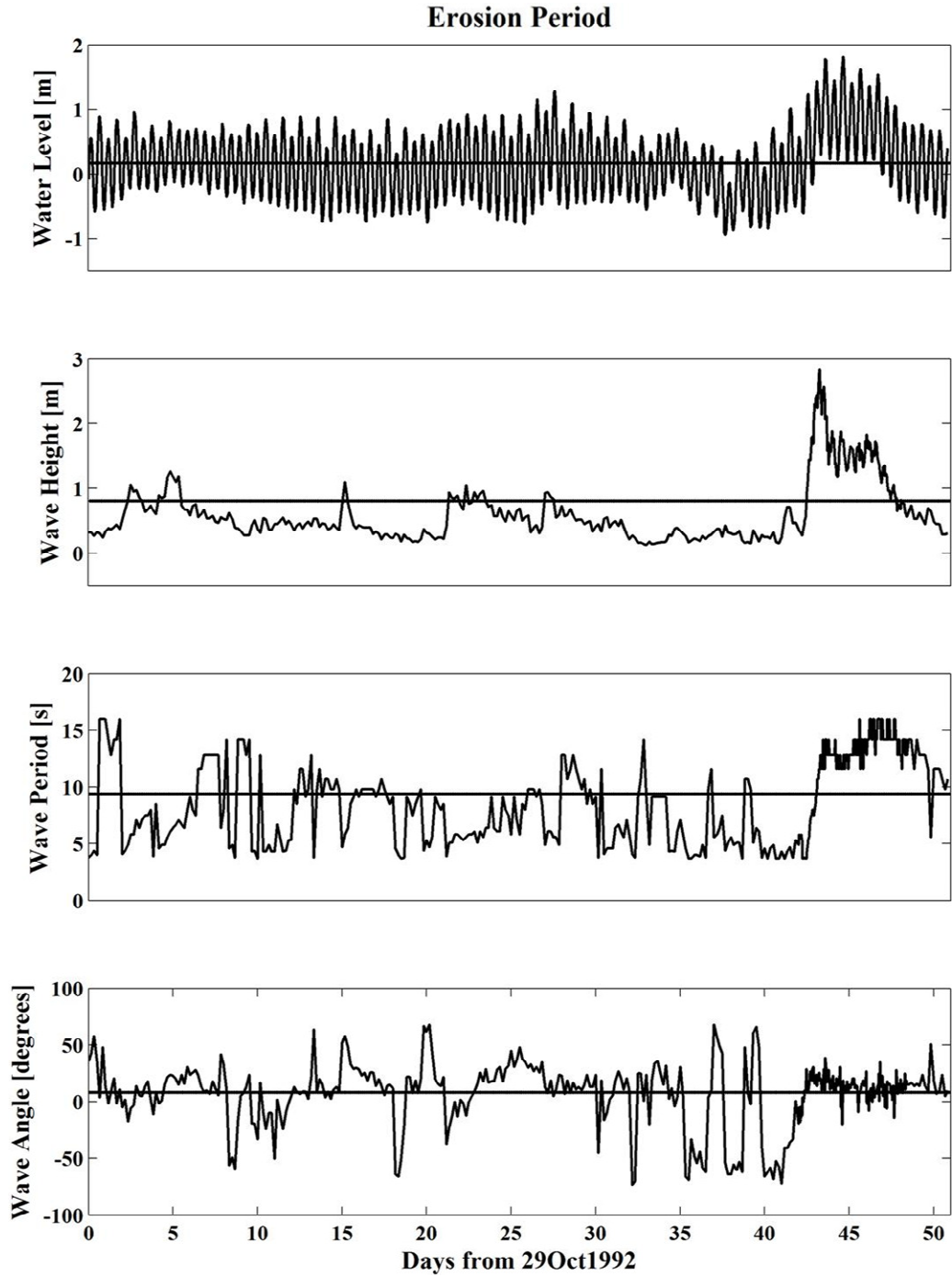


Figure 2.2 Water level, root-mean-square wave height, spectral peak period, and peak spectral wave direction for erosion period

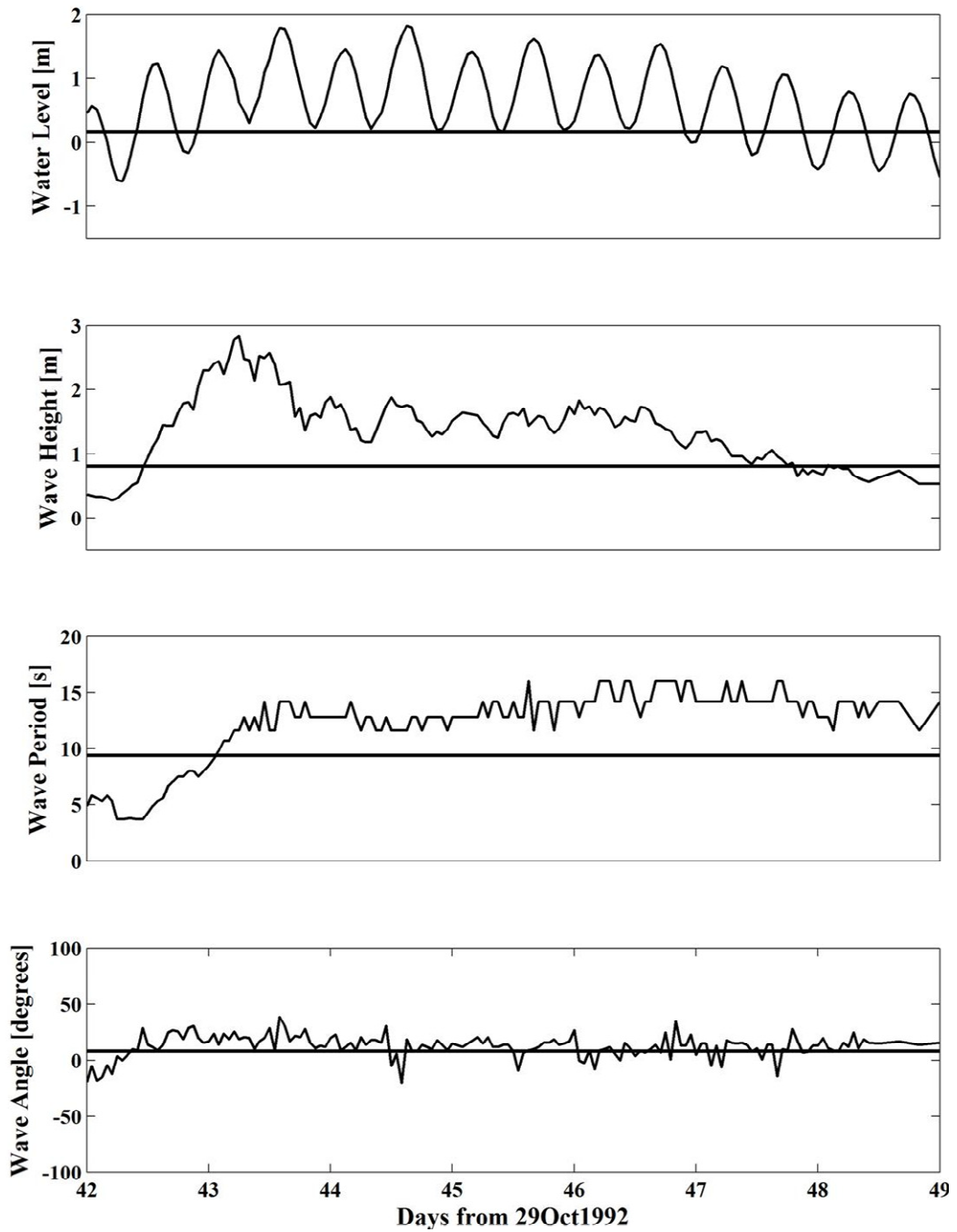


Figure 2.3 Storm of 10 December 1992 during erosion period

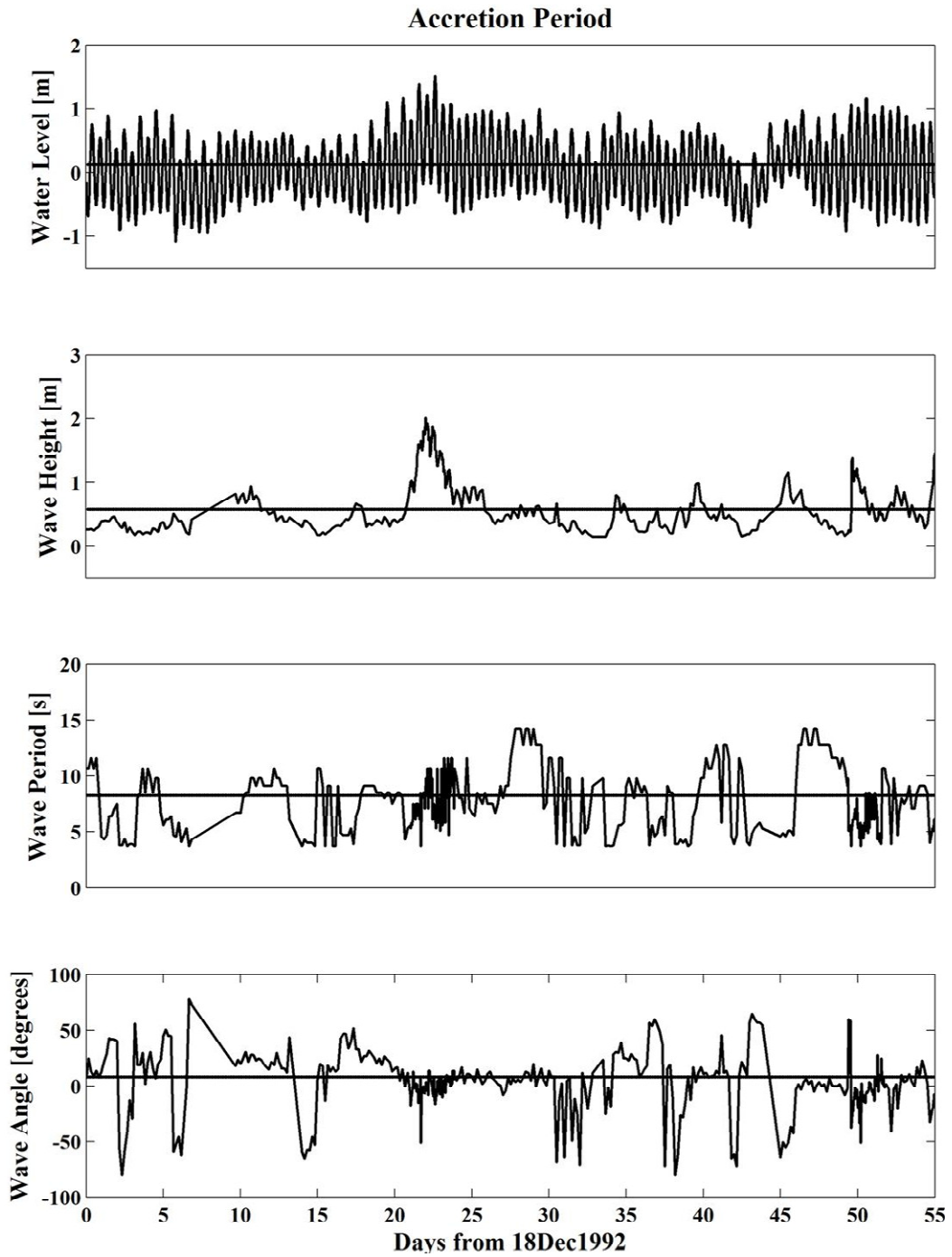


Figure 2.4 Water level, root-mean-square wave height, spectral peak period, and peak spectral wave direction during 0 to 55 days of accretion period

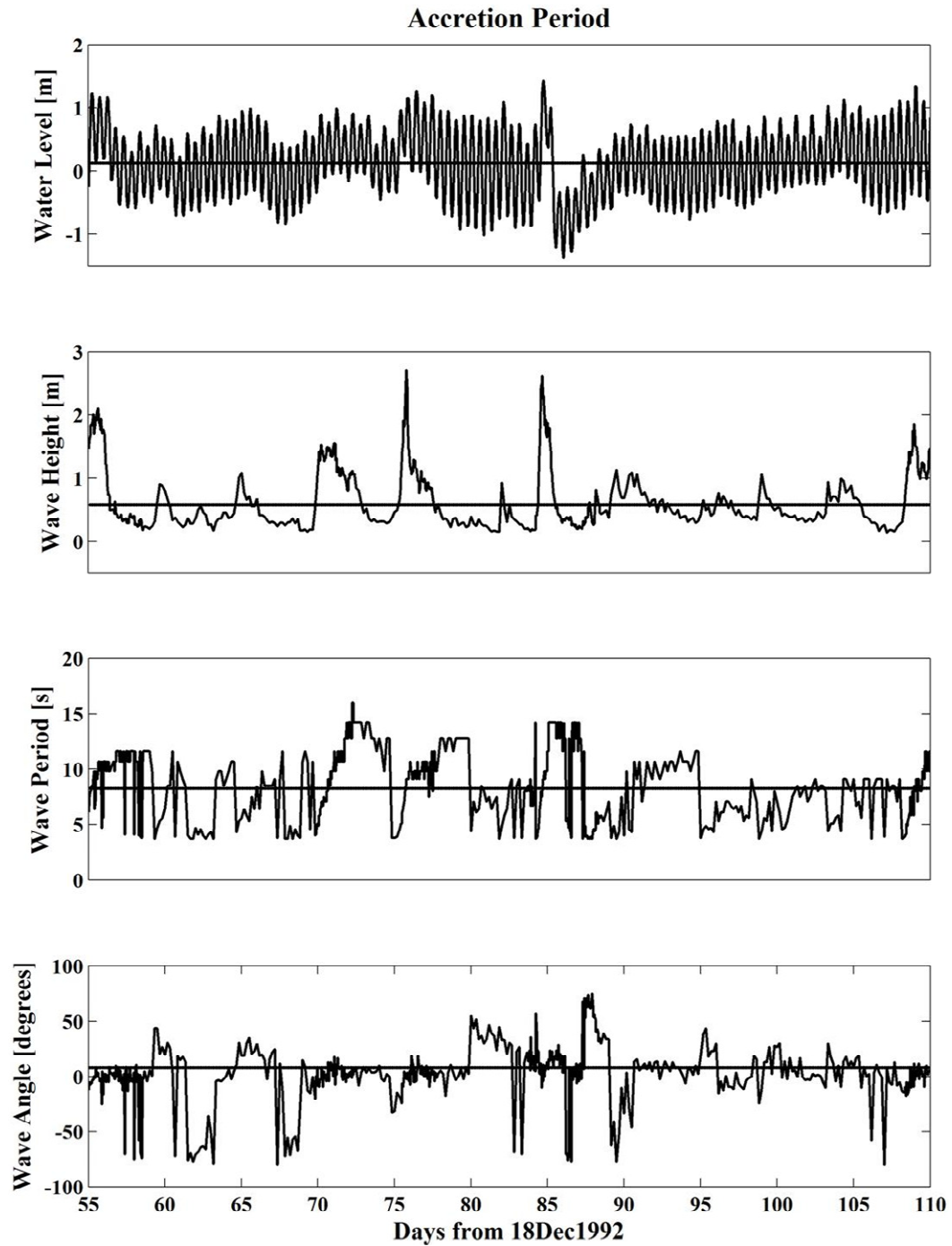


Figure 2.5 Water level, root-mean-square wave height, spectral peak period, and peak spectral wave direction during 55 to 110 days of accretion period

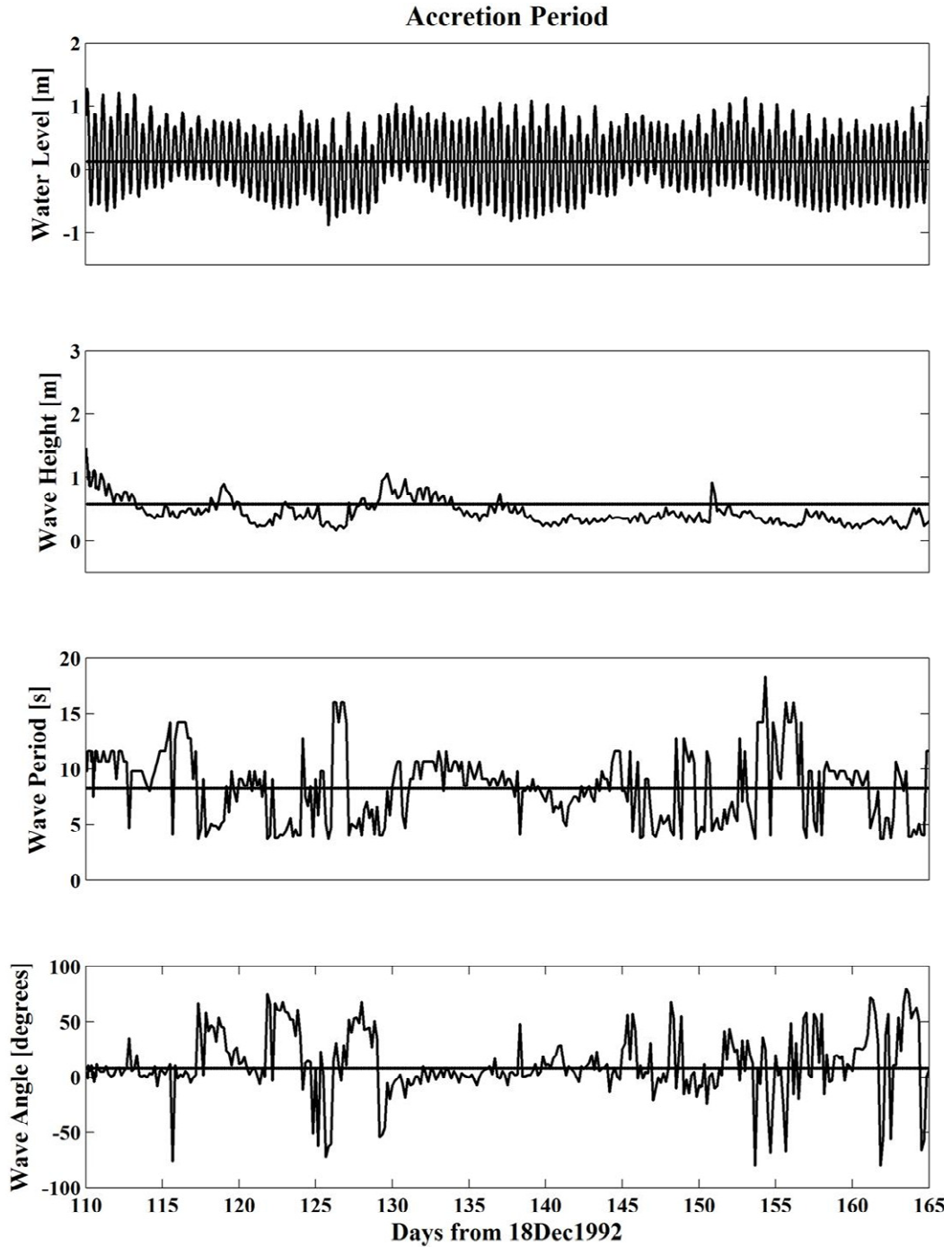


Figure 2.6 Water level, root-mean-square wave height, spectral peak period, and peak spectral wave direction during 110 to 165 days of accretion period

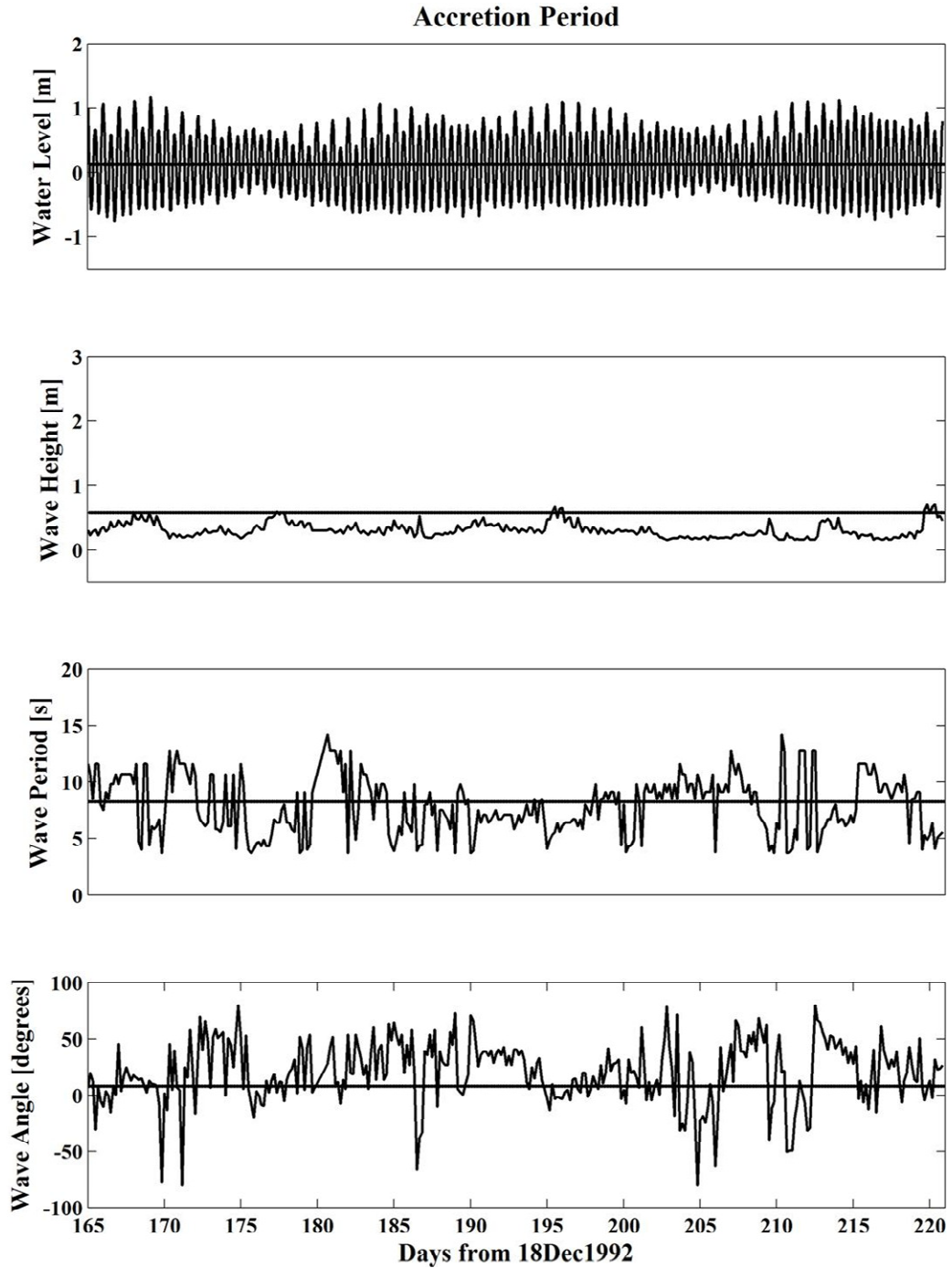


Figure 2.7 Water level, root-mean-square wave height, spectral peak period, and peak spectral wave direction during 165 to 220.8 days of accretion period

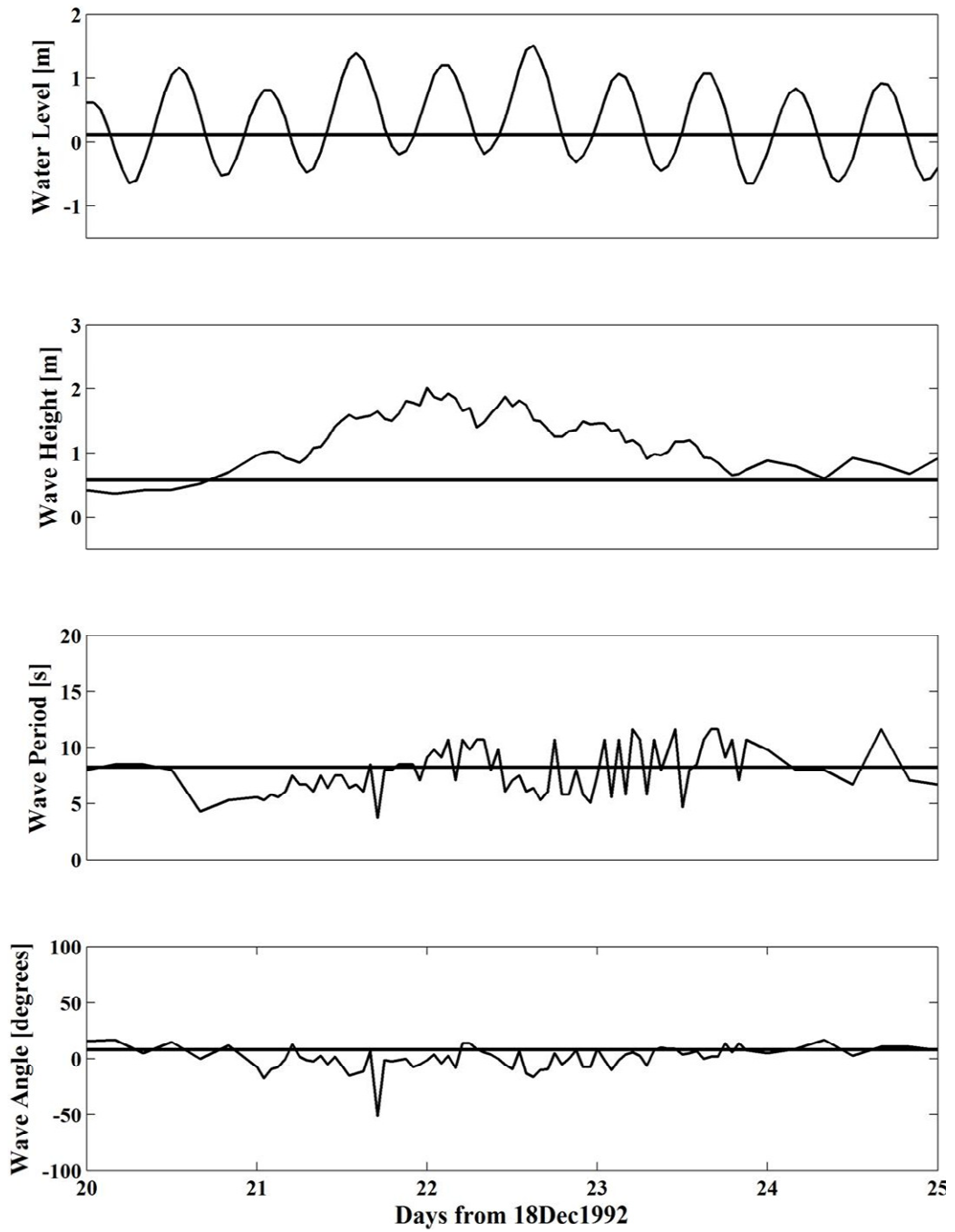


Figure 2.8 Storm of 8 January 1993 during accretion period

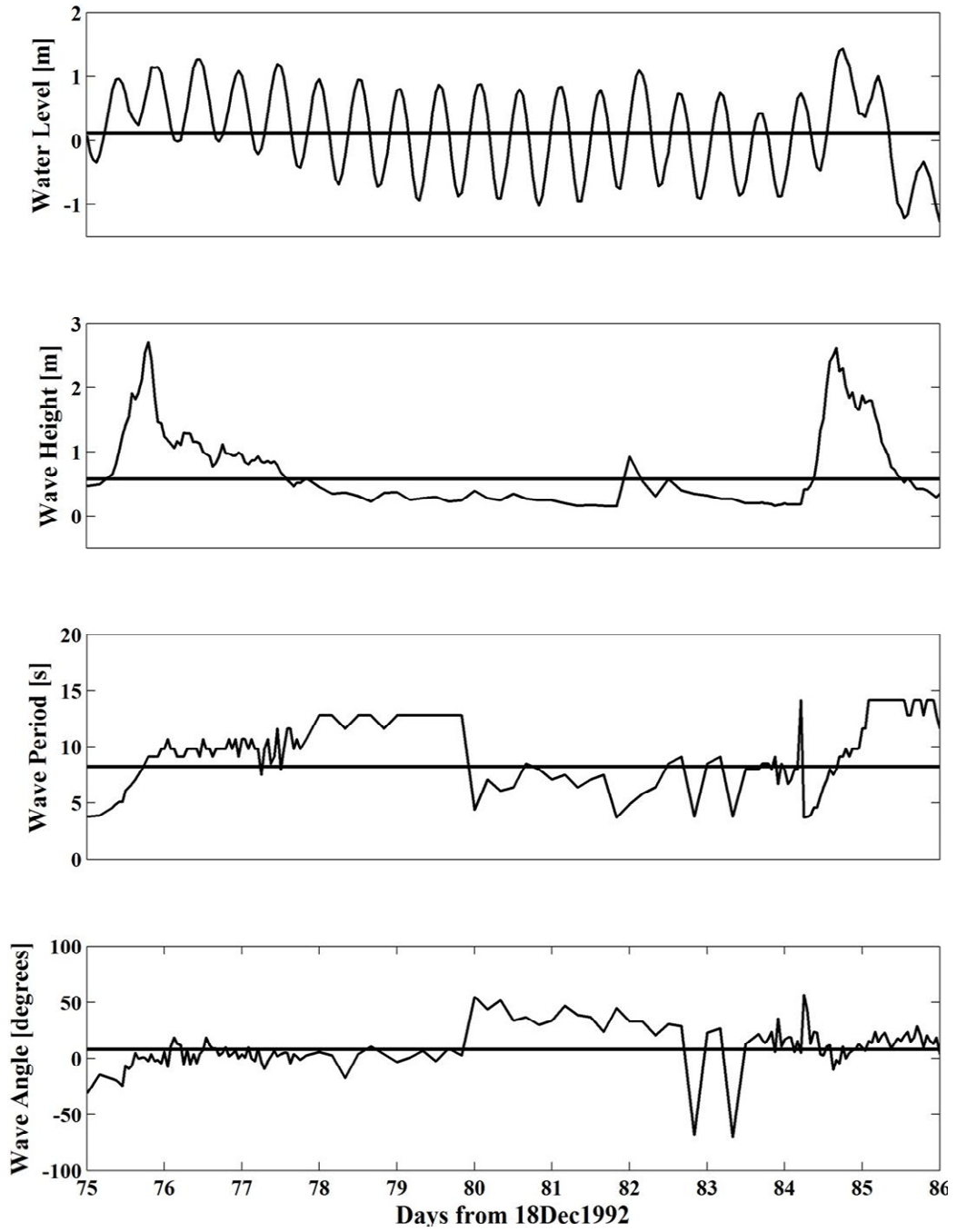


Figure 2.9 Storms of 3 March and 12 March 1993 during accretion period

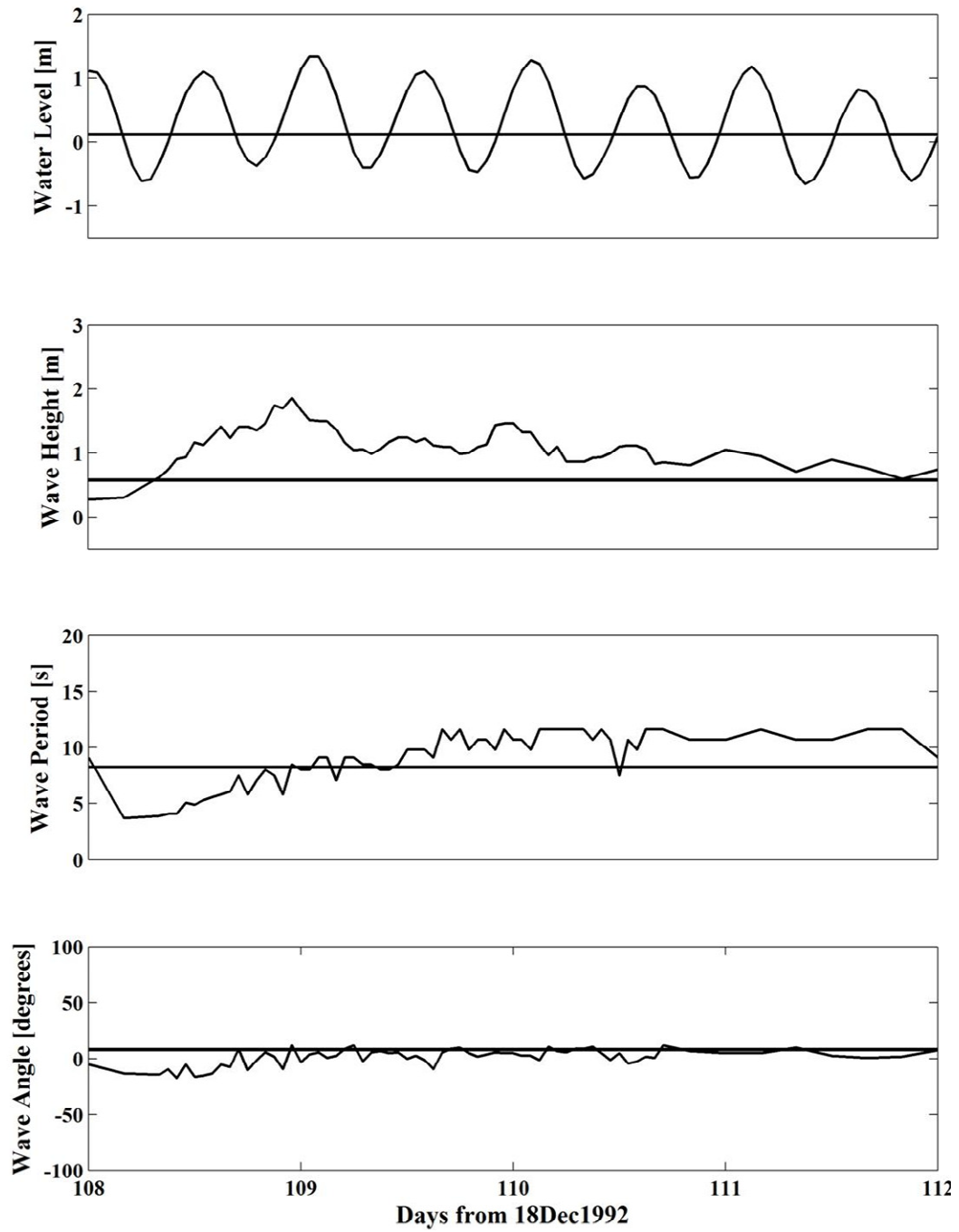


Figure 2.10 Storm of 5 April 1993 during accretion period

2.3 Beach Profile Data

The three beach profiles along each of the 16 cross-shore lines measured on 29 October 1992, 18 December 1992, and 27 July 1993 are plotted together to determine the cross-shore overlapping zone of the three profiles along each cross-shore line. The onshore coordinate x along each cross-shore line is taken as $x = 0$ at the seaward boundary of CSHORE and $x = x_m$ at the landward boundary of the overlapping zone above MSL. The values of x_m among the 16 profiles varied in the range of 309 to 634 m and the average value of x_m was 417 m. During the erosion period, erosion and deposition occurred above and below MSL, respectively, and the shoreline location at MSL did not vary much. During the accretion period, accretion and erosion occurred above and below MSL, respectively, and the beach profile at the beginning of the erosion period was similar to the corresponding profile at the end of the accretion period. The measured profiles are presented in the following. The shoreline location did not represent the observed erosion and accretion on these beaches.

Figure 2.11 shows the cross-shore survey lines on the two beaches. Table 2.2 summarizes the profile data for Rehoboth (R) and Dewey (D) beaches where N and S indicate the northern and southern segments of each beach. The numeral after N or S is related to the alongshore distance from the middle (numeral = 0) of each beach. The alongshore coordinate y is taken to be positive northward in the direction of the net longshore sediment transport with $y = 0$ at the most southern line DS40. The landward extent of some of the overlapped profiles was too short to resolve the dune profile change adequately. The top panel of Figure 2.12 shows a 3-D display of surveyed data points for the 16 profiles on Rehoboth and Dewey beaches measured on 29 October 1992.

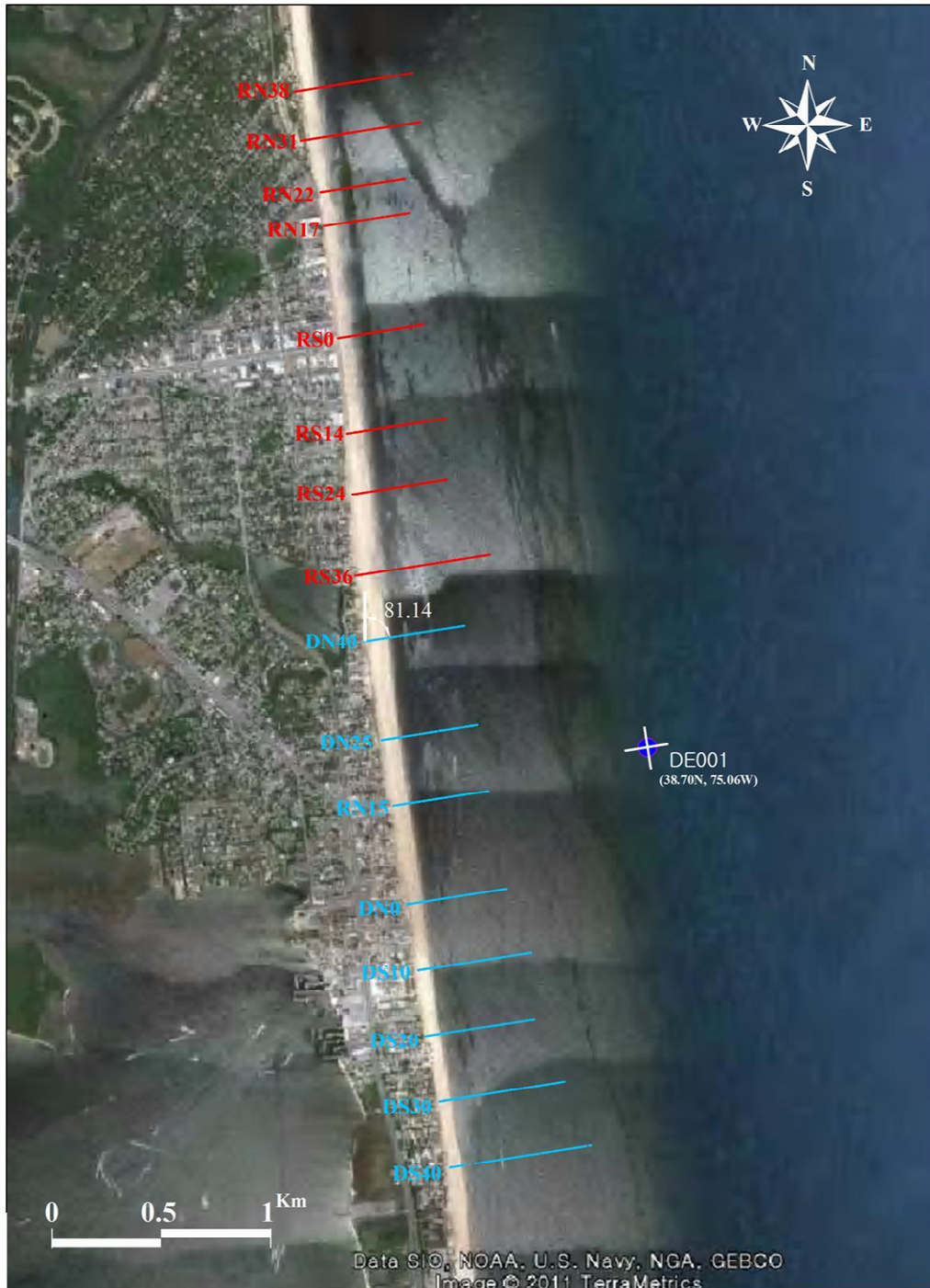


Figure 2.11 Eight cross-shore lines (RN38 to RS36) for Rehoboth beach and eight cross-shore lines (DN40 to DS40) for Dewey beach

Table 2.2 Alongshore Distance y , Increment Δy , and Cross-Shore Distance x_m Used for Computation

Beach	Line	$y(m)$	$\Delta y(m)$	$x_m(m)$
Rehoboth	RN38	4975	225	479
	RN31	4750	246	466
	RN22	4504	159	379
	RN17	4345	515	355
	RS0	3830	441	309
	RS14	3389	277	363
	RS24	3112	368	400
	RS36	2744	305	575
Dewey	DN40	2439	457	391
	DN25	1982	305	331
	DN15	1677	457	326
	DN0	1220	305	359
	DS10	915	305	374
	DS20	610	305	411
	DS30	305	305	520
	DS40	0	0	634
	Average		311	417

Note: y = alongshore distance from the most southward profile DS40

x_m = landward limit of each cross-shore profile starting from seaward boundary

$x = 0$ of CSHORE computation

The bottom panel of Figure 2.12 shows the 16 survey lines with the landward limits of $x = 0$ and $x_m = x$, respectively, along each survey line.

Figures 2.13 to 2.16 show the measured profiles on 29 October 1992, 18 December 1992, and 27 July 1993 for each of the 16 survey lines. Dune overwash

occurred at DN0 in Figure 2.15 and at DS10 in Figure 2.16 during the storm before the profile measurement on 18 December 1992. The sand volume per unit alongshore length above MSL is calculated using the beach profile measured on 29 October 1992 for each line to indicate the relatively large alongshore variation of the beach profile above MSL as listed in Table 2.3. The erosion volume per unit length above MSL is calculated using the measured profiles at the beginning and end of the erosion period. The accretion volume per unit length above MSL is calculated using the measured profiles at the beginning and end of the accretion period. As shown in Table 2.3, the erosion and accretion volumes were similar and did not vary alongshore as much as the initial sand volume. The erosion and accretion above MSL were more uniform alongshore than the initial 16 beach profiles. Figure 2.7 plots the volumes listed in Table 2.3 to indicate the recovery of the eroded beach above MSL at the end of the accretion period.

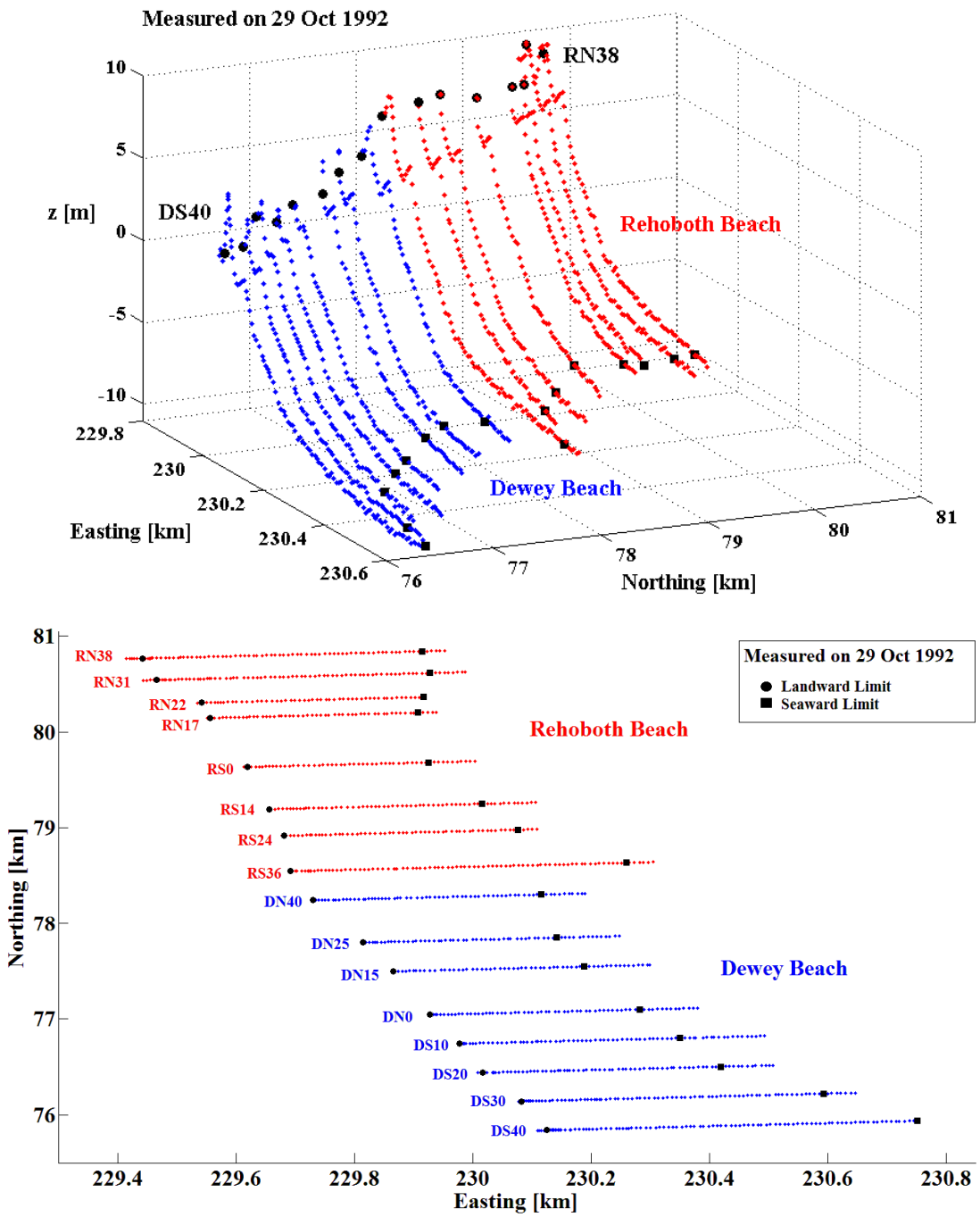


Figure 2.12 Profile survey data(top) and survey lines(bottom)
 Note: x = Normal to shoreline(8.86° counterclockwise from Easting)
 y = Alongshore(8.86° counterclockwise from Northing)

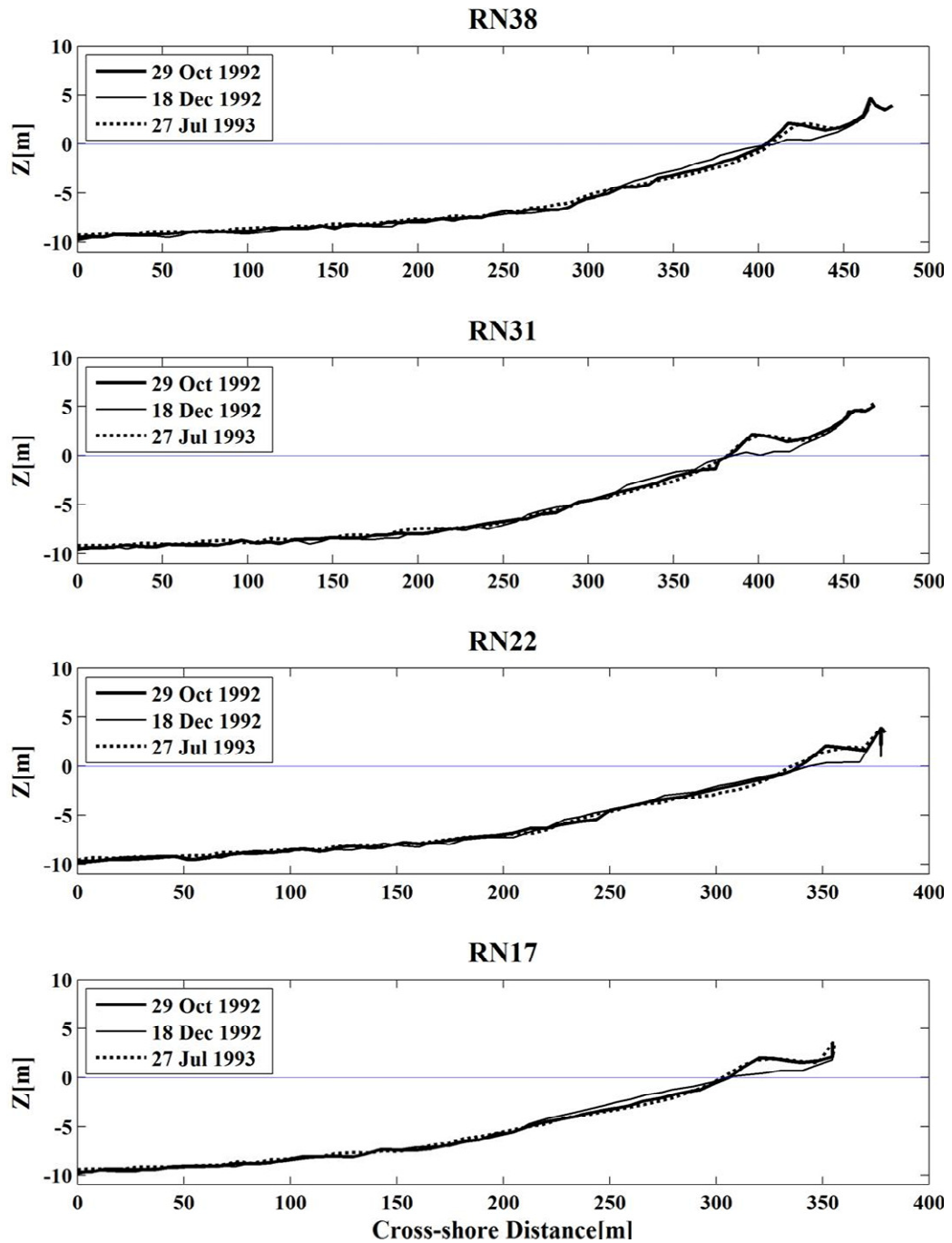


Figure 2.13 Measured profiles along lines RN38, RN31, RN22, and RN17 on 29 October 1992, 18 December 1992, and 27 July 1993

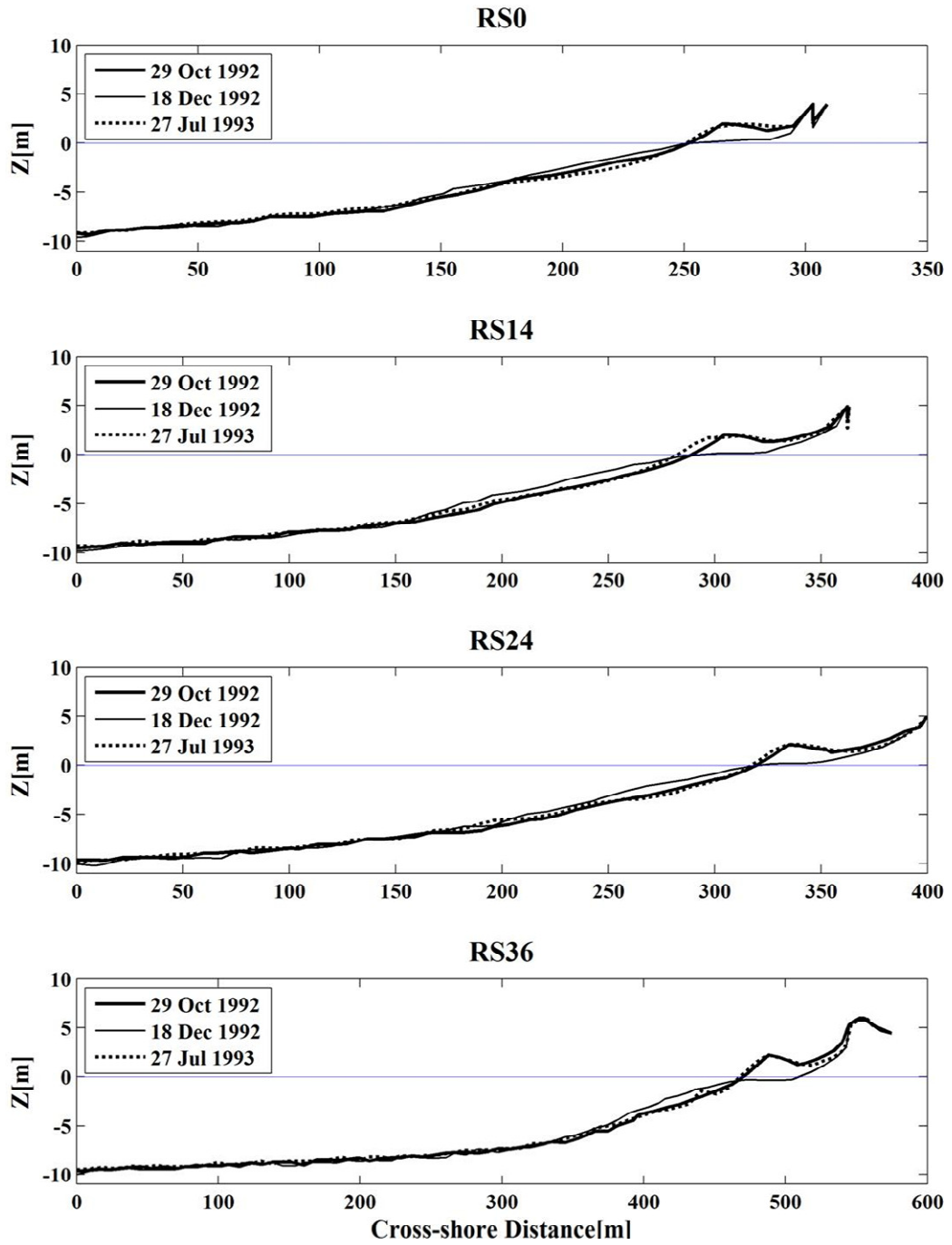


Figure 2.14 Measured profiles along lines RS0, RS14, RS24, and RS36 on 29 October 1992, 18 December 1992, and 27 July 1993

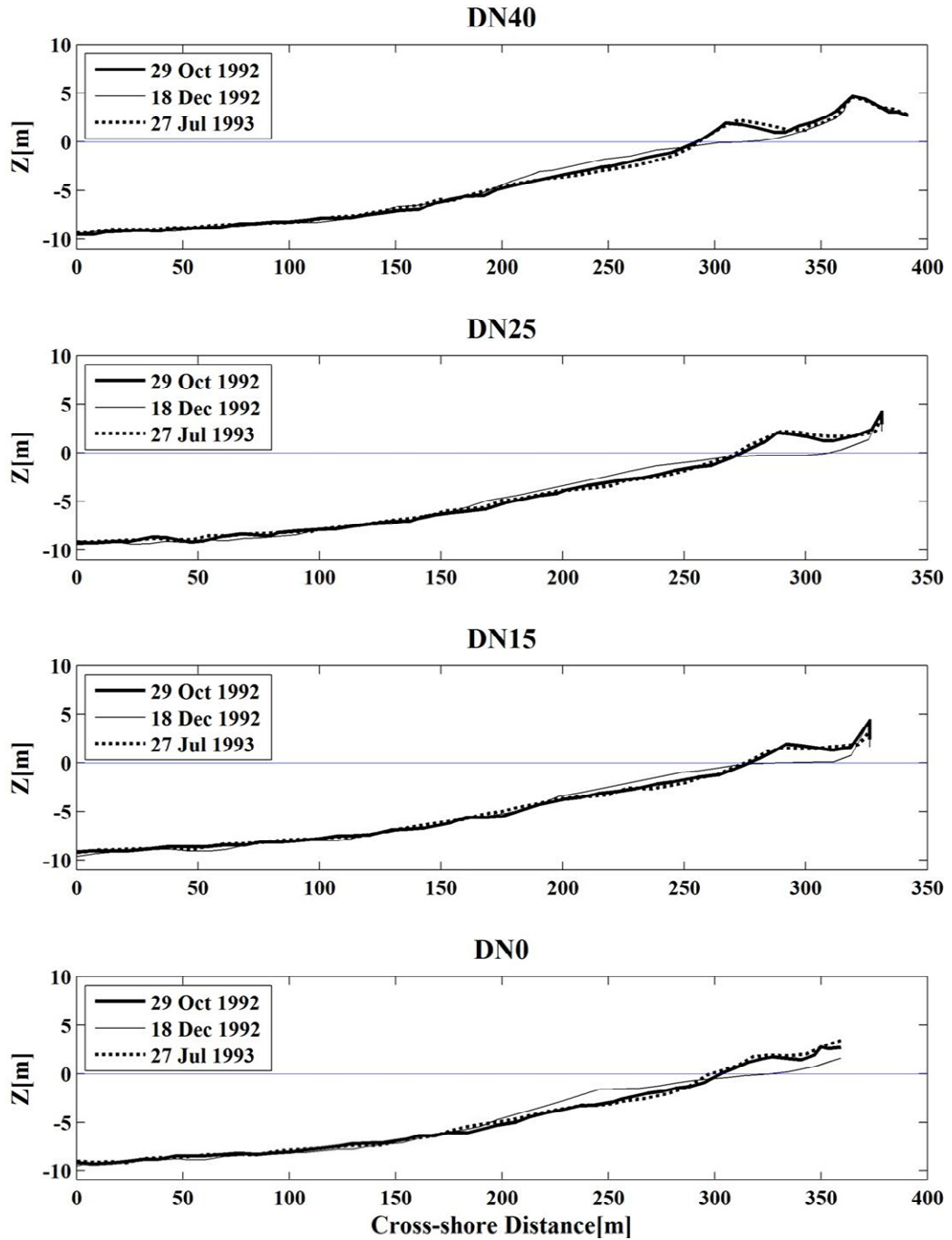


Figure 2.15 Measured profiles along lines DN40, DN25, DN15, and DN0 on 29 October 1992, 18 December 1992, and 27 July 1993

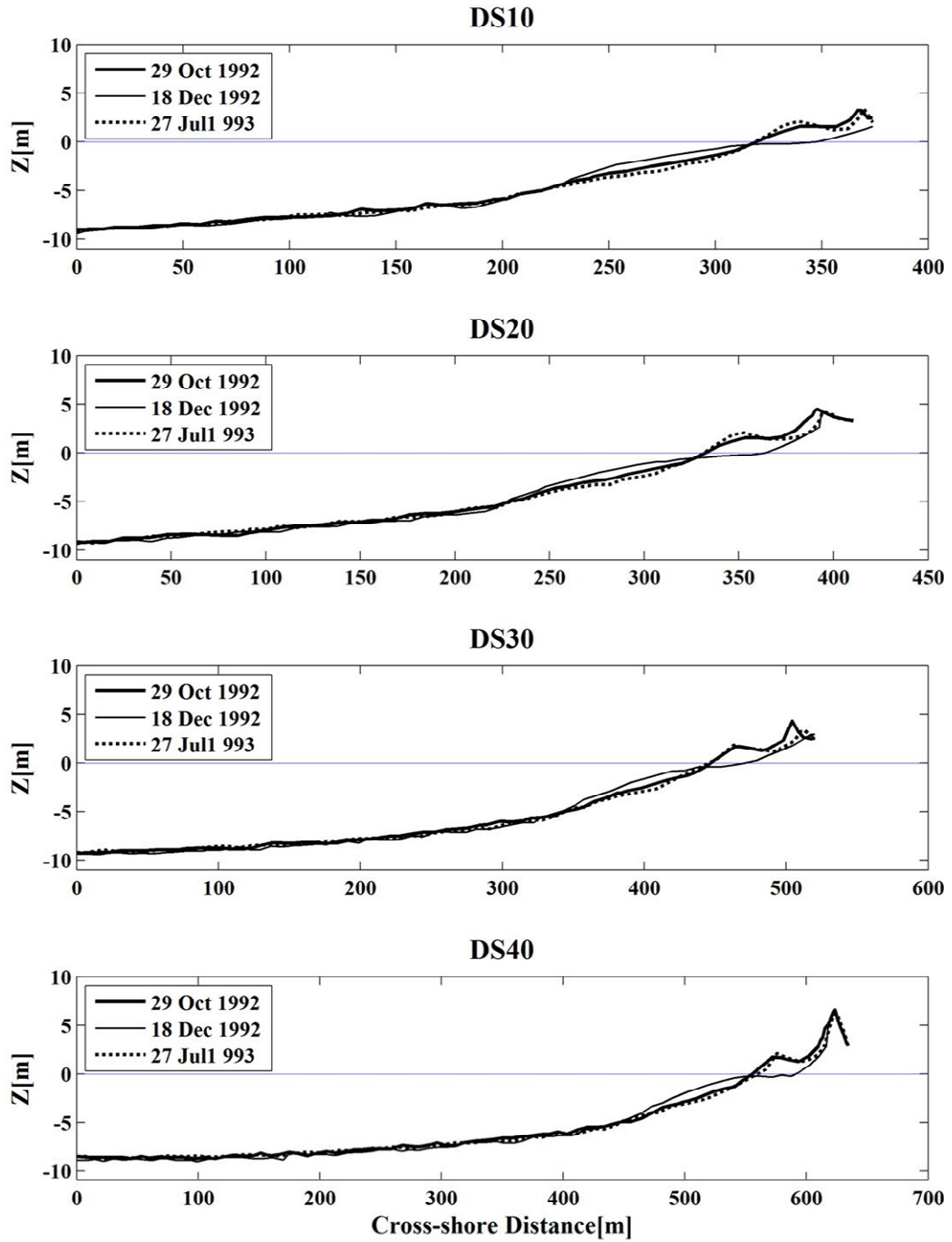


Figure 2.16 Measured profiles along lines DS10, DS20, DS30, and DS40 on 29 October 1992, 18 December 1992, and 27 July 1993

Table 2.3 Sediment Volume above MSL on 29 October 1992, Erosion Volume above MSL during Erosion Period, Accretion Volume above MSL during Accretion Period, and Net Erosion Volume above MSL for Entire Duration

Line	y(m)	Sediment Volume(m²)	Erosion Volume	Accretion Volume(m²)	Net Erosion Volume(m²)
RN38	4975	162.19	49.02	42.74	6.28
RN31	4750	199.82	59.40	58.56	0.84
RN22	4504	73.46	37.18	38.11	-0.93
RN17	4345	79.52	41.88	48.64	-6.77
RS0	3830	102.25	49.90	55.63	-5.73
RS14	3389	142.31	65.84	77.17	-11.33
RS24	3112	166.00	65.36	63.77	1.59
RS36	2744	302.24	90.78	77.26	13.52
DN40	2439	226.50	63.15	63.61	-0.45
DN25	1982	92.66	67.54	77.33	-9.79
DN15	1677	79.98	55.92	51.57	4.35
DN0	1220	89.09	67.34	86.14	-18.80
DS10	915	86.52	67.61	69.74	-2.14
DS20	610	173.43	72.09	61.77	10.32
DS30	305	138.00	72.38	57.95	14.44
DS40	0	193.89	75.45	56.48	18.97

Note: sediment volume including voids above Mean Sea Level(MSL) per unit longshore length

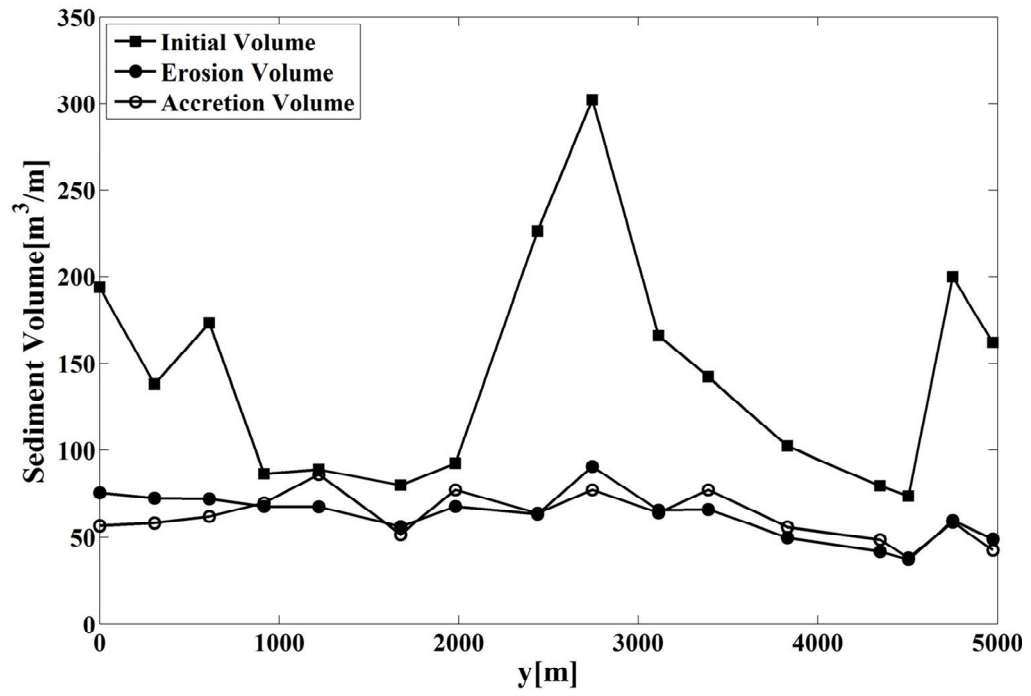


Figure 2. 17 Measured initial sediment volume, erosion volume, and accretion volume per unit longshore length

Chapter 3

NUMERICAL MODEL CSHORE

3.1 Hydrodynamic Model

The cross-shore numerical model CSHORE assumes unidirectional irregular waves and alongshore uniformity along each cross-shore line. The hydrodynamic model in CSHORE predicts the mean and standard deviation of the free surface elevation above the still water level (SWL) and depth-averaged cross-shore and longshore velocities. The time-averaged continuity, cross-shore momentum, longshore momentum and wave energy equations together with Snell's law are used in the wet zone seaward of the still water shoreline (Kobayashi et al. 2007) where the roller effect is found to be negligible in the present profile evolution comparison and is not included in the following computed results. The breaker ratio parameter γ is taken as its typical value of $\gamma = 0.7$ where the computed profile evolution is not sensitive to $\gamma = 0.7$ or 0.8 . The bottom friction factor f_b is taken as $f_b = 0.02$ calibrated for longshore current and sediment transport by Kobayashi et al. (2007). In the wet and dry zone, the wave angle is assumed to be small and remain the same as the wave angle at the still water shoreline. The time-averaged continuity and cross-shore momentum equations derived from the nonlinear shallow-water wave equations are used together with the exponential probability distribution of the instantaneous water depth (Kobayashi et al. 2010).

3.2 Sediment Transport Model

The sediment transport model in CSHORE consists of separate formulas for bed load and suspended load. The volume of suspended sediment per unit bottom area is expressed in terms of the wave energy dissipation rates due to wave breaking and bottom friction (Kobayashi et al. 2008). The suspended sediment is assumed to be transported by the cross-shore and longshore currents (Kobayashi et al. 2007). The effect of onshore flow due to wave overtopping is included to estimate the cross-shore suspended sediment transport rate q_{sx} (Figlus et al. 2011) where the wave overwash parameter a_o is taken as $a_o = 0.1$ but the computed profile evolution is not very sensitive to a_o in the range of 0.1 to 1.0. The longshore suspended sediment transport rate q_{sy} is proportional to the longshore current which is sensitive to the bottom friction factor $f_b = 0.02$ assumed in the following.

The cross-shore and longshore bed load transport rates q_{bx} and q_{by} are expressed as a function of the standard deviation and direction of the oscillatory wave velocity and the cross-shore and longshore currents (Kobayashi et al. 2009). The effect of the cross-shore bottom slope on q_{bx} is included to reduce the onshore bed load transport rate q_{bx} on a steep upward slope. The rates q_{bx} and q_{by} are proportional to the empirical bed load parameter b . Kobayashi et al. (2008) calibrated b using 20 water tunnel tests, 4 large-scale wave flume tests, and 24 sheet flow tests. The calibrated range for these tests with nonbreaking waves was $b = 0.001 - 0.004$ and the typical value of $b = 0.002$ has been used to predict beach and dune erosion for which offshore suspended sediment transport is dominant. For the present comparison with the beach erosion and recovery data, $b = 0.002$ is found to reproduce the 16 eroded profiles as well as for the previous comparisons (e.g., Kobayashi et al. 2010) but could not reproduce the 16 accreted profiles because of the deposition near the shoreline at MSL

unlike the observed upward berm reconstruction above MSL. To cause the landward increase of the onshore bed load transport rate q_{bx} inside the surf zone, use is made of $b = B (0.5 + Q)$ with $B = 0.002$ where the computed fraction Q of irregular breaking waves is zero for no wave breaking and unity when all waves break. Consequently, b increases from 0.001 outside the surf zone to 0.003 near the still water shoreline in the wet zone and in the wet and dry zone. The sensitivity of the computed profile change to the input value of B is presented after the comparison using $B = 0.002$.

3.3 Profile Evolution Model

The cross-shore beach profile evolution along each of the 16 lines is predicted using the continuity equation of bottom sediment

$$(1 - n_p) \frac{\partial z_b}{\partial t} + \frac{\partial q_x}{\partial x} + \frac{\partial q_y}{\partial y} = 0 \quad (1)$$

where n_p = porosity of bottom sediment assumed as $n_p = 0.4$; t = morphological time; z_b = bottom elevation with $z_b = 0$ at MSL; q_x = total cross-shore sediment transport rate per unit width given by $q_x = (q_{sx} + q_{bx})$; and q_y = total longshore sediment transport rate per unit width given by $q_y = (q_{sy} + q_{by})$. The alongshore gradient of q_y is included in Eq. (1) to allow the gradual alongshore variation of longshore sediment transport although the alongshore uniformity is assumed for each cross-shore line. CSHORE is modified to allow the simultaneous computation of the multiple cross-shore lines and include the effect of the alongshore gradient of q_y on the temporal variation of z_b along each line in approximate but computationally efficient manners. It is noted that the modified CSHORE is not a horizontally two-dimensional model like Xbeach (Roelvink et al. 2009).

To solve Eq. (1) numerically, the bottom elevation z_b is expressed as $z_b = (z_x + z_y)$ and Eq. (1) is rewritten as

$$(1 - n_p) \frac{\partial z_x}{\partial t} + \frac{\partial q_x}{\partial x} = 0 \quad (2)$$

$$(1 - n_p) \frac{\partial z_y}{\partial t} + \frac{\partial q_y}{\partial y} = 0 \quad (3)$$

Eq. (2) is solved using the same numerical method as that used for the case of no alongshore gradient of q_y in Eq. (1) (Kobayashi et al. 2007). Eq. (3) is integrated with respect to time t for the duration of constant water level and wave conditions where $\Delta t = 1h$ in the present computation. The bottom elevation change Δz_y is expressed as

$$(1 - n_p) \Delta z_y + \frac{\partial v_y}{\partial y} = 0 \quad ; \quad v_y = \int_t^{t+\Delta t} q_y dt \quad (4)$$

where v_y = longshore sediment transport volume per unit width for the duration of Δt which is obtained during the computation of z_x . The value of Δz_y based on Eq. (4) is added to the bottom elevation z_x computed using Eq. (2) at the interval of Δt . This numerical procedure assumes that the time scale of z_x in Eq. (2) is smaller than that of z_y in Eq. (3). This procedure is also convenient because the time step size used to solve Eq. (2) is constrained by the numerical stability criterion and can vary among the cross-shore lines.

The alongshore length scale is assumed to be larger than the cross-shore length scale to be consistent with the profile layout in Table 2.2 where the spacing of the cross-shore lines is as large as the cross-shore distance x_m . No additional cross-shore line is added to estimate the alongshore gradient of v_y in Eq. (4) which is expressed as

$$\frac{\partial v_y}{\partial y} = \frac{1}{L_x} \frac{\partial V_y}{\partial y} ; V_y = \int_0^{x_m} v_y dx ; \int_0^{x_m} \frac{dx}{L_x} = 1 \quad (5)$$

where V_y = longshore sediment transport volume across the entire cross-shore line; and L_x = cross-shore length related to the cross-shore variation of Δz_y in view of Eq. (4). If $L_x = x_m$ is assumed, the alongshore gradient of V_y causes the uniform change of Δz_y across the cross-shore line.

In the following computation, the length scale L_x is intuitively assumed to be given by

$$L_x = \frac{A_x}{|\Delta z_x|} ; A_x = \int_0^{x_m} |\Delta z_x| dx \quad (6)$$

where Δz_x = bottom elevation change based on Eq. (2) during time t to $(t + \Delta t)$. Eq. (6) satisfies the requirement of L_x in Eq. (5). Substitution of Eqs. (5) and (6) into Eq. (4) yields

$$\Delta z_y = \frac{-|\Delta z_x|}{(1-n_p) A_x} \frac{\partial V_y}{\partial y} \quad (7)$$

which shows that Δz_y is proportional to the magnitude of the bottom elevation change Δz_x due to the cross-shore sediment transport. This eliminates the need to specify the seaward and landward limit of the profile change for one-line models. The sign (accretion or erosion) of Δz_y in Eq. (7) depends on the alongshore gradient of V_y and remains the same along the cross-shore line. The alongshore gradient of V_y is approximated by an upstream differencing method (e.g., Anderson et al. 1984) for its numerical stability where the upstream direction is determined by the direction of V_y . Eq. (6) may not be rigorous but allows the use of a large alongshore spacing of two adjacent cross-shore lines.

3.4 CSHORE Input

The input to CSHORE includes the hourly time series of the water level above MSL and the incident wave conditions represented by H_{rms} , T_p and θ at the seaward boundary $x = 0$. Wave setup is assumed to be zero at $x = 0$. The beach sand is characterized by the median diameter of 0.33 mm and the fall velocity of 5 cm/s. The initial beach profile at time = 0 is the measured profile along each of the 16 cross-shore lines on 29 October 1992 for the erosion period and that on 18 December 1992 for the accretion period to assess the capability and limitation of CSHORE for predicting beach erosion and recovery separately. The cross-shore nodal spacing is 3 m for each cross-shore line. The computation time was 9 min for the erosion period of 50.8 days and 30 min for the accretion period of 220.8 days. The short computation time facilitated the above modifications of CSHORE which required a number of trial computations.

Chapter 4

COMPARISON OF NUMERICAL MODEL WITH FIELD DATA

The measured and computed profiles at the end of each period are compared for each of the 16 lines. Comparisons from the northern end(RN38) to the southern end(DS40) including the dune overwash zone(DN0 and DS10) in Figures 2.15 and 2.16 are presented in the following to represent the alongshore variation of the agreement among the 16 lines. The computed rates q_{bx} , q_{sx} , q_x , q_{by} , q_{sy} and q_y are integrated with time to obtain the cumulative sediment volumes per unit width transported during each period and to examine the computed cross-shore and longshore sediment transport. It is noted that the summary of the following comparison is presented in the paper by Kobayashi and Jung(2011).

4.1 Erosion Period

The measured initial profile and the measured and computed profiles at the end of the erosion period are presented in the top panel of each of Figures. 4.1 to 4.8. The elevation z is zero at the mean sea level (MSL). The offshore zone of the negligible profile change is omitted in these figures. The eroded berm and dune profile is predicted well for the northern profiles in Figure 4.1. Dune overwash occurred in the middle of the Dewey beach(DS0 in Figure 4.6 and DS10 in Figure 4.7) but the measured profile did not extend sufficiently landward. The eroded profile above MSL at DS0 and DS10 is underpredicted partly because of the boundary condition of zero cross-shore gradient of q_x at $x = x_m$ used to solve Eq. (2). The accreted profile below

MSL at DS0 and DS10 may be related to the erosion above MSL but its cause is not certain for lack of the landward profile data because the eroded sand must have also been transported landward. The erosion of the berm and dune for the southern profiles such as the profile at DS40 in Figure 4.8 is underpredicted and the nearly horizontal eroded profile near MSL cannot be predicted by CSHORE.

The cumulative cross-shore sediment volumes per unit width transported during the erosion period are plotted in the middle panel of each of Figures 4.1 to 4.8. CSHORE predicts the onshore (positive) bed load transport and the offshore (negative) suspended load transport for the case of negligible wave overwash. The total load is the sum of bed load and suspended load. The onshore bed load and offshore suspended load are computed to be of similar magnitude and the maximum near MSL. The small total load is plotted in Figures 4.9 to 4.12 where small numerical fluctuations occur near and above MSL. For the lines with no or minor dune overwash, the offshore total load is the maximum near MSL and approaches zero landward. CSHORE predicts the small onshore sediment transport outside the surf zone where the onshore bed load transport is predicted to exceed the offshore suspended sediment transport. This onshore sediment transport rate varies gradually in the cross-shore direction and causes very small profile changes. For DS0 and DS10 with major dune overwash, the total load is small seaward of MSL and increases landward of MSL because of the onshore flow associated with dune overwash.

On the other hand, the cumulative longshore sediment volumes per unit width transported during the erosion period are plotted in the bottom panel of each of Figures 4.1 to 4.8. The net longshore transport of bed load and suspended load is positive and northward along the Delaware Atlantic coast. The suspended load is

dominant for the longshore sediment transport and the maximum near MSL. It is noted that CSHORE has been shown to predict the cross-shore distribution of longshore sediment transport under constant water level and wave conditions (Kobayashi et al. 2007). The large longshore sediment transport in the swash zone explains the maximum cumulative load near MSL.

An option is provided in CSHORE to compute the beach profile change without (IQYDY=0) and with (IQYDY=1) the correction term given by Eq. (7). The computed bottom elevation z_b at the end of the erosion period for IQYDY=0 is subtracted from that for IQYDY=1. The elevation difference indicates the effect of the alongshore gradient of the longshore sediment transport on the cross-shore profile change. The computed elevation difference shown in Figures 4.13 to 4.16 turns out to be of the order of 10 cm or less. The positive (negative) elevation difference implies accretion (erosion) due to the longshore sediment transport gradient. The cross-shore variation of the elevation difference depends on the length scale L_x which is assumed to be given by Eq. (6). The computed elevation difference is much smaller than the profile changes of the order of 1 m or more in Figures 4.1 to 4.8

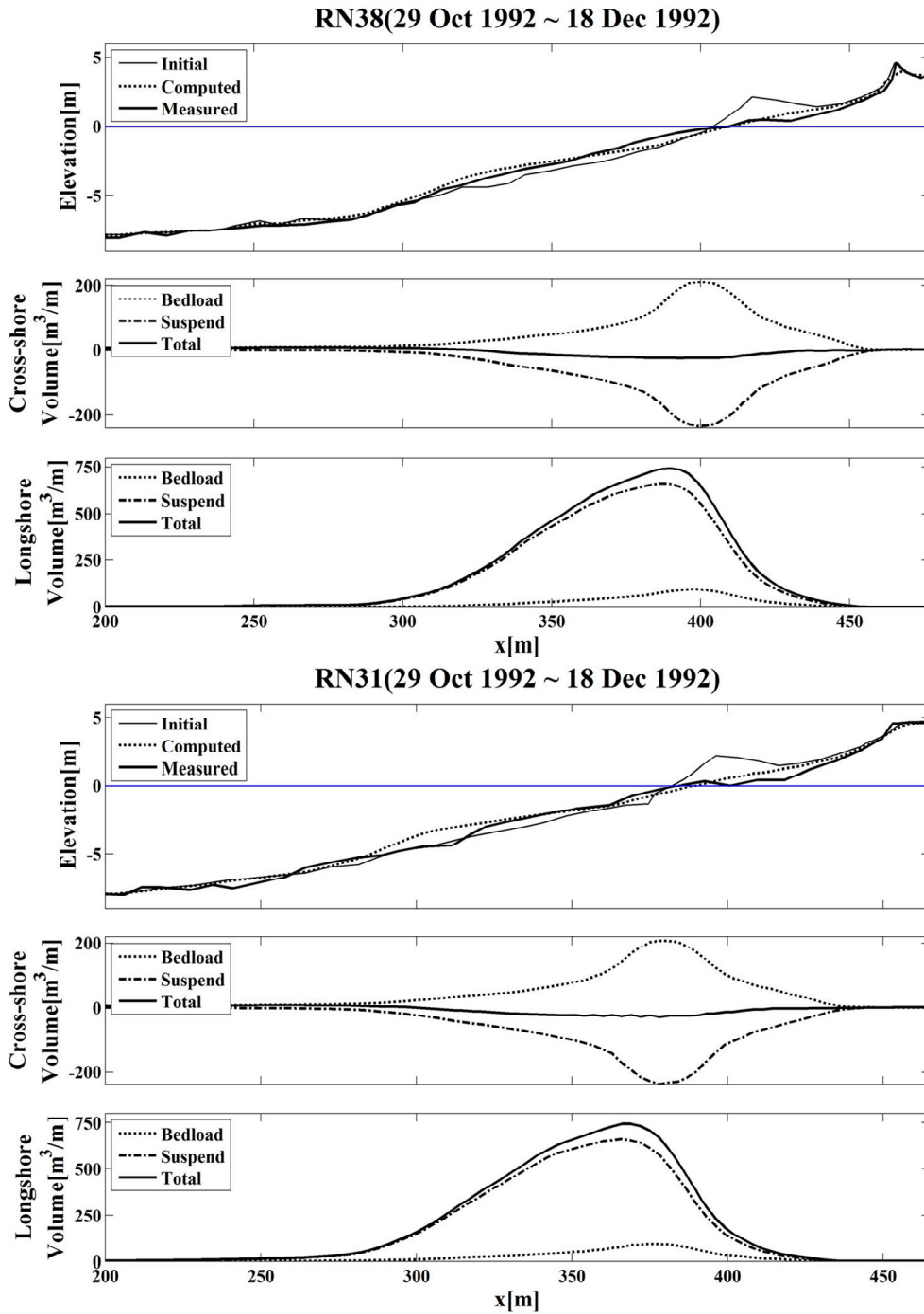


Figure 4.1 Measured and computed beach profiles (top), cumulative cross-shore (middle) and longshore (bottom) sand transport volume per unit width during erosion period for RN38 and RN31.

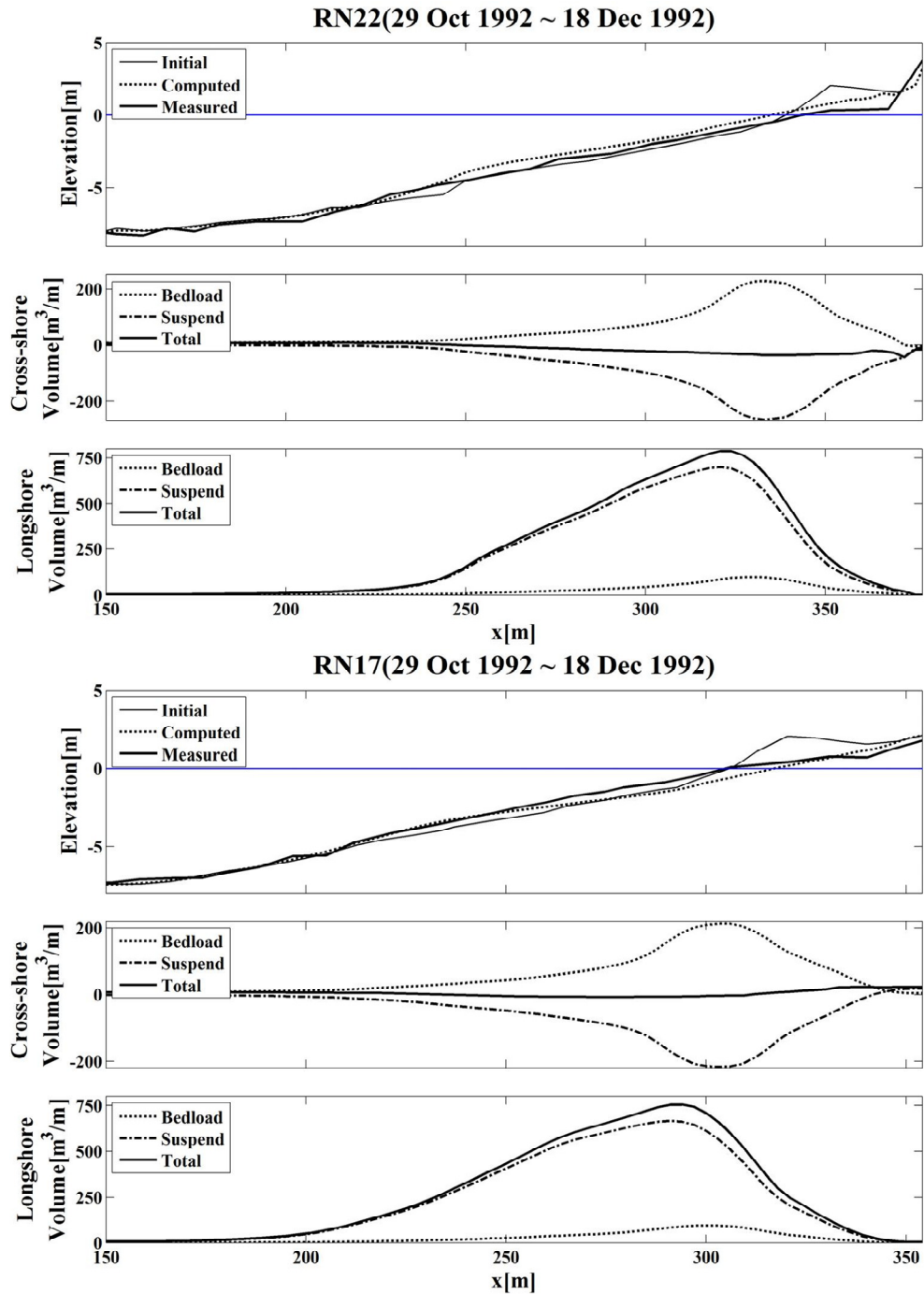


Figure 4.2 Measured and computed beach profiles (top), cumulative cross-shore (middle) and longshore (bottom) sand transport volume per unit width during erosion period for RN22 and RN17.

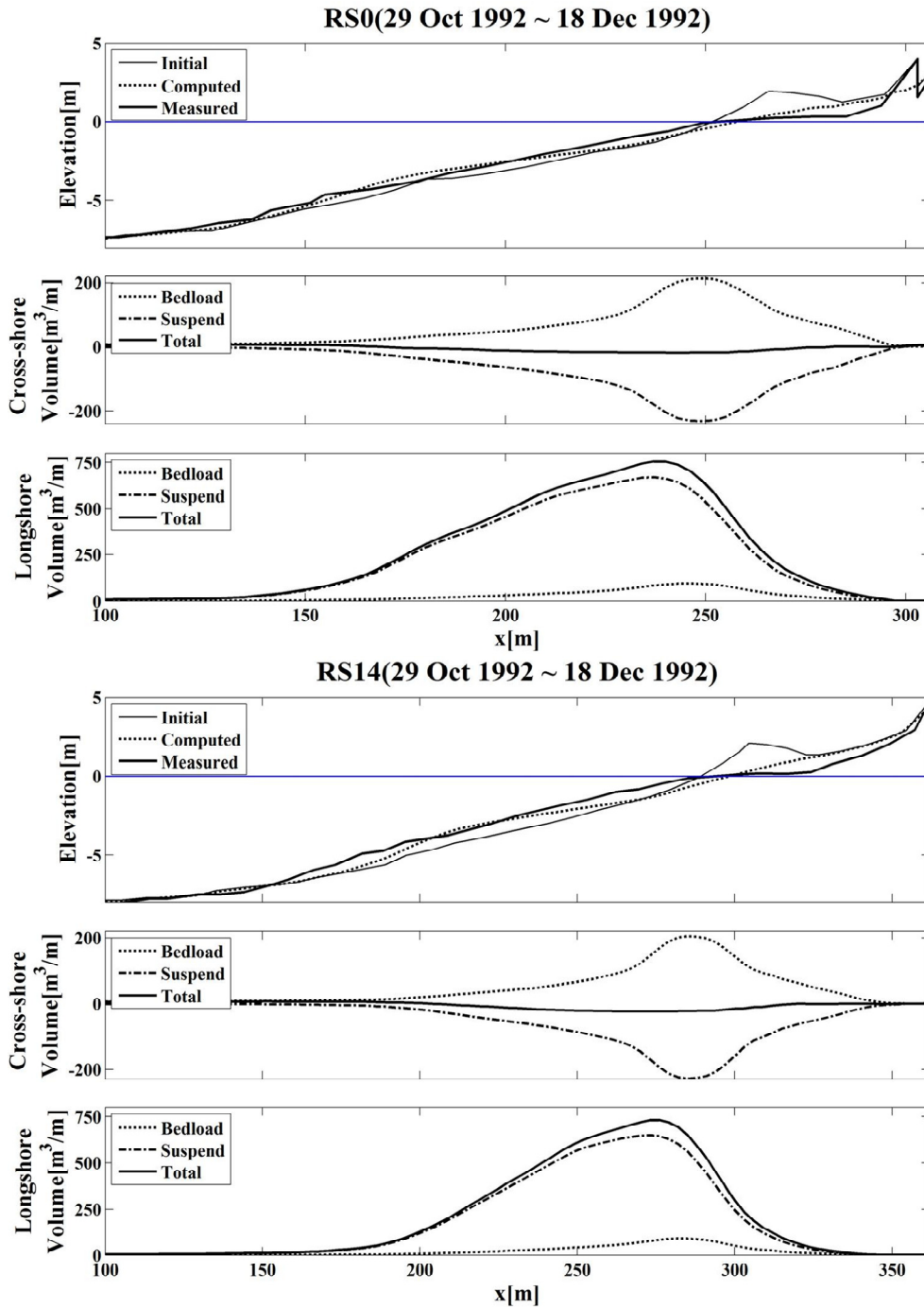


Figure 4.3 Measured and computed beach profiles (top), cumulative cross-shore (middle) and longshore (bottom) sand transport volume per unit width during erosion period for RS0 and RS14.

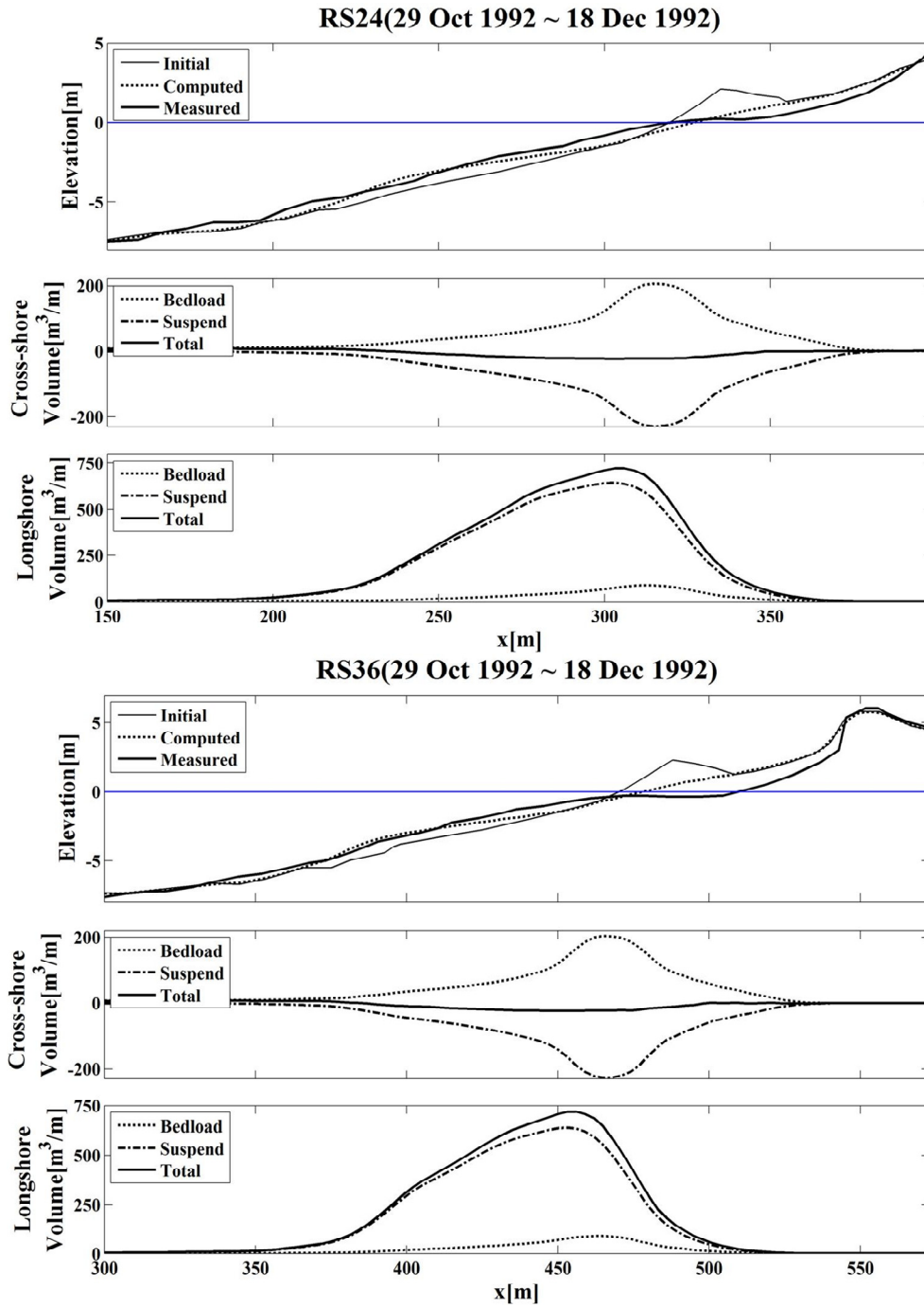


Figure 4.4 Measured and computed beach profiles (top), cumulative cross-shore (middle) and longshore (bottom) sand transport volume per unit width during erosion period for RS24 and RS36.

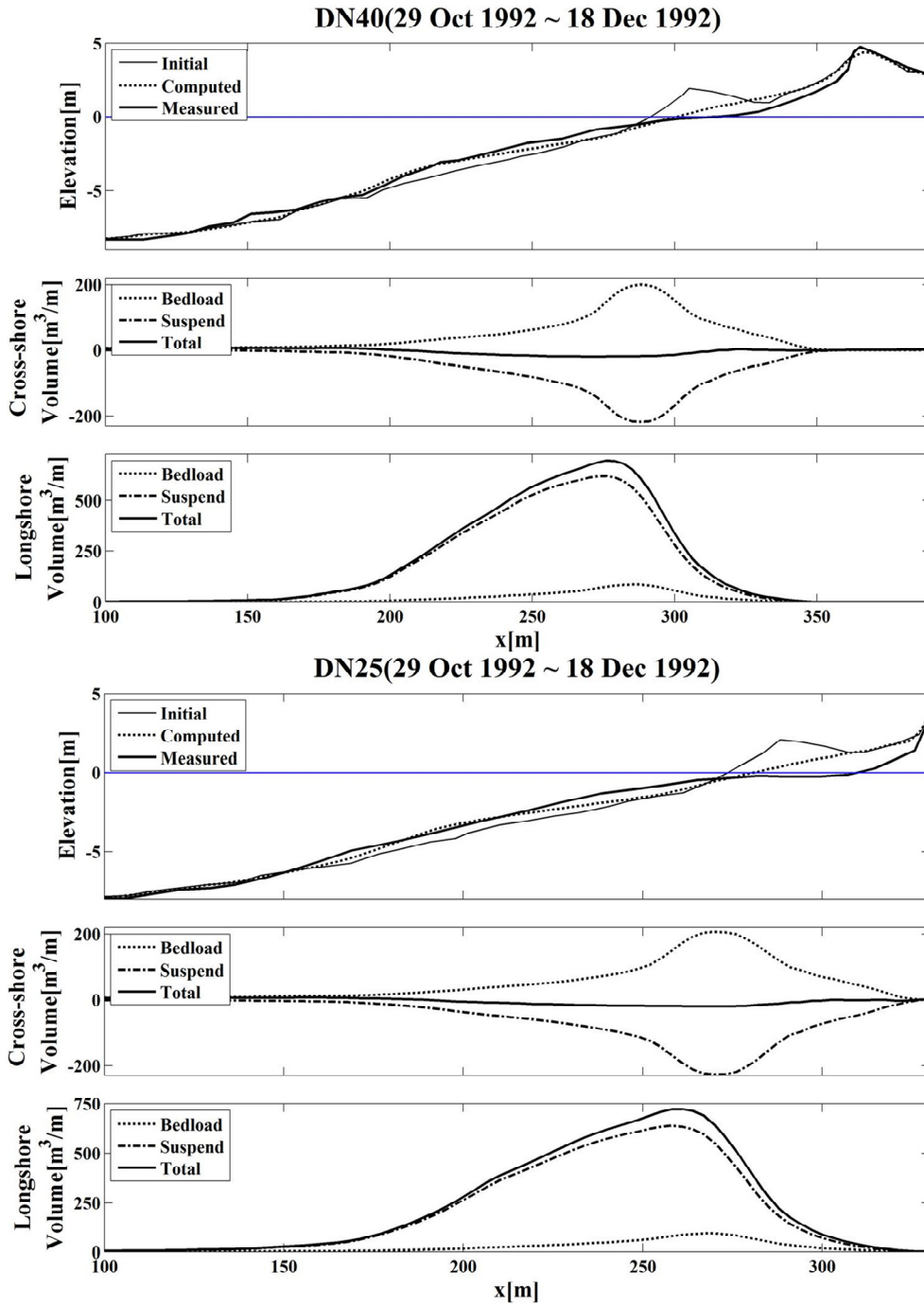


Figure 4.5 Measured and computed beach profiles (top), cumulative cross-shore (middle) and longshore (bottom) sand transport volume per unit width during erosion period for DN40 and DN25.

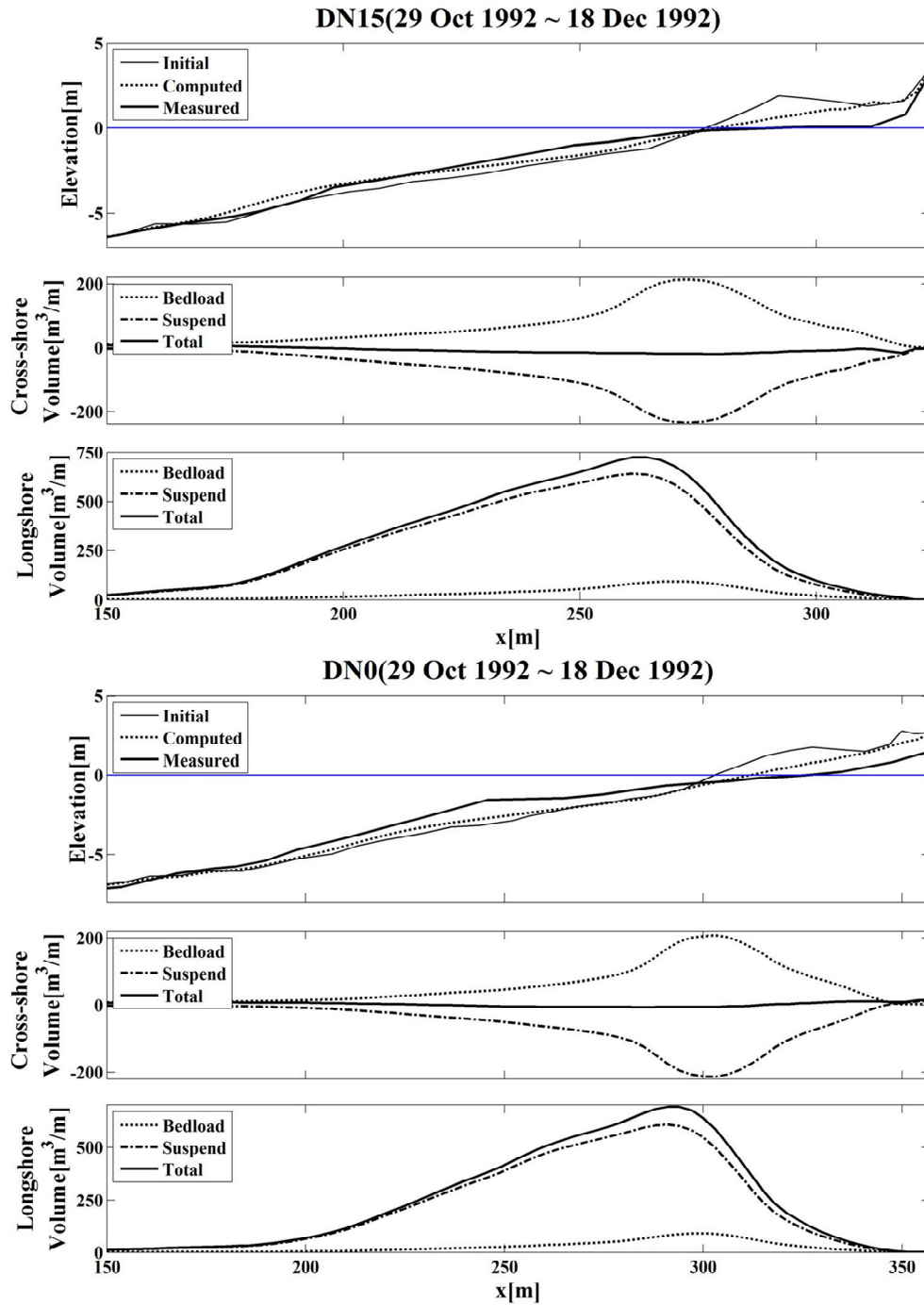


Figure 4.6 Measured and computed beach profiles (top), cumulative cross-shore (middle) and longshore (bottom) sand transport volume per unit width during erosion period for DN15 and DN0.

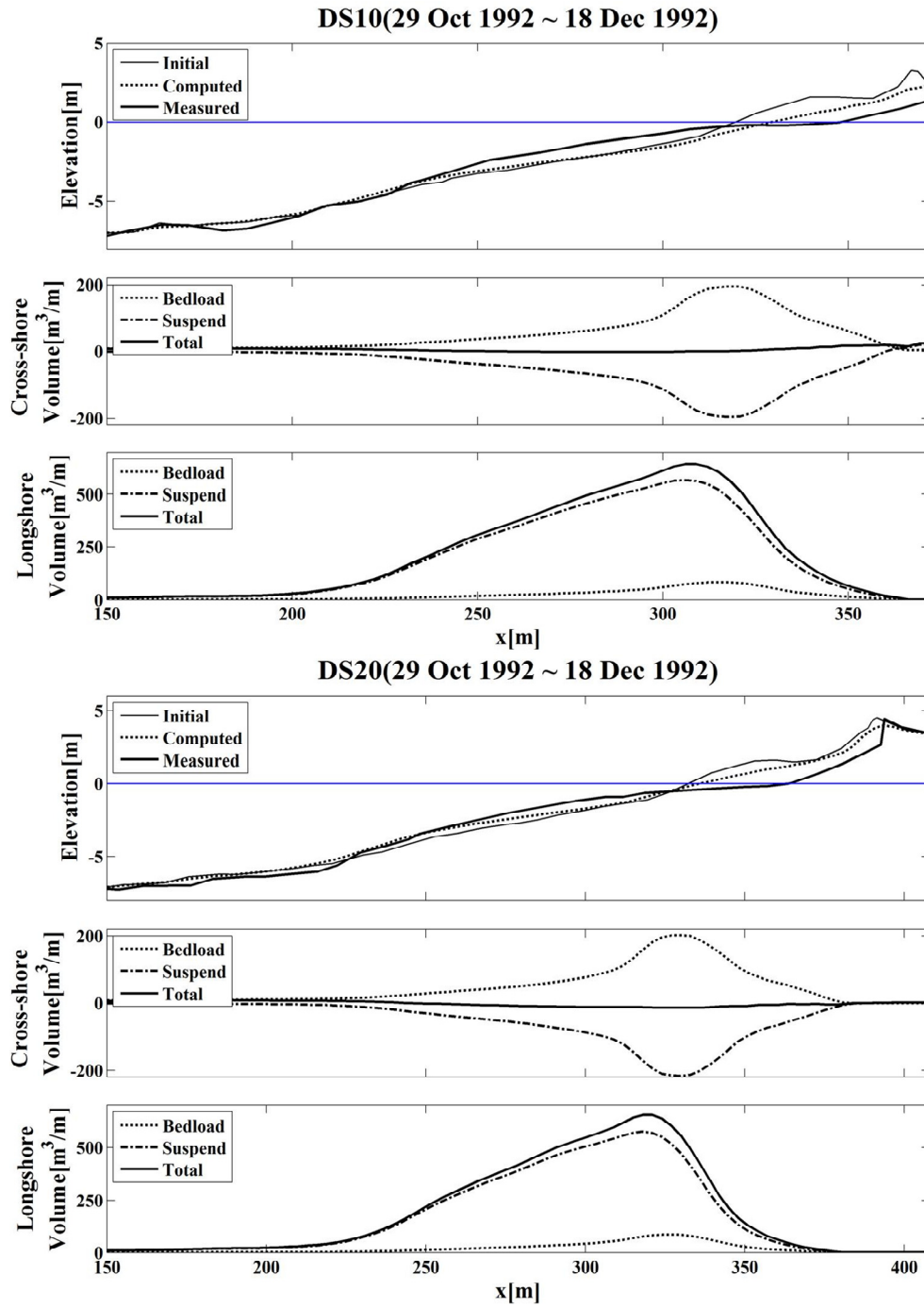


Figure 4.7 Measured and computed beach profiles (top), cumulative cross-shore (middle) and longshore (bottom) sand transport volume per unit width during erosion period for DS10 and DS20.

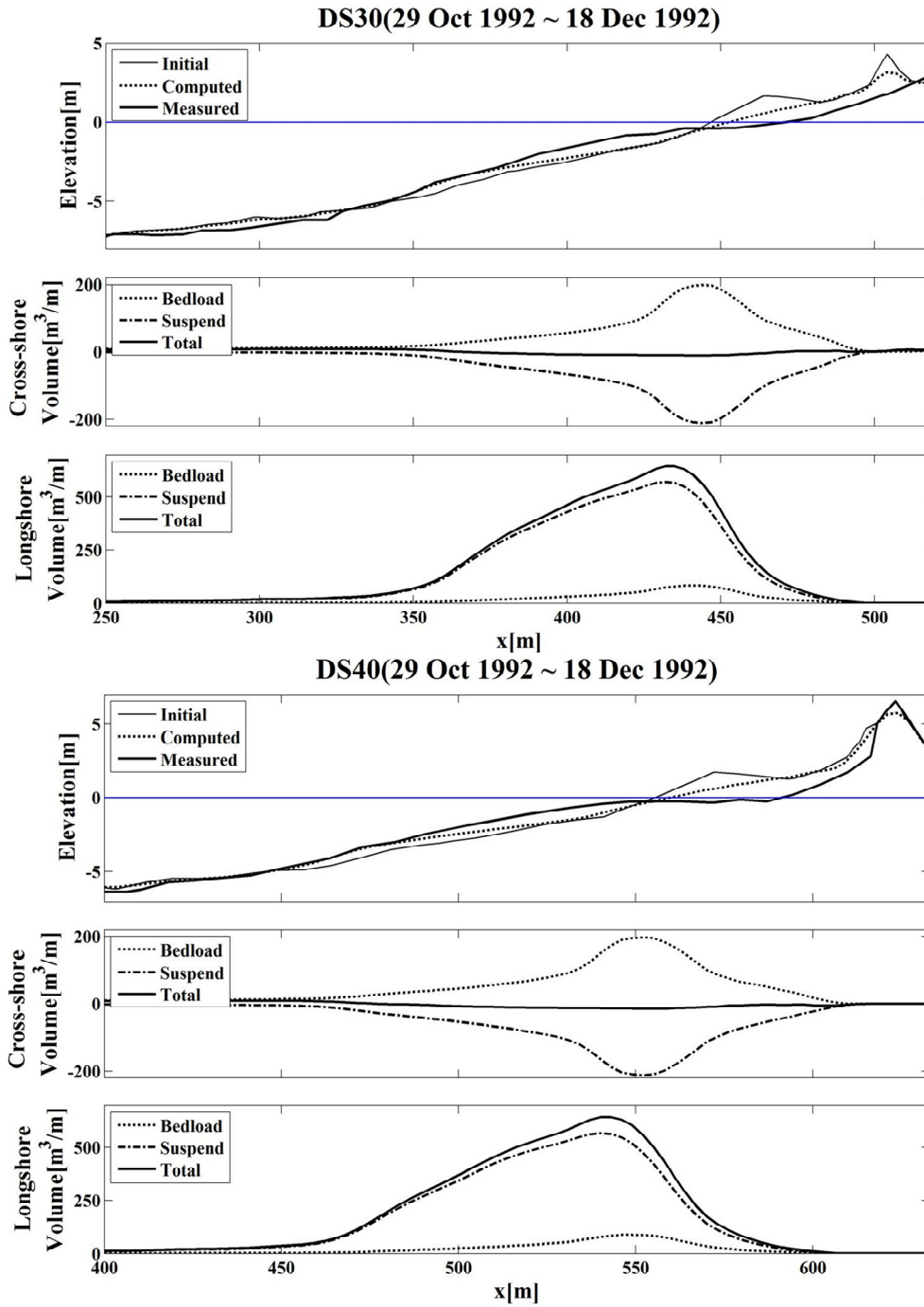


Figure 4.8 Measured and computed beach profiles (top), cumulative cross-shore (middle) and longshore (bottom) sand transport volume per unit width during erosion period for DS30 and DS40.

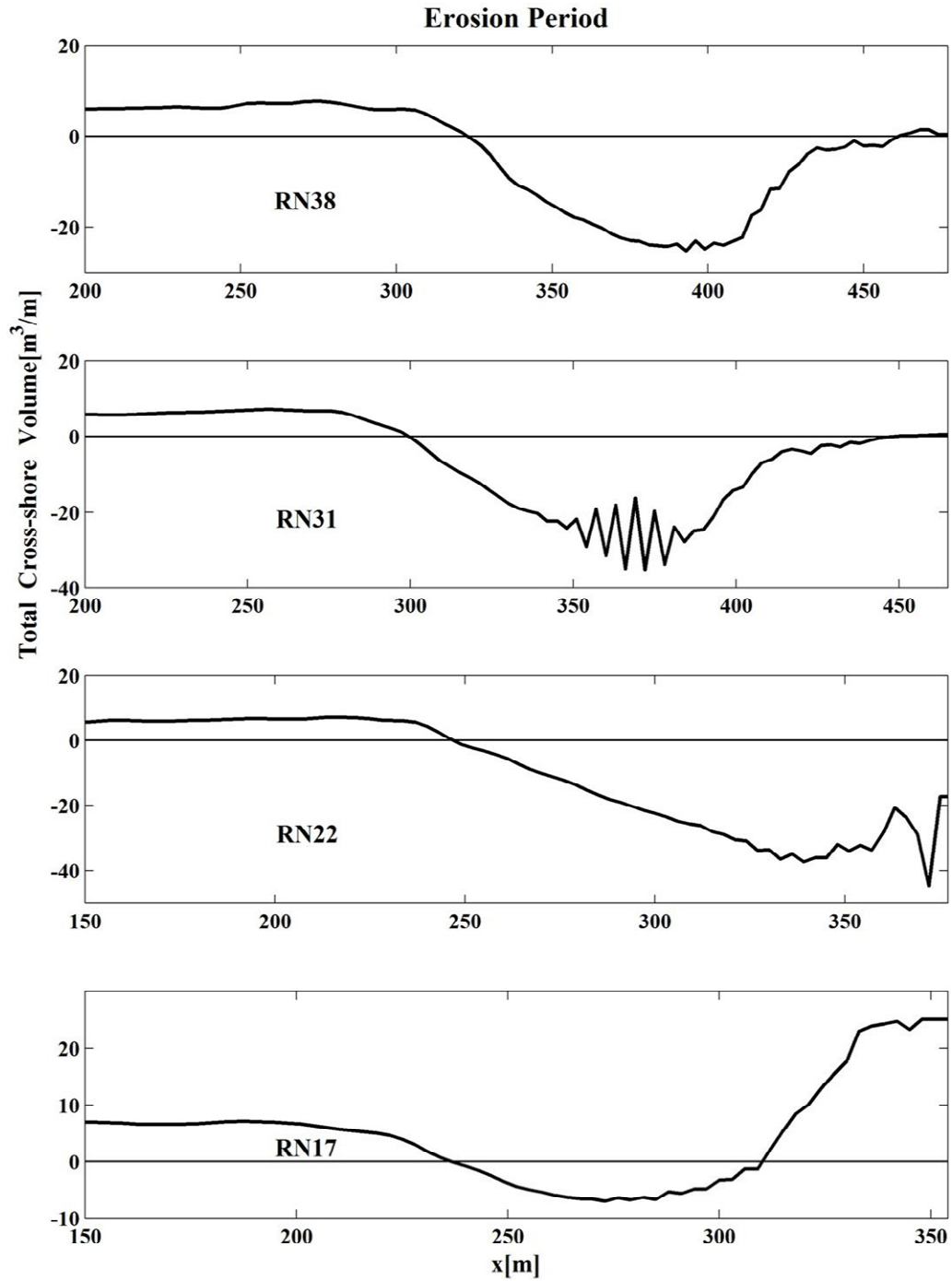


Figure 4.9 Cumulative total cross-shore sand transport volume per unit width during erosion period for RN38, RN31, RN22, and RN17.

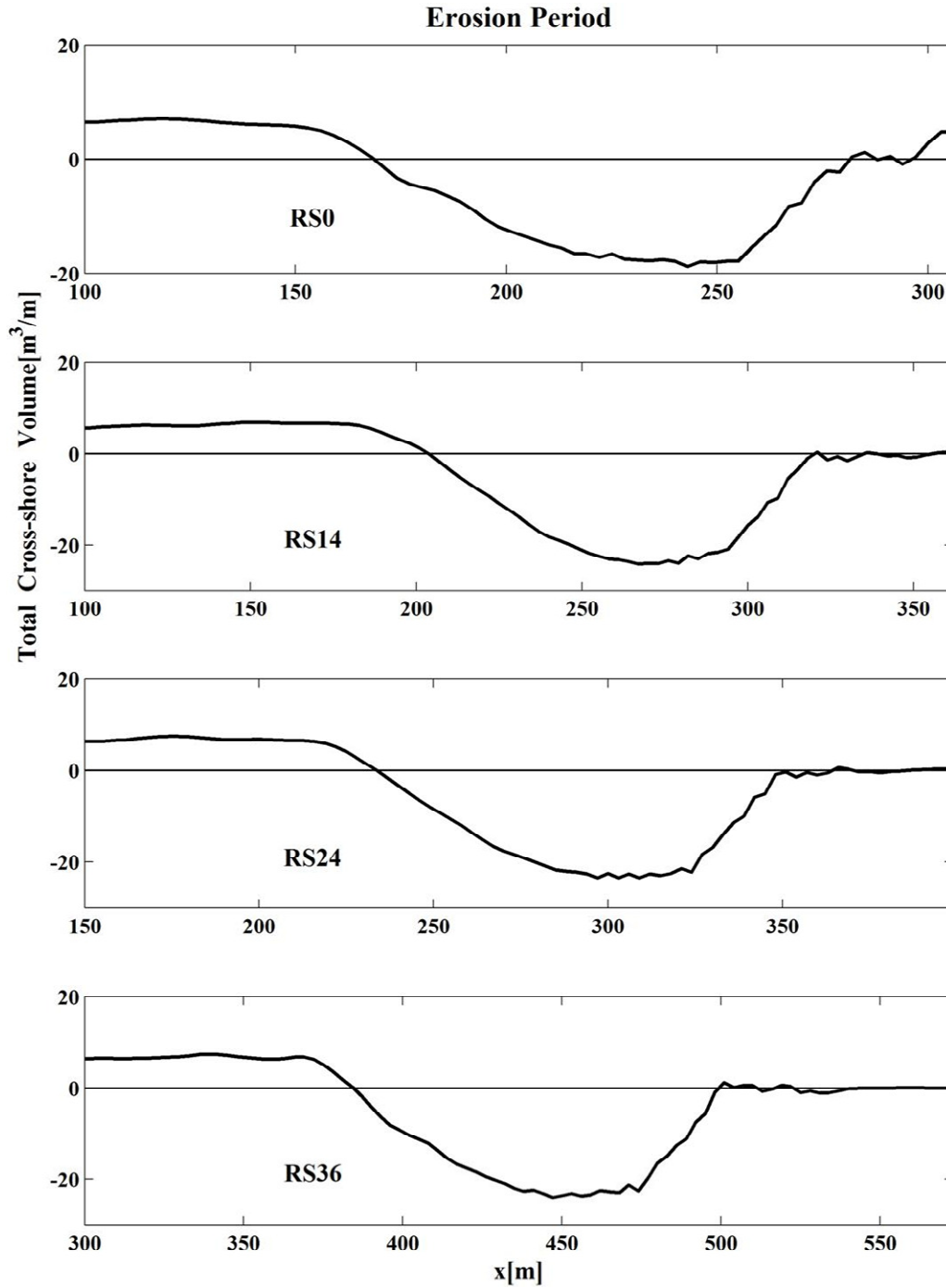


Figure 4.10 Cumulative total cross-shore sand transport volume per unit width during erosion period for RS0, RS14, RS24, and RS36.

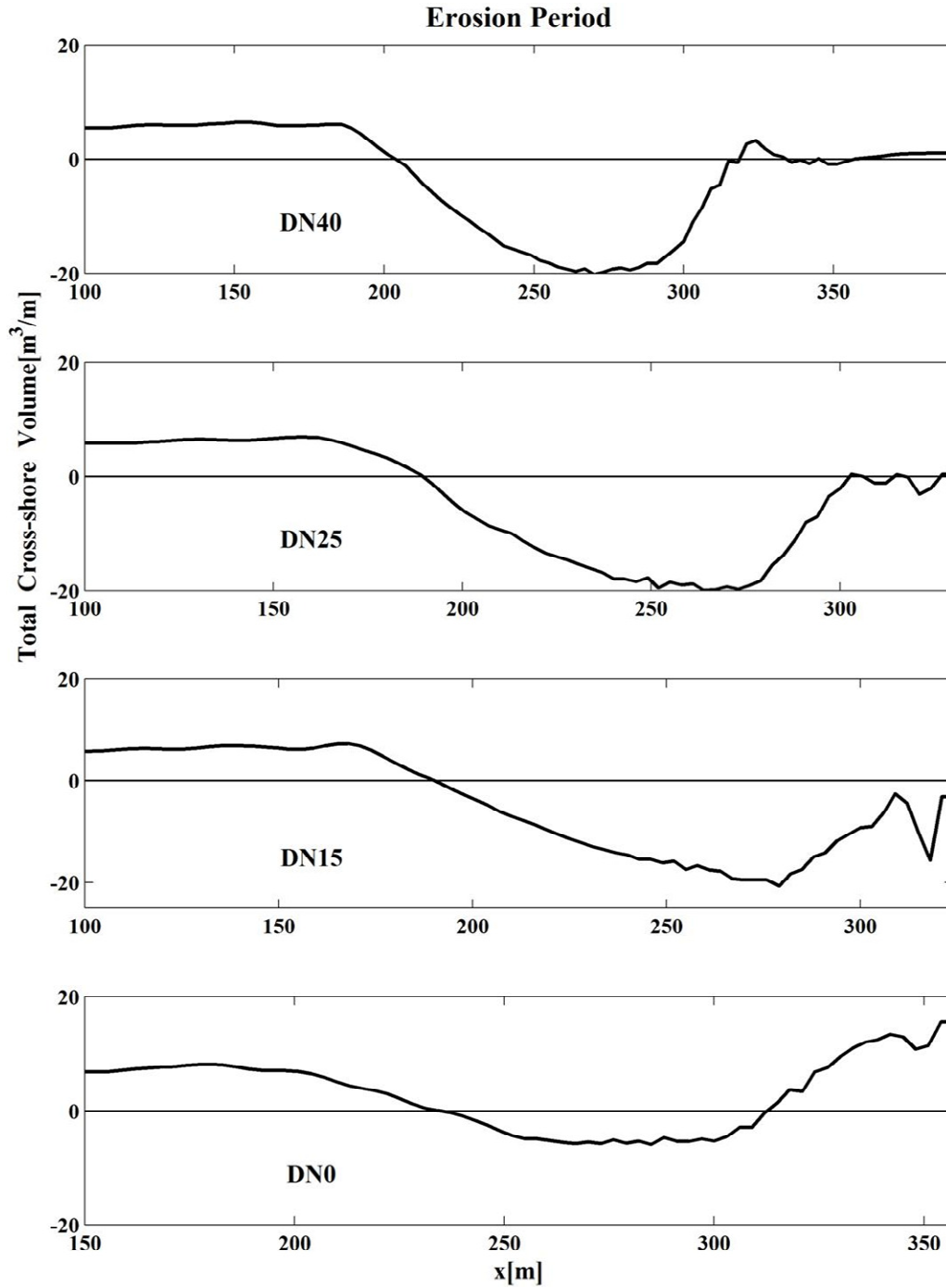


Figure 4.11 Cumulative total cross-shore sand transport volume per unit width during erosion period for DN40, DN25, DN15, and DN0.

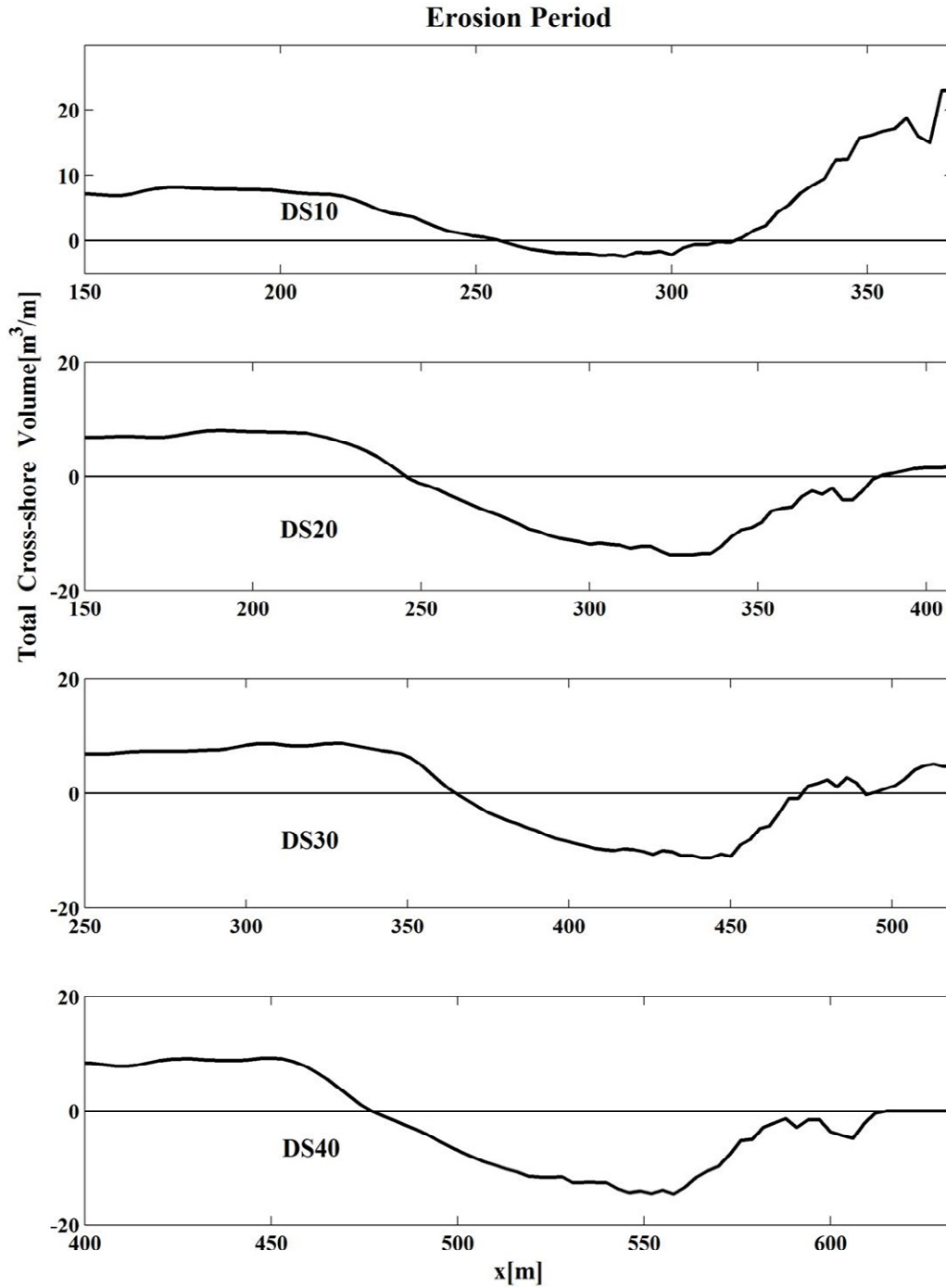


Figure 4.12 Cumulative total cross-shore sand transport volume per unit width during erosion period for DS10, DS20, DS30, and DS40.

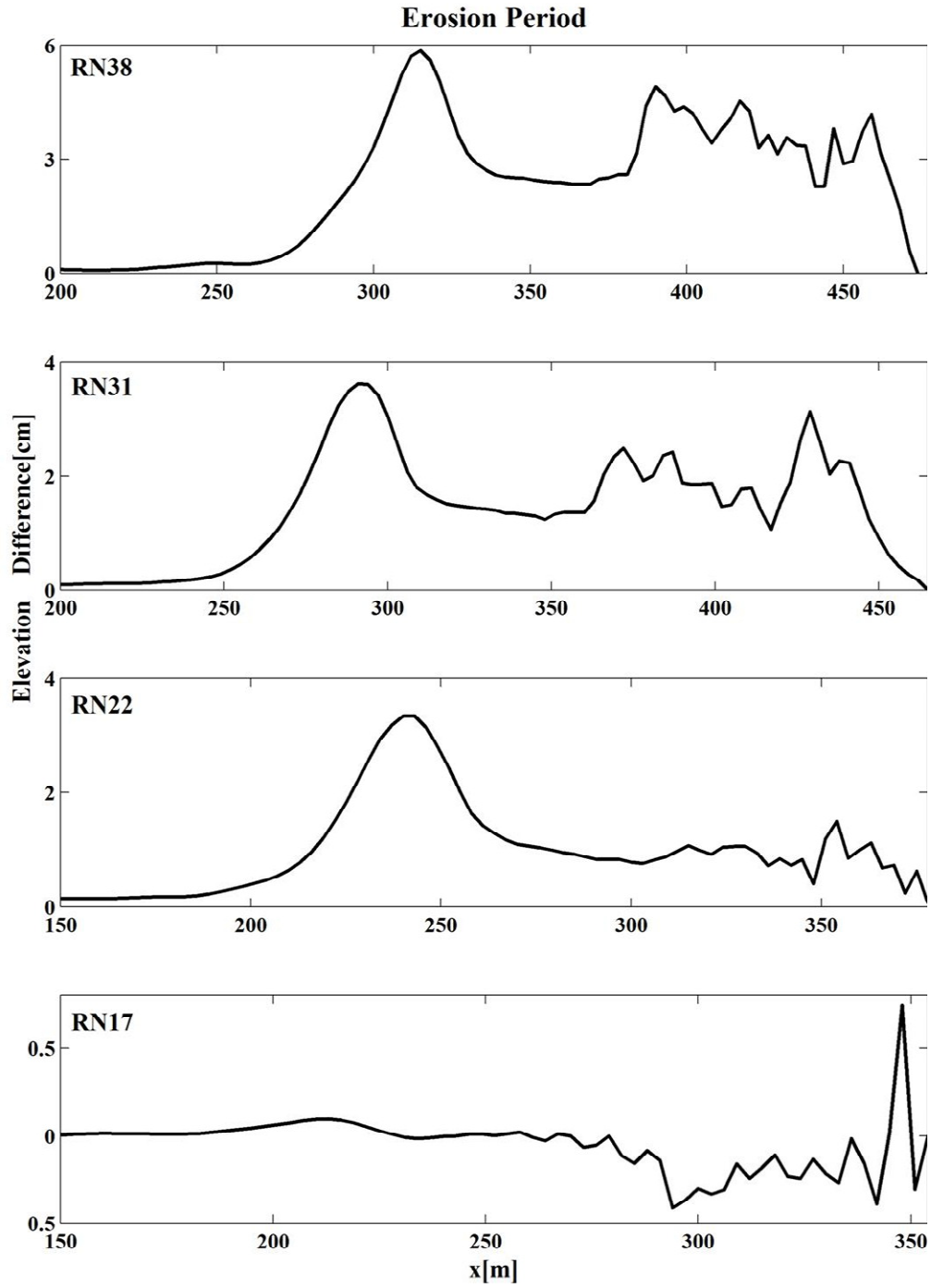


Figure 4.13 Bottom elevation difference on 18 December 1992 caused by alongshore gradient of longshore sediment transport rate for RN38, RN31, RN22, and RN17.

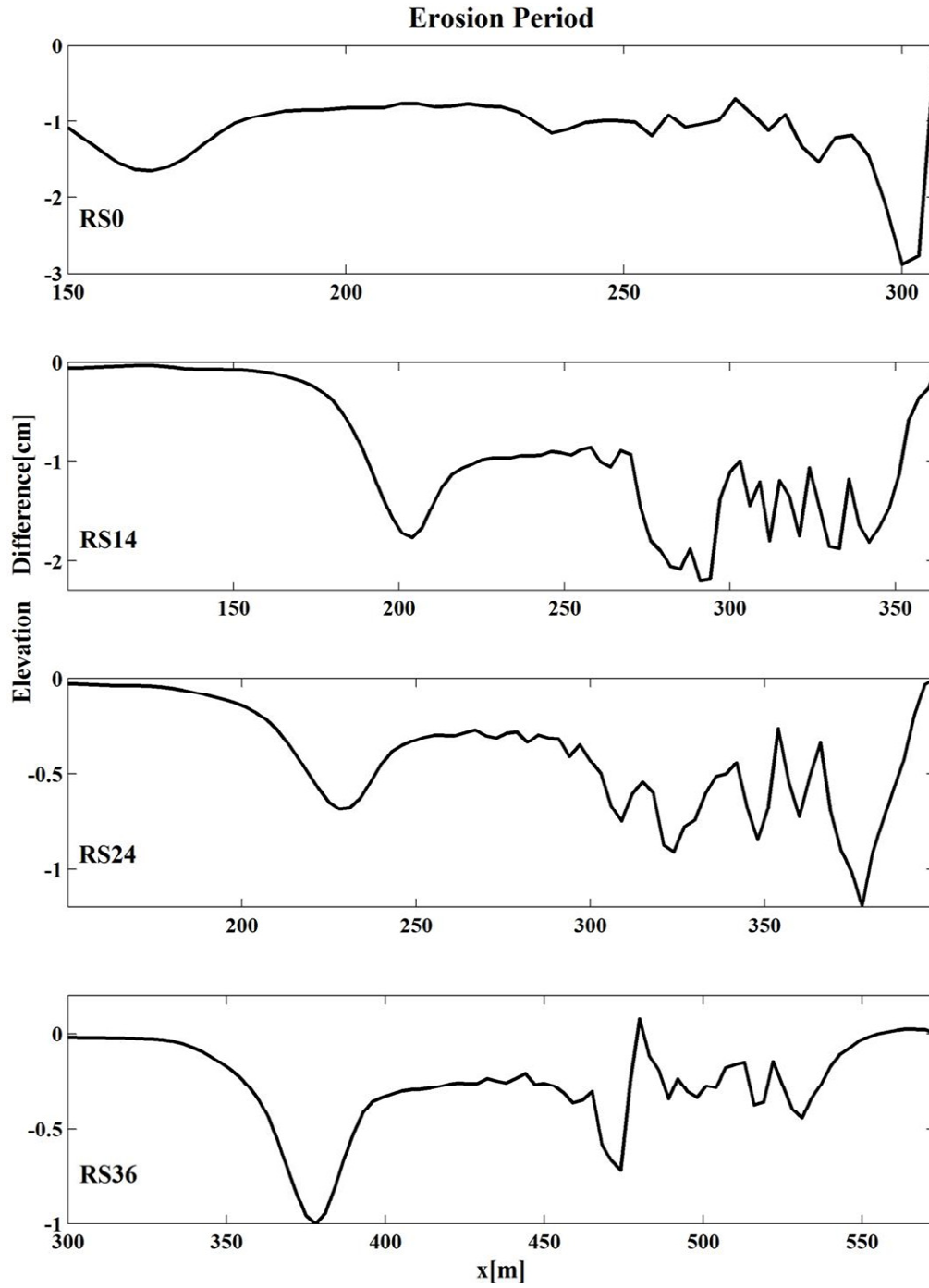


Figure 4.14 Bottom elevation difference on 18 December 1992 caused by alongshore gradient of longshore sediment transport rate for RS0, RS14, RS24, and RS36.

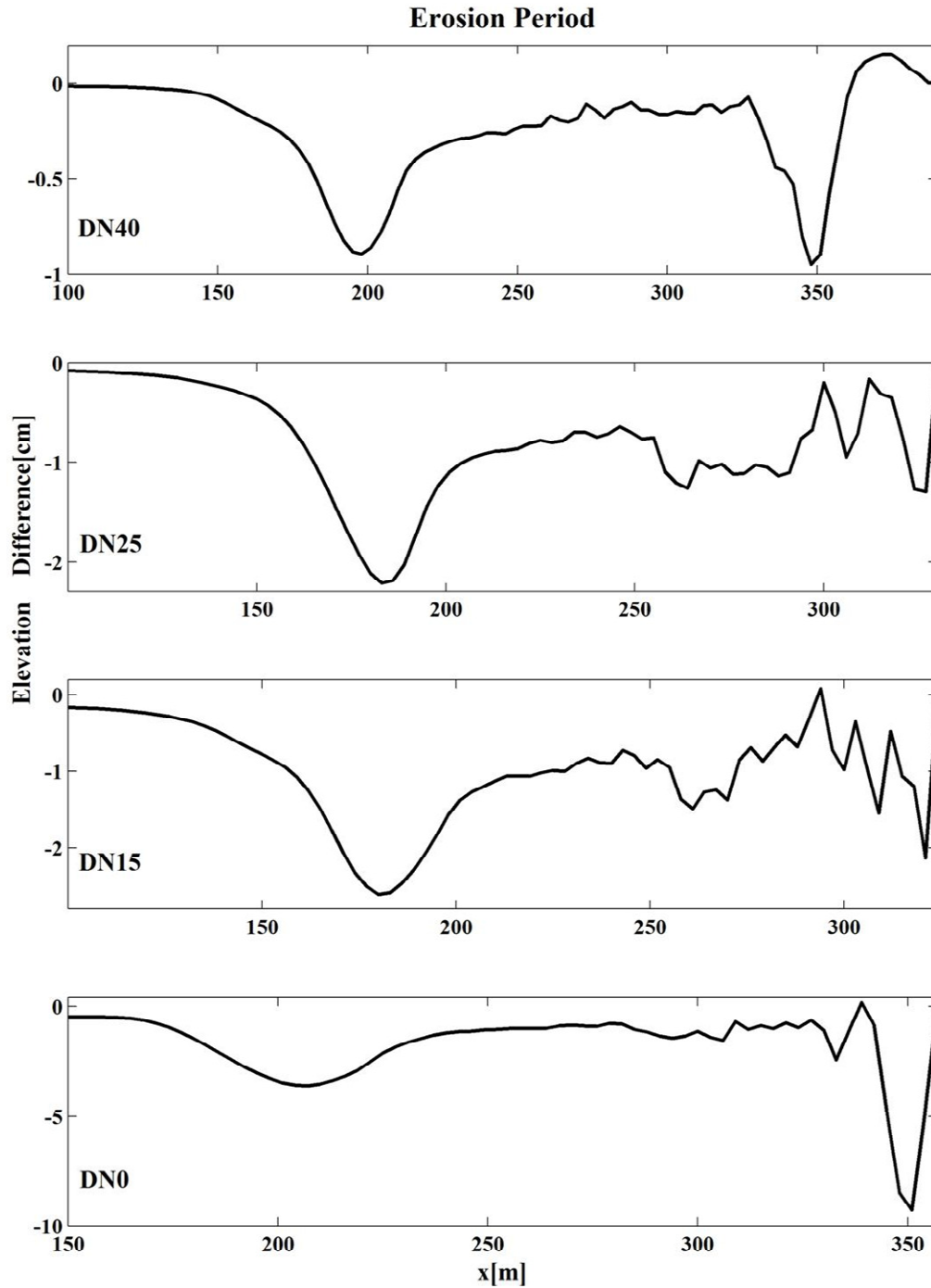


Figure 4.15 Bottom elevation difference on 18 December 1992 caused by alongshore gradient of longshore sediment transport rate for DN40, DN25, DN15, and DN0.

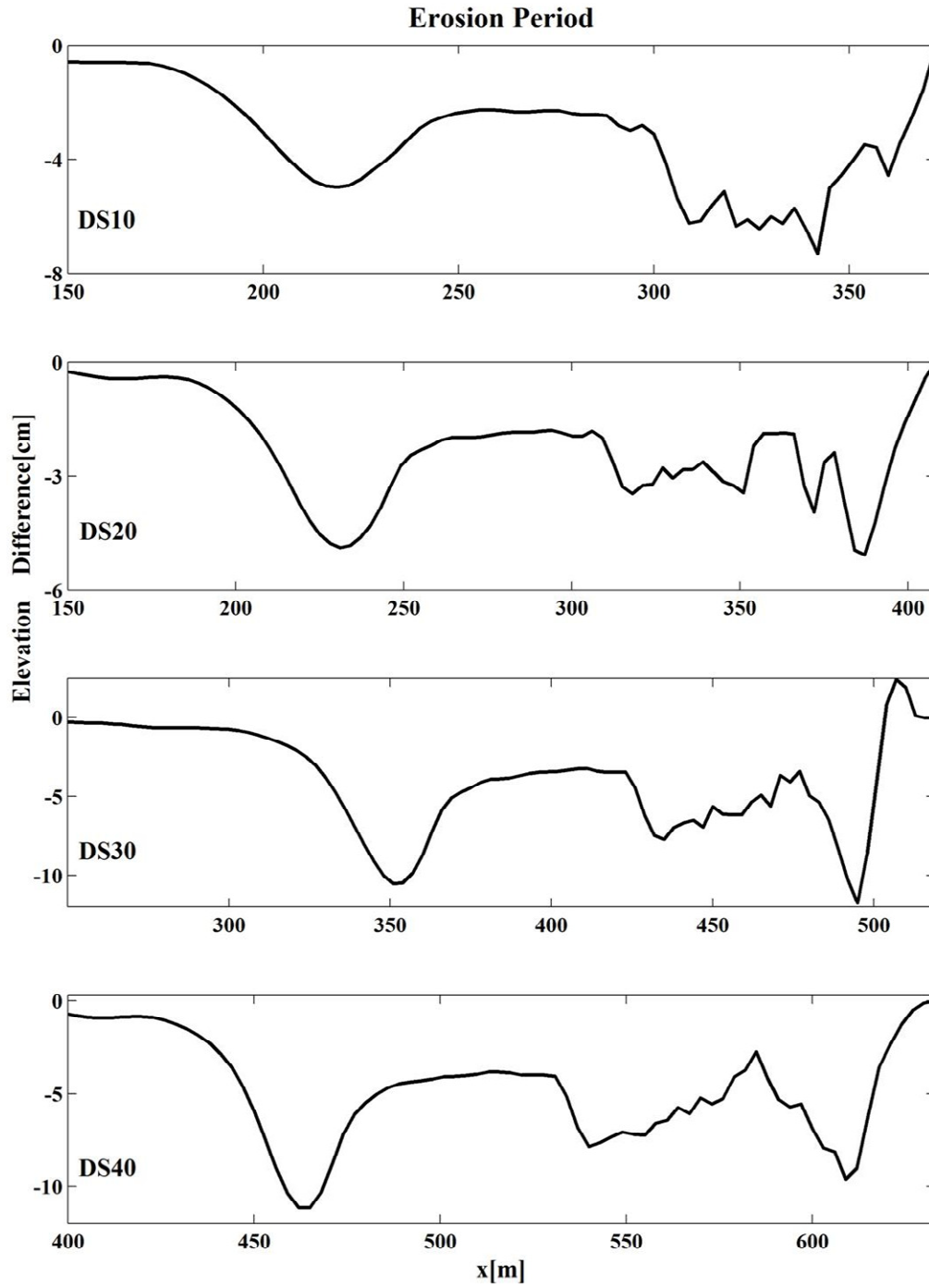


Figure 4.16 Bottom elevation difference on 18 December 1992 caused by alongshore gradient of longshore sediment transport rate for DS10, DS20, DS30, and DS40.

4.2 Accretion Period

Figures 4.17 to 4.24 show the comparison at the end of the accretion period for the 16 lines. CSHORE cannot reproduce the berm sufficiently for most of the lines but predicts the accreted profile at DS40 well. The total cross-shore sand transport volume is plotted separately in Figures 4.25 to 4.28. The effect of the alongshore gradient of the longshore sediment transport is quantified by computing the elevation difference in the same way as in Figures 4.13 to 4.16. The computed elevation difference is less than 5 cm and small for the accretion period as shown in Figures 4.29 to 4.32. The dune at DS0 and DS10 (dune overwash zone) on 27 July 1993 may be related to the emergency nourishment of 4,400 m³ in July 1993 (Garriga and Dalrymple 2002) which is not included in the computed profile for lack of the fill placement information. Assuming the placement of 4,400 m³ between DN0 and DS10 with the alongshore distance of 305 m, the placement volume per unit length is 14 m³/m which is small in comparison to the accretion volume per unit length of 86 and 70 m³/m at DN0 and DS10, respectively, as listed in Table 2.3. It is also noted that wind-blown sediment transport (e.g., U.S. Army Engineer Research and Development Center 2002) may not be negligible for the accretion period of 220.8 days.

The cumulative cross-shore bed load and suspended load in the middle panel of each of Figures 4.17 to 4.24 are larger than those in Figures 4.1 to 4.8 for the erosion period of 50.8 days. The cumulative cross-shore total load appears to be almost zero in these figures but Figures 4.25 to 4.28 show that the total load is positive (onshore) and the maximum near MSL even at DS0 and DS10. The magnitude of the onshore total load in Figures 4.25 to 4.28 is similar to the magnitude of the offshore total load in Figures 4.9 to 4.12. This explains the recovery of the eroded profile. On the other hand, the cumulative longshore bed load, suspended load and total load in

the bottom panel in Figures 4.17 to 4.24 are similar in their magnitudes to those in Figures 4.1 to 4.8 for the erosion period but the cross-shore extent is narrower for the accretion period with smaller wave heights as indicated in Table 2.1.

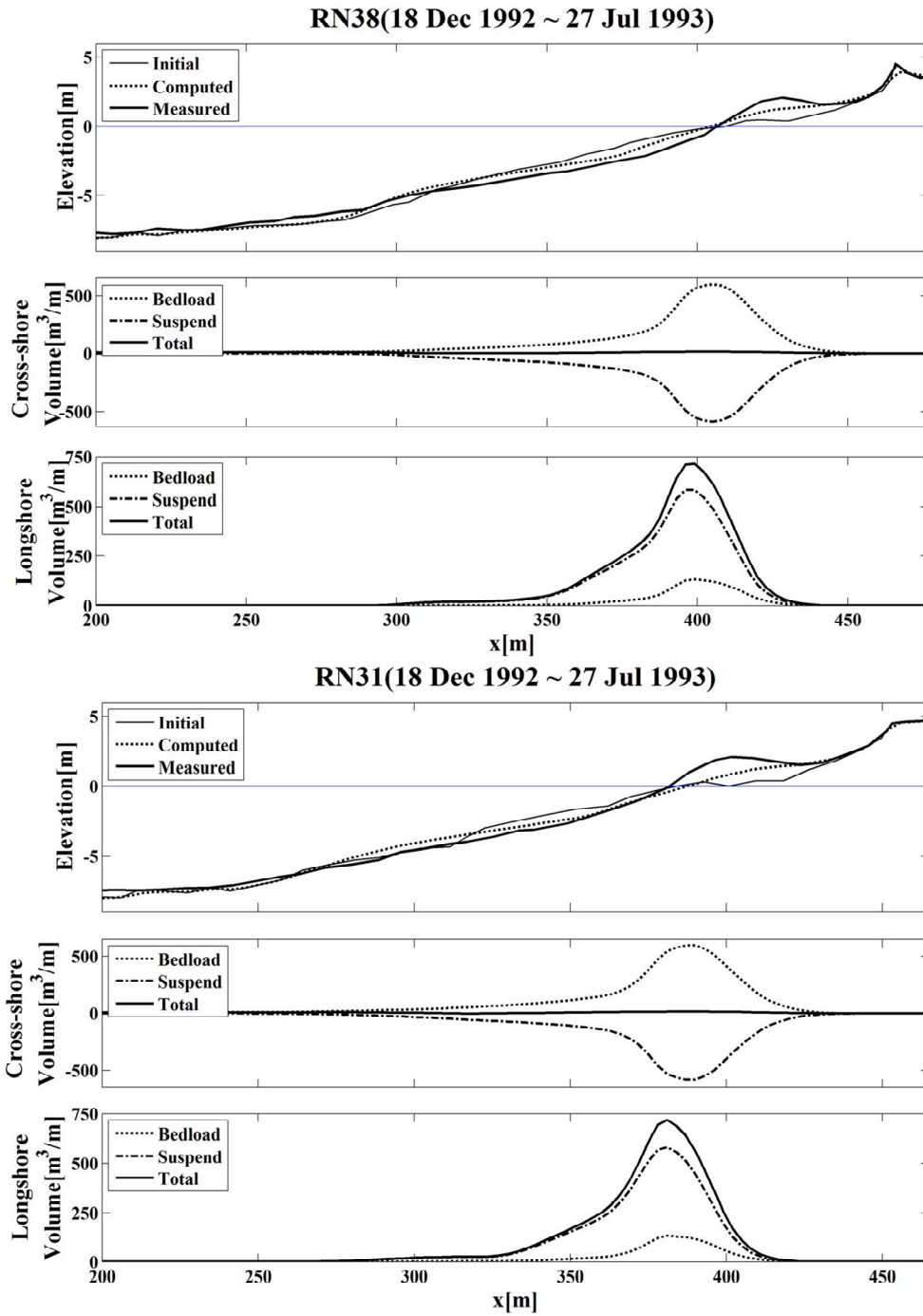


Figure 4.17 Measured and computed beach profiles (top), cumulative cross-shore (middle) and longshore (bottom) sand transport volume per unit width during accretion period for RN38 and RN31.

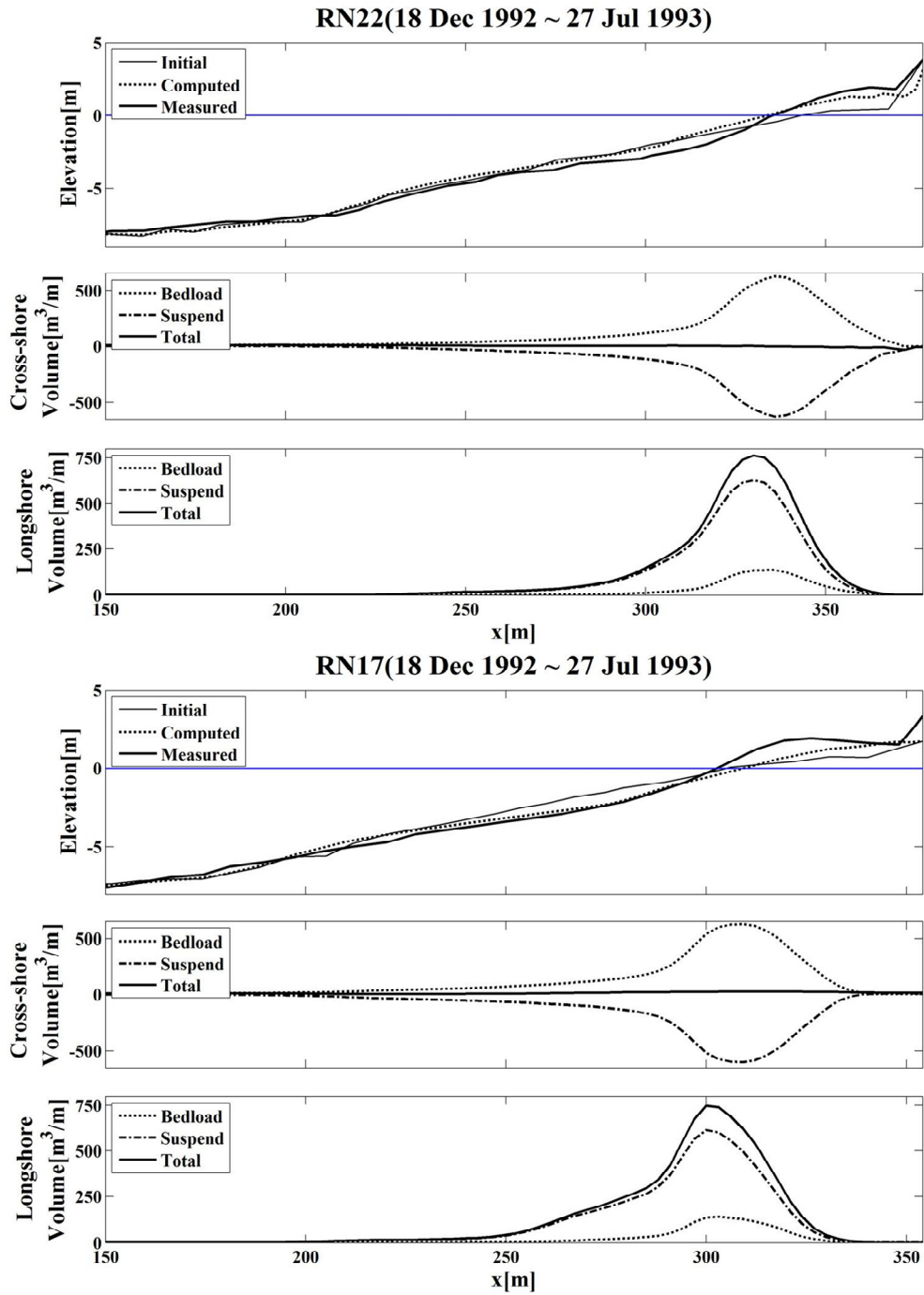


Figure 4.18 Measured and computed beach profiles (top), cumulative cross-shore (middle) and longshore (bottom) sand transport volume per unit width during accretion period for RN22 and RN17.

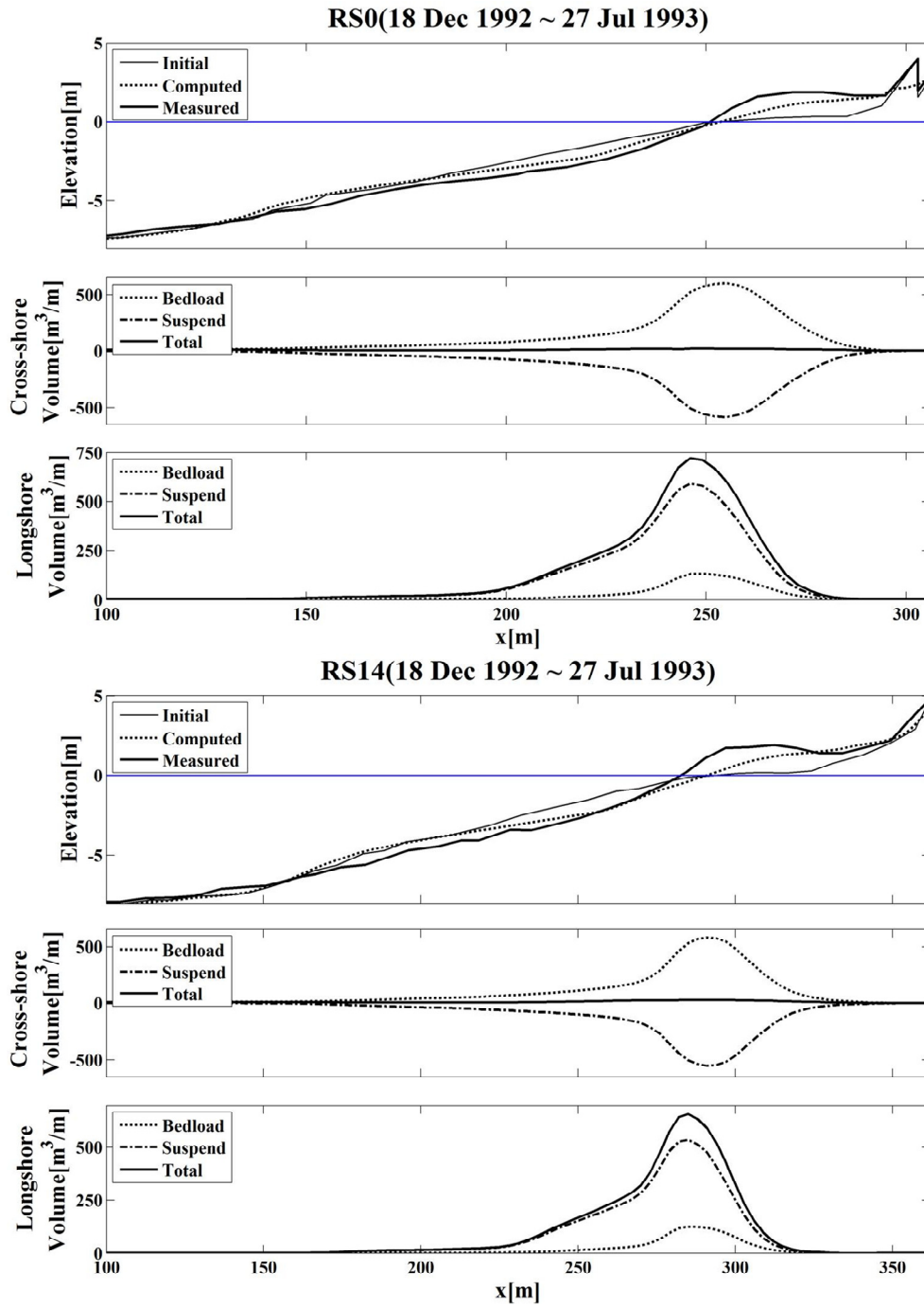


Figure 4.19 Measured and computed beach profiles (top), cumulative cross-shore (middle) and longshore (bottom) sand transport volume per unit width during accretion period for RS0 and RS14.

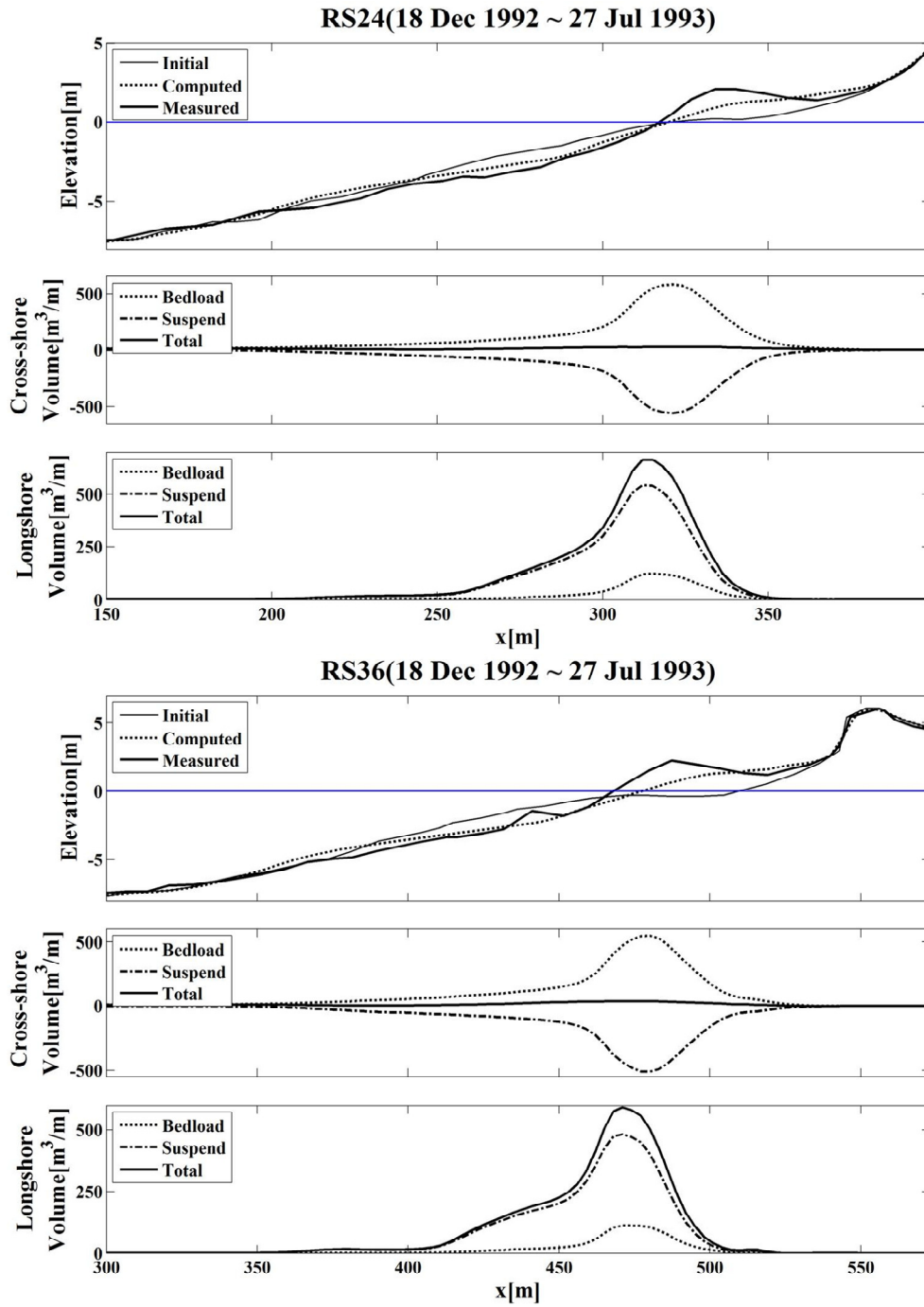


Figure 4.20 Measured and computed beach profiles (top), cumulative cross-shore (middle) and longshore (bottom) sand transport volume per unit width during accretion period for RS24 and RS36.

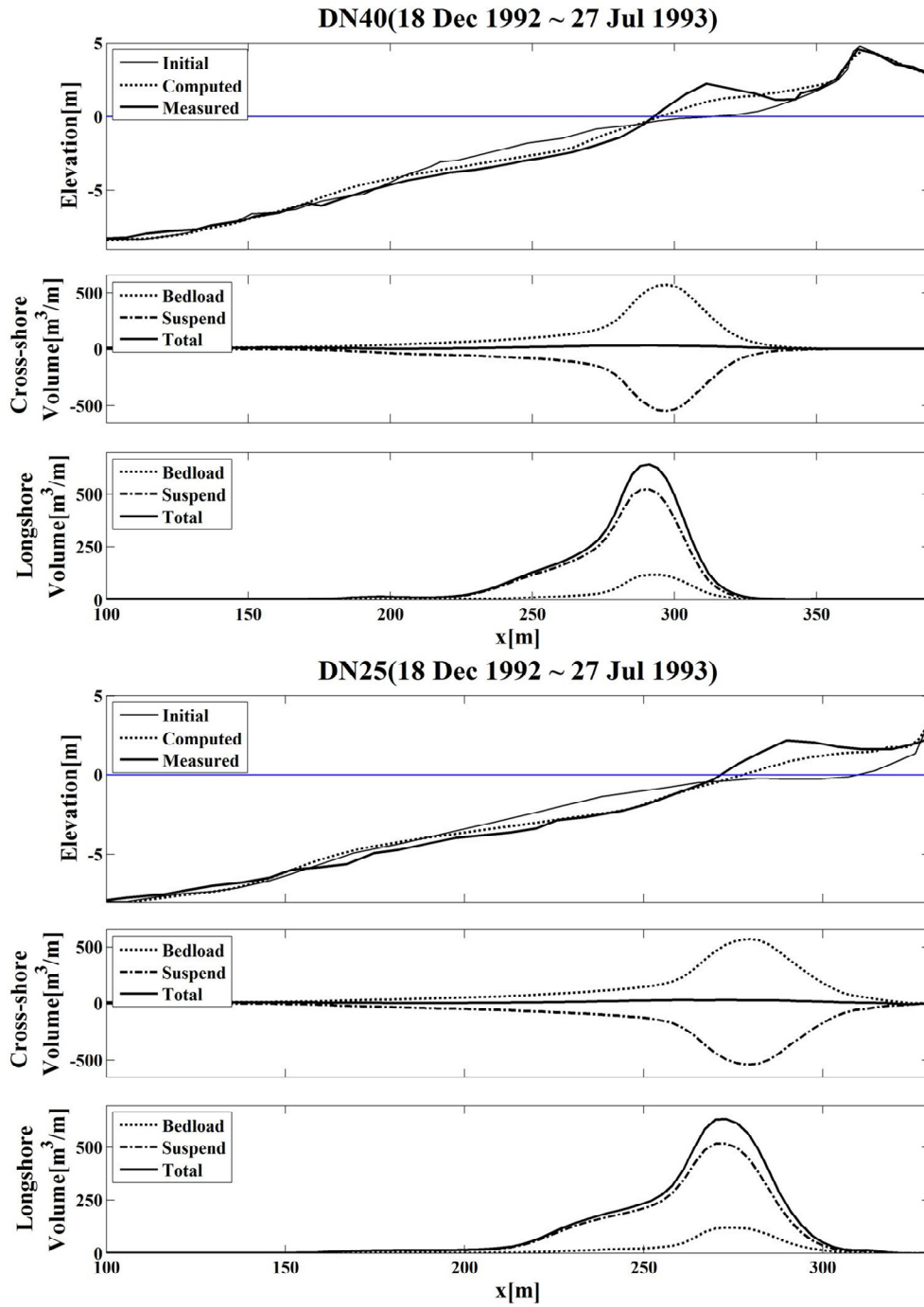


Figure 4.21 Measured and computed beach profiles (top), cumulative cross-shore (middle) and longshore (bottom) sand transport volume per unit width during accretion period for DN40 and DN25.

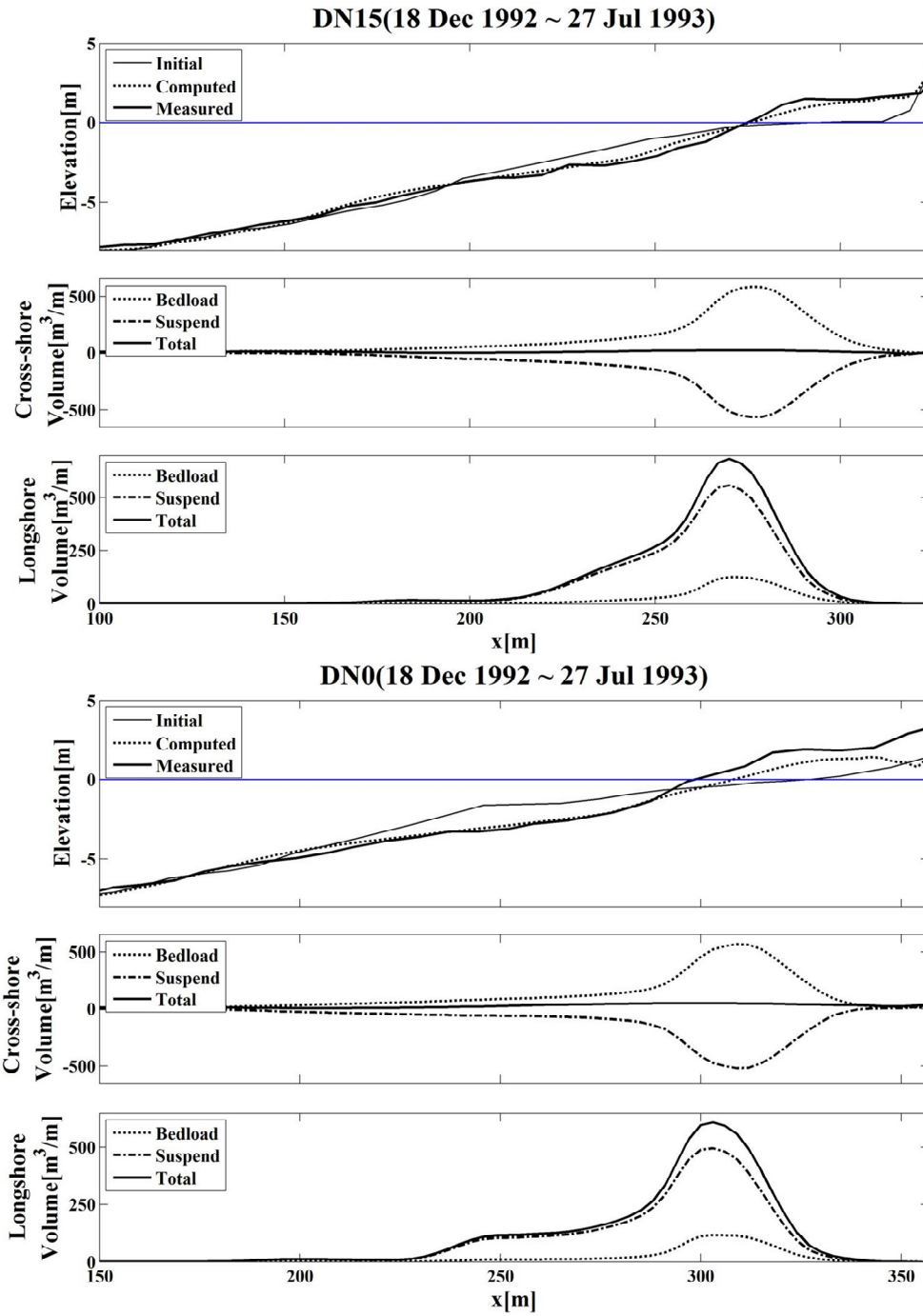


Figure 4.22 Measured and computed beach profiles (top), cumulative cross-shore (middle) and longshore (bottom) sand transport volume per unit width during accretion period for DN15 and DN0.

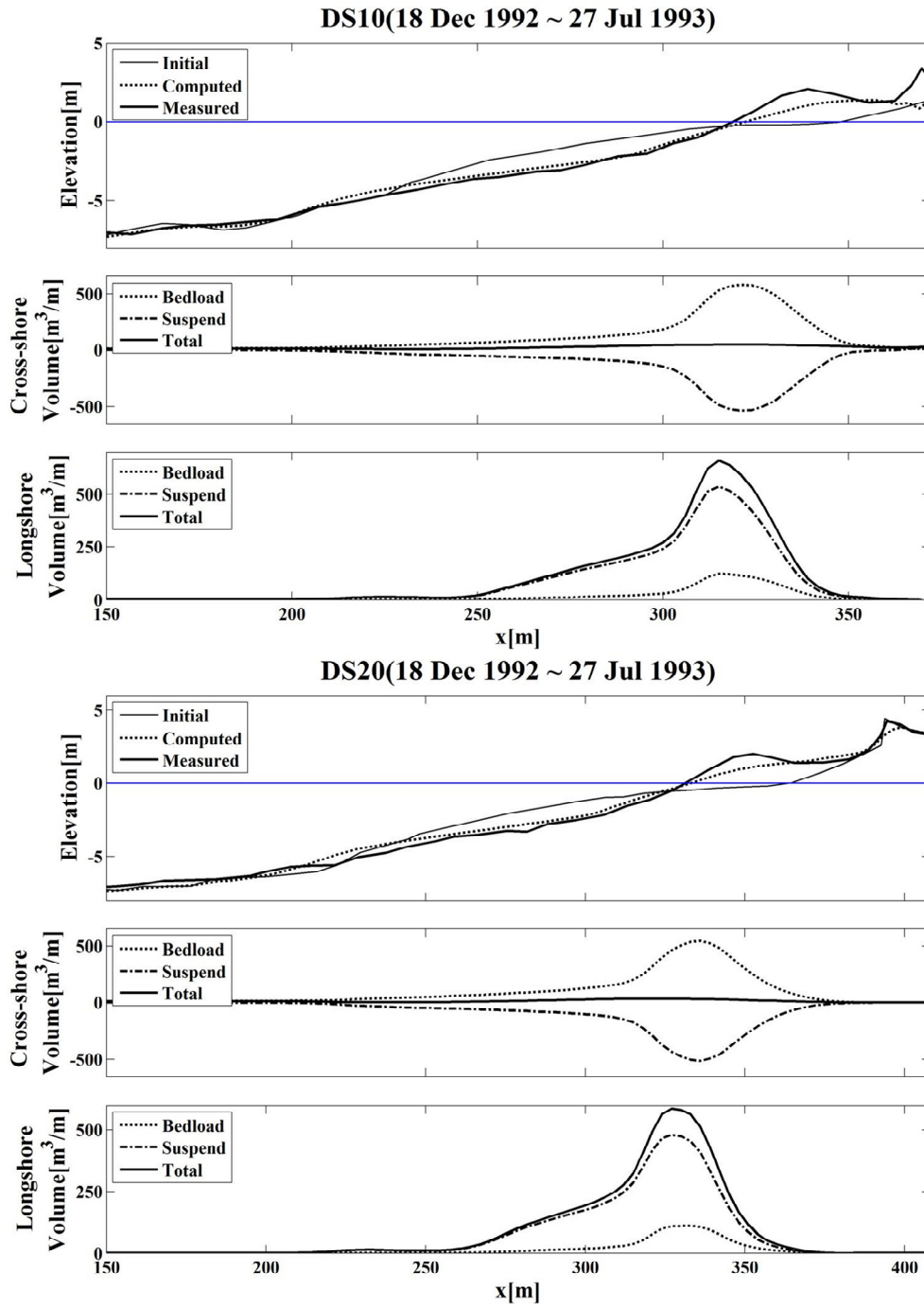


Figure 4.23 Measured and computed beach profiles (top), cumulative cross-shore (middle) and longshore (bottom) sand transport volume per unit width during accretion period for DS10 and DS20.

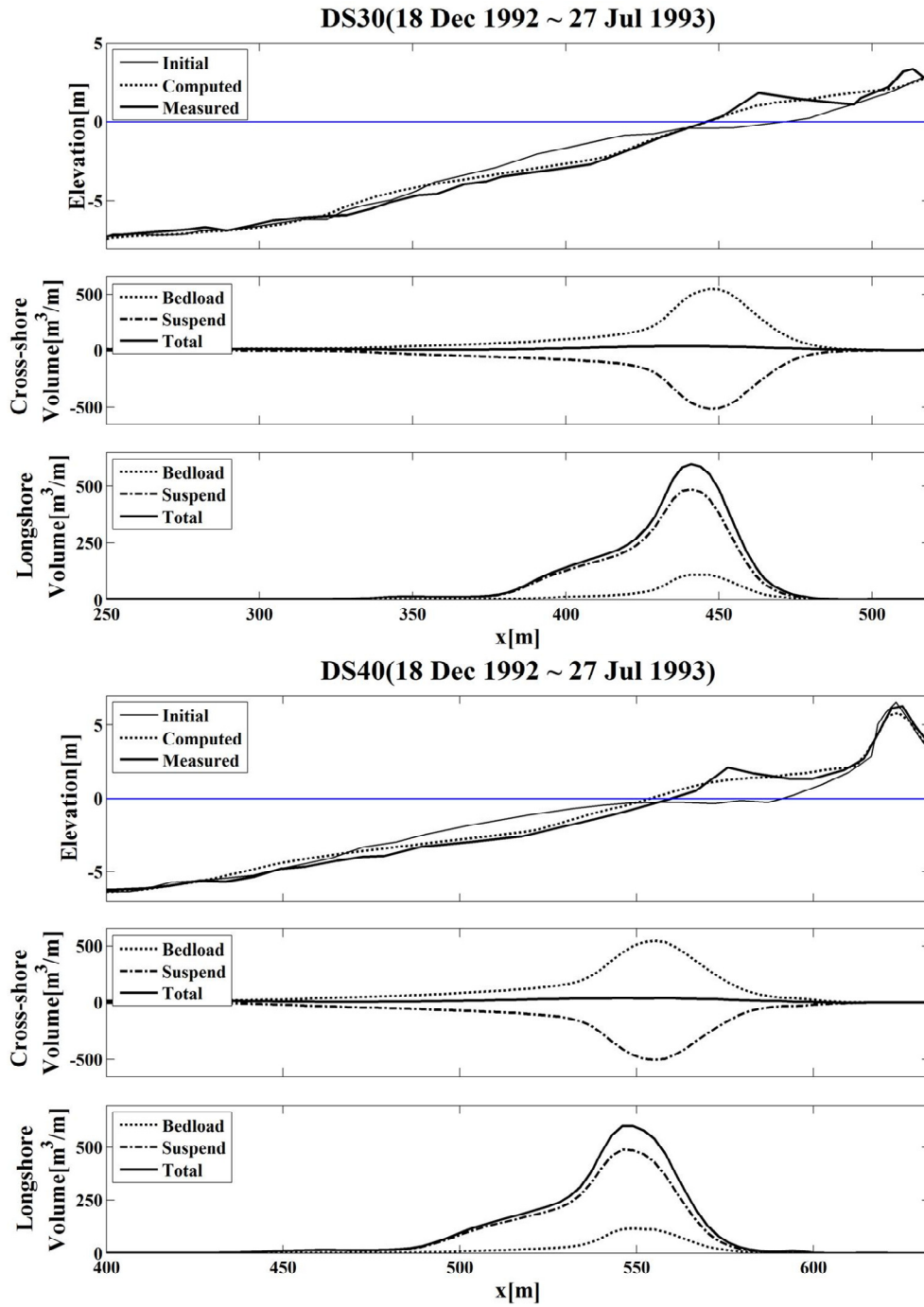


Figure 4.24 Measured and computed beach profiles (top), cumulative cross-shore (middle) and longshore (bottom) sand transport volume per unit width during accretion period for DS30 and DS40.

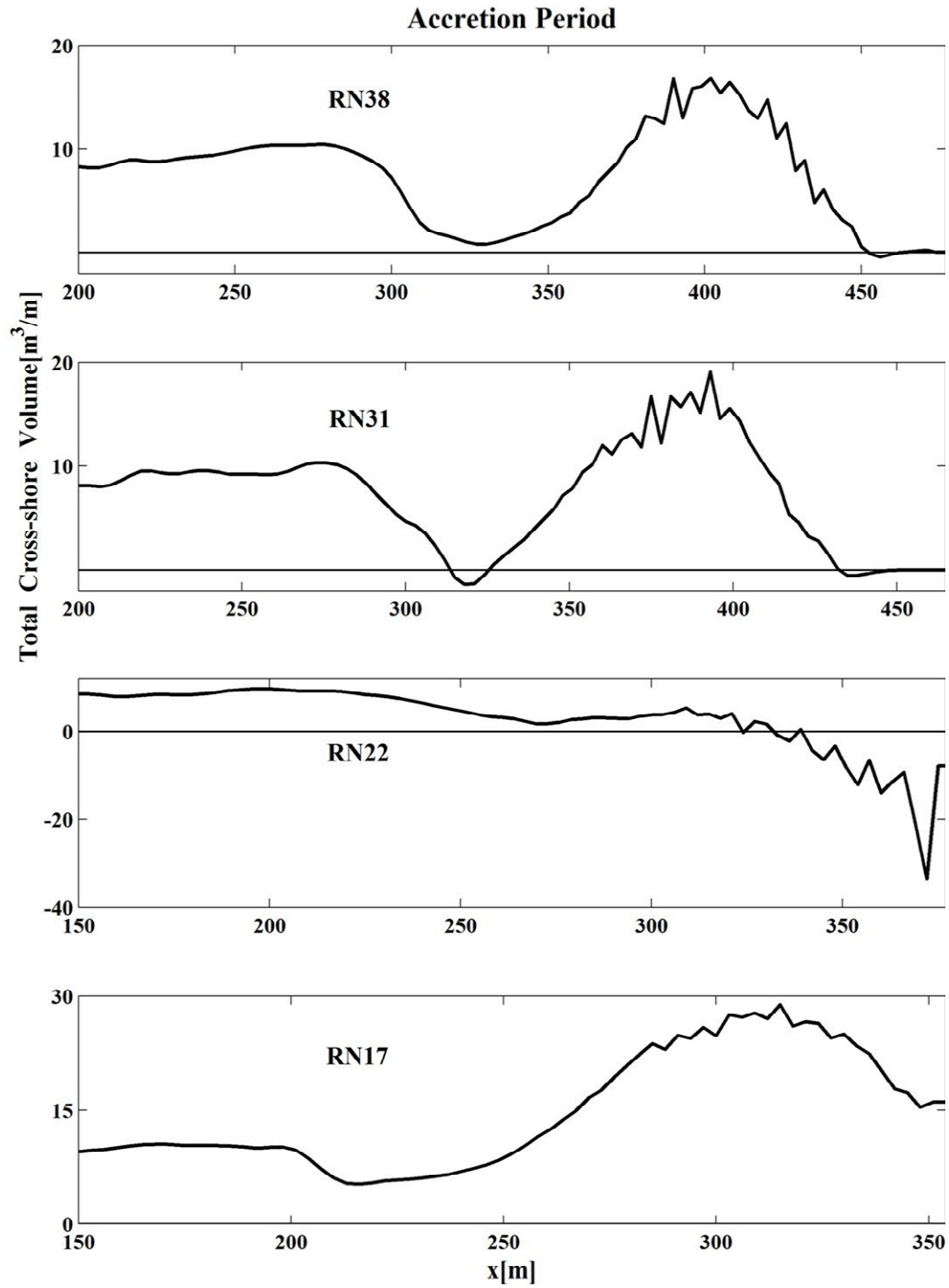


Figure 4.25 Cumulative total cross-shore sand transport volume per unit width during accretion period for RN38, RN31, RN22, and RN17.

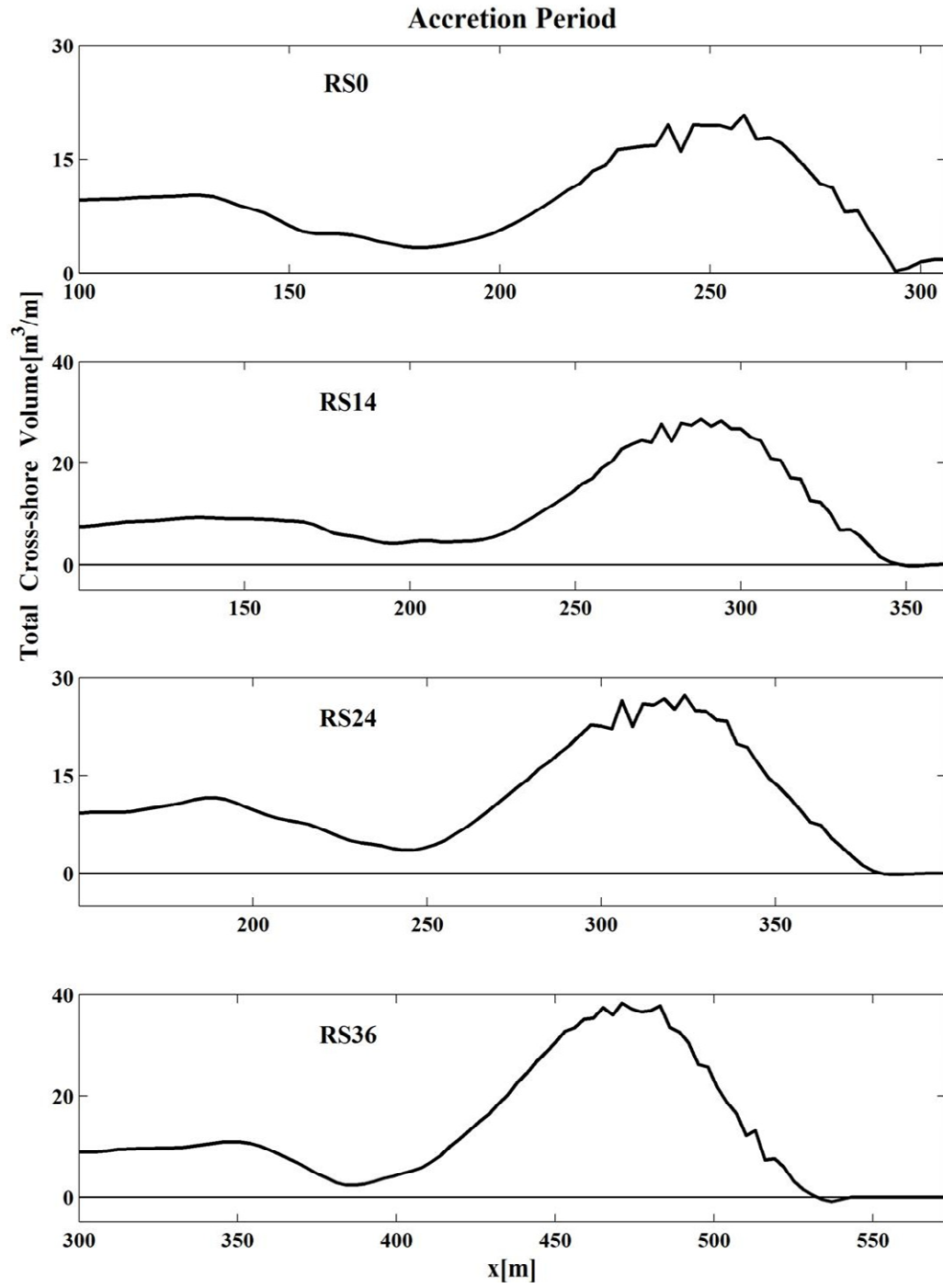


Figure 4.26 Cumulative total cross-shore sand transport volume per unit width during accretion period for RS0, RS14, RS24, and RS36.

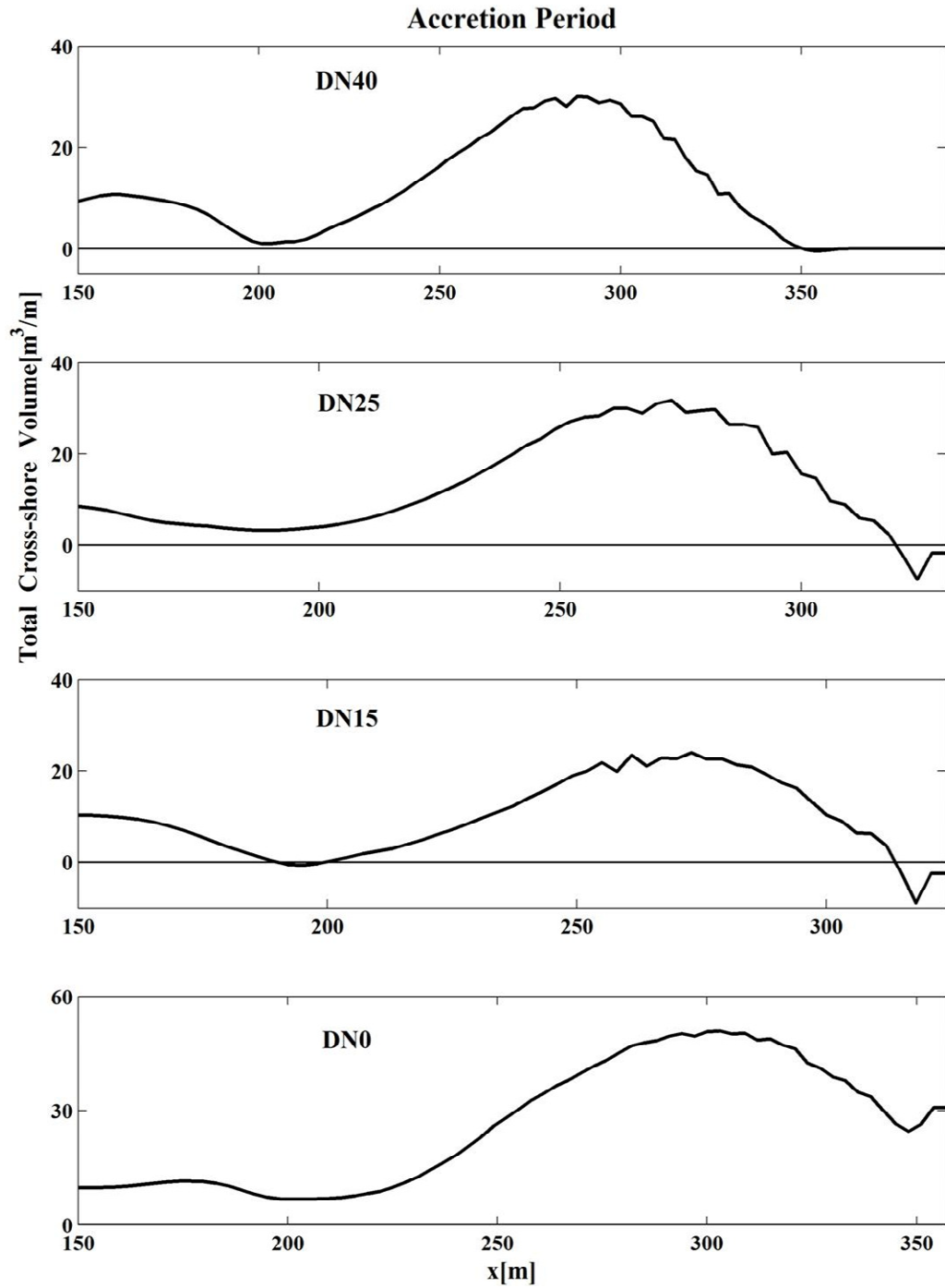


Figure 4.27 Cumulative total cross-shore sand transport volume per unit width during accretion period for DN40, DN25, DN15, and DN0.

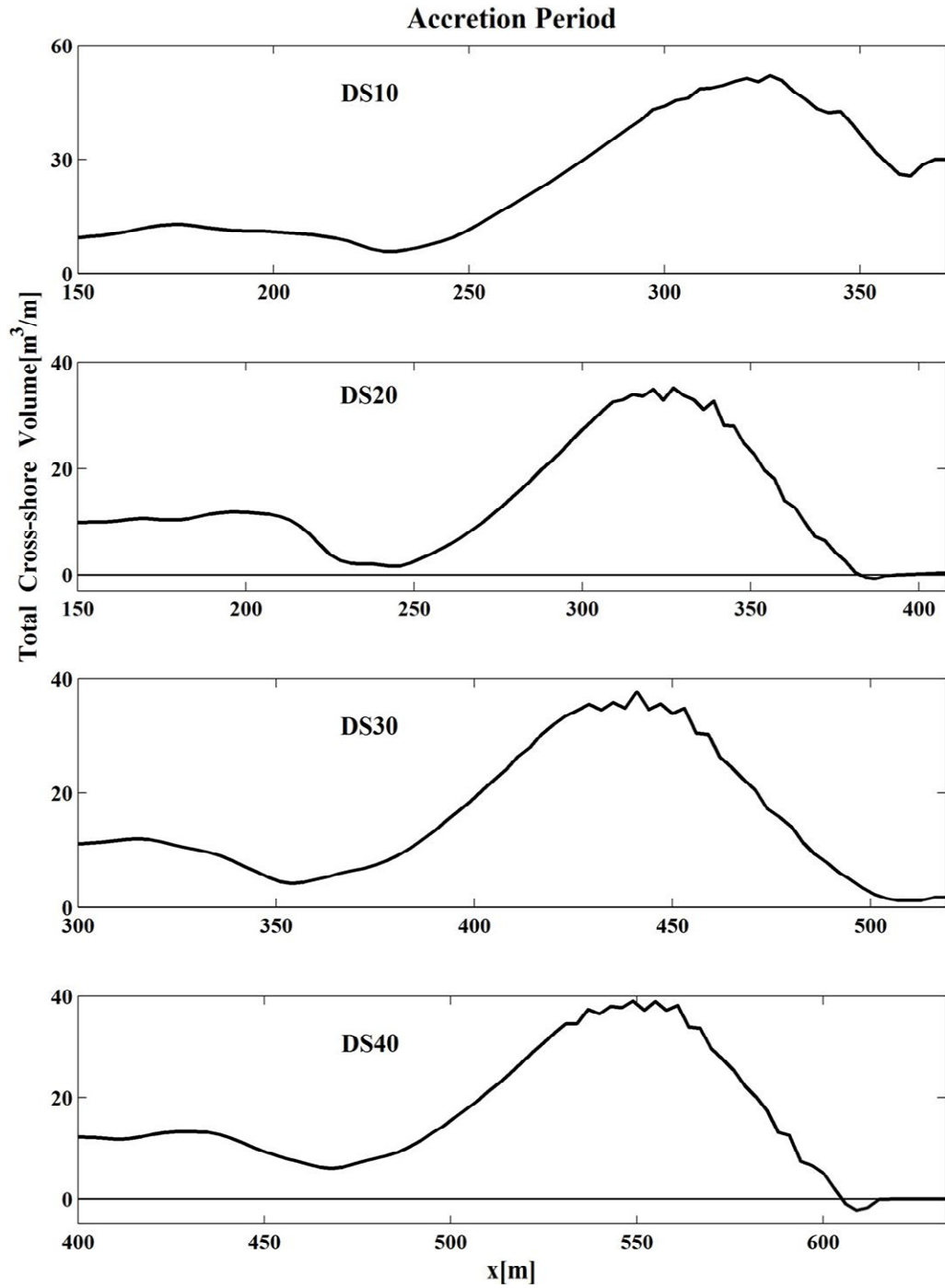


Figure 4.28 Cumulative total cross-shore sand transport volume per unit width during accretion period for DS10, DS20, DS30, and DS40.

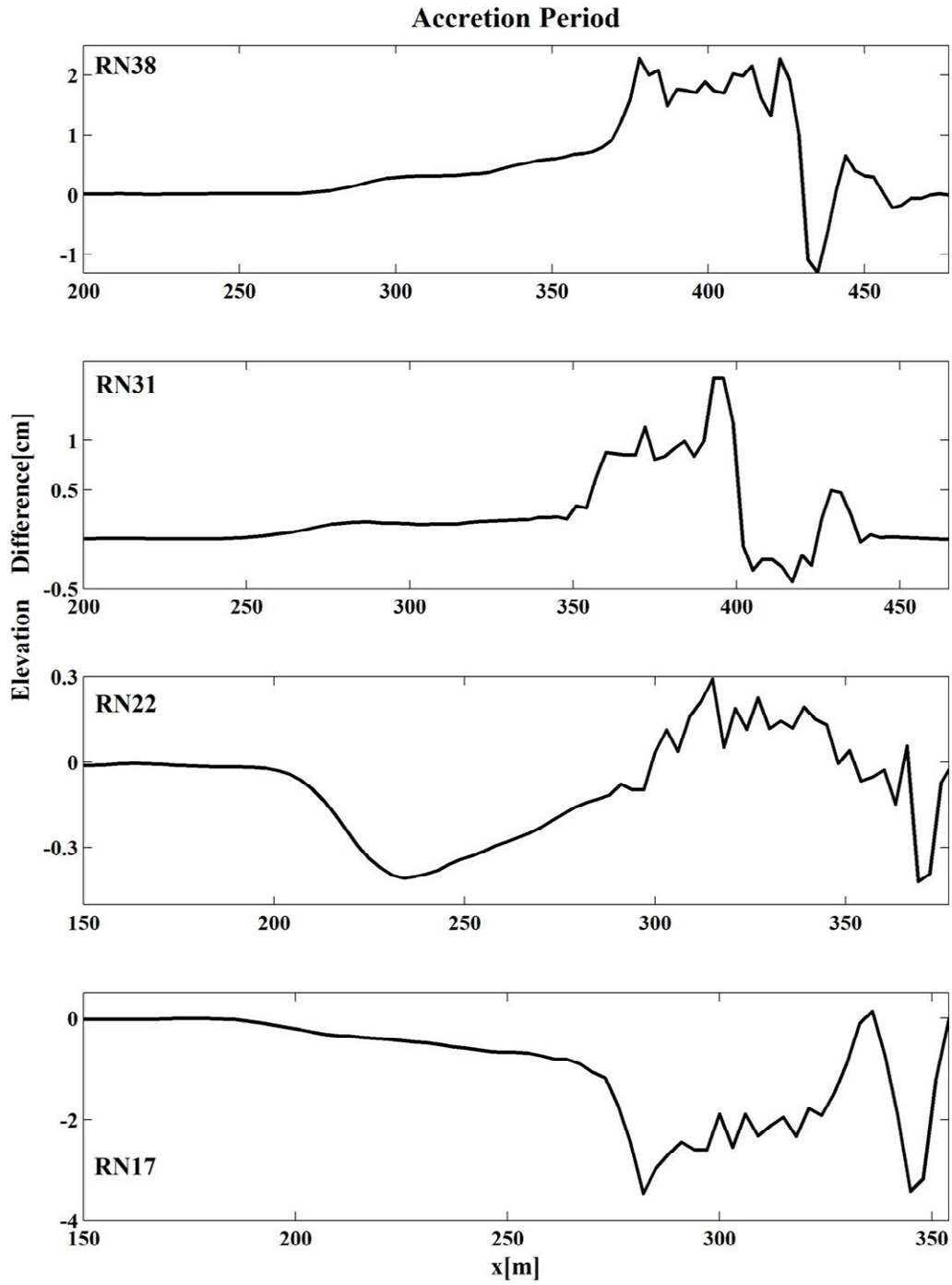


Figure 4.29 Bottom elevation difference on 27 July 1993 caused by alongshore gradient of longshore sediment transport rate for RN38, RN31, RN22, and RN17.

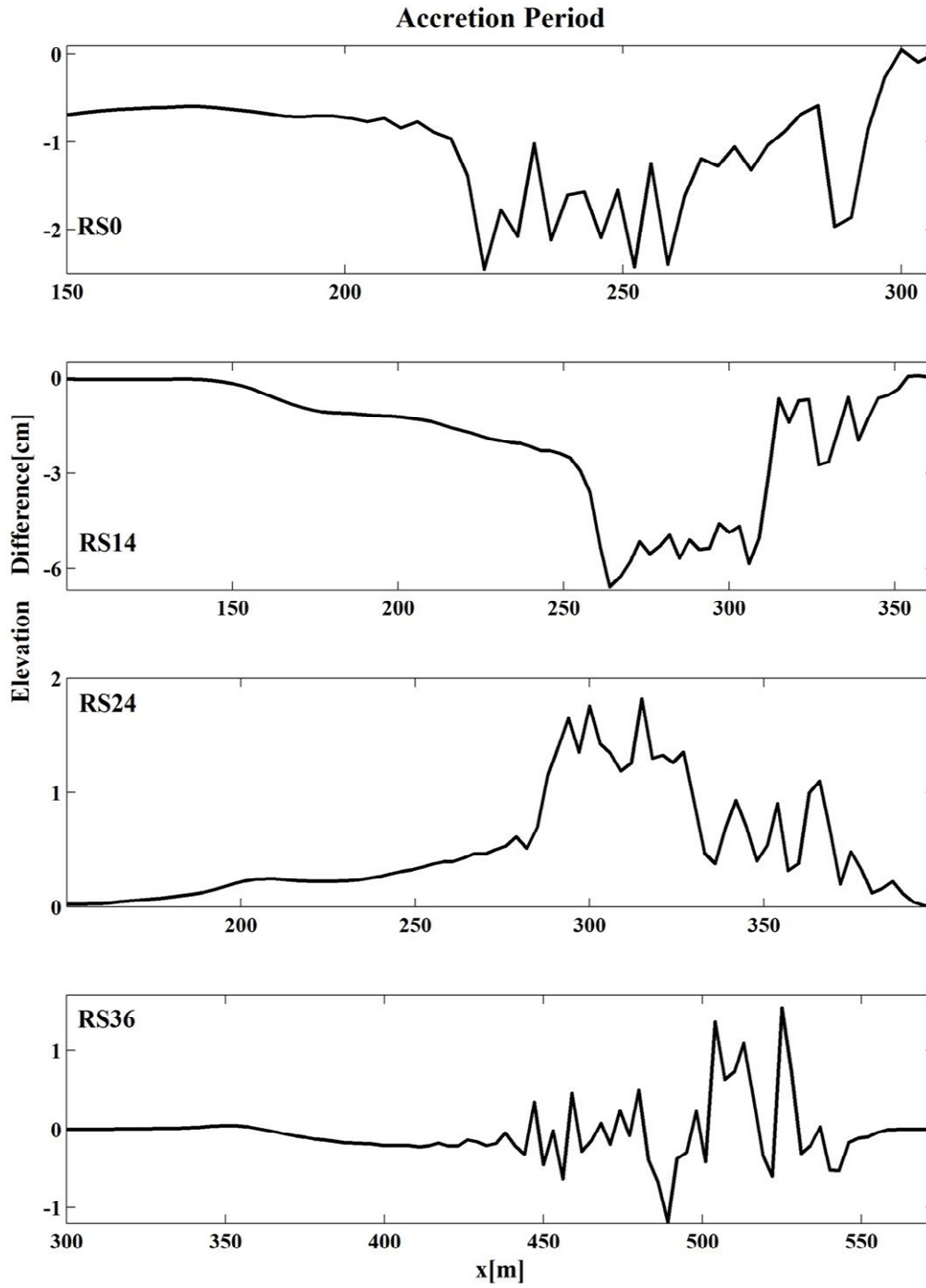


Figure 4.30 Bottom elevation difference on 27 July 1993 caused by alongshore gradient of longshore sediment transport rate for RS0, RS14, RS24, and RS36.

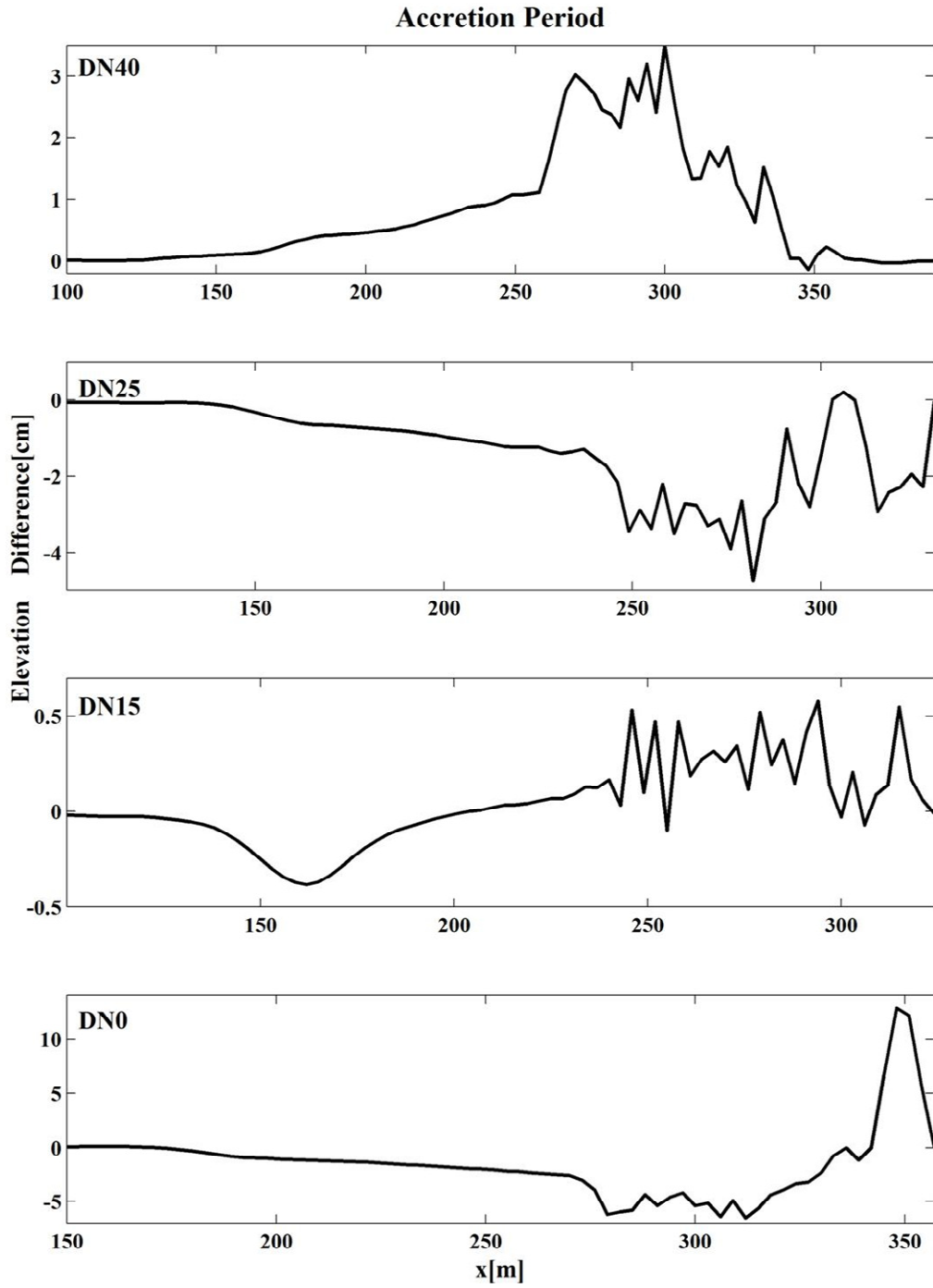


Figure 4.31 Bottom elevation difference on 27 July 1993 caused by alongshore gradient of longshore sediment transport rate for DN40, DN25, DN15, and DN0.

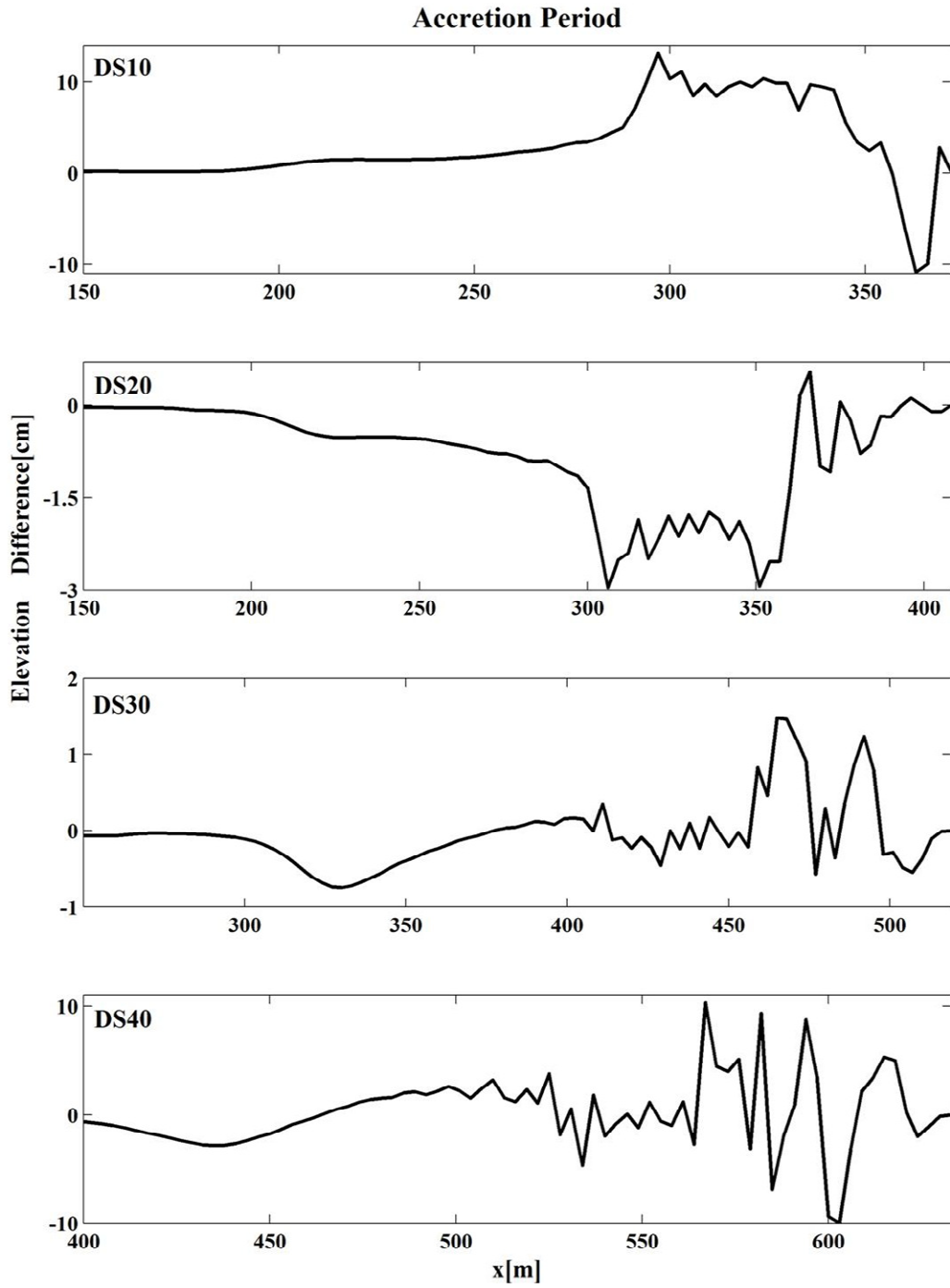


Figure 4.32 Bottom elevation difference on 27 July 1993 caused by alongshore gradient of longshore sediment transport rate for DS10, DS20, DS30, and DS40.

4.3 Sensitivity to Bed Load Parameter B

The computed results shown in Figures 4.1 to 4.32 are based on the bed load parameter $b = B (0.5 + Q)$ with $B = 0.002$. The onshore bed load transport rate is proportional to the value of B specified as input to CSHORE. Figures 4.1 to 4.8 for the 16 lines indicate that $B = 0.002$ does not produce sufficient erosion above MSL. The computed results with $B = 0.001$ are shown in Figures 4.33 to 4.40. The reduction of B by the factor of 2 reproduces the eroded profile above MSL but the offshore deposition is overpredicted. The cumulative cross-shore and longshore bed load transport volumes per unit width are reduced by the factor of about 2 but the corresponding suspended load volumes are reduced as well. This is because the modified bed load changes the beach profile which affects the computed hydrodynamics and the offshore transport of suspended sediment by undertow current. The hydrodynamics, sediment dynamics and beach profile changes are closely interconnected for the beach profile evolution. Figures 4.41 to 4.44 show the total cross-shore volumes for $B=0.002$ and 0.001. The offshore total load transport volume is increased in the surf and swash zones by the reduction of B .

Figures 4.45 to 4.52 show the computed results with $B = 0.003$ for the 16 lines in comparison to those with $B = 0.002$ shown in Figures 4.17 to 4.24. Figures 4.53 to 4.56 show the corresponding total cross-shore volumes. The increase of B by the factor of 1.5 increases the accretion above MSL and the cumulative bed load and suspended load. The value of $B = 0.003$ improves the agreement for the accretion volume per unit width above MSL but the accretion occurs on the seaward side of the shoreline at MSL instead of the upward berm reconstruction. This computed profile looks similar to the accreted profile predicted using $b=B$ with $B = 0.002$ before the

present modification of $b=B(0.5 + Q)$. The reproduction of the accreted profile above MSL is found to be more difficult than that of the eroded profile above MSL.

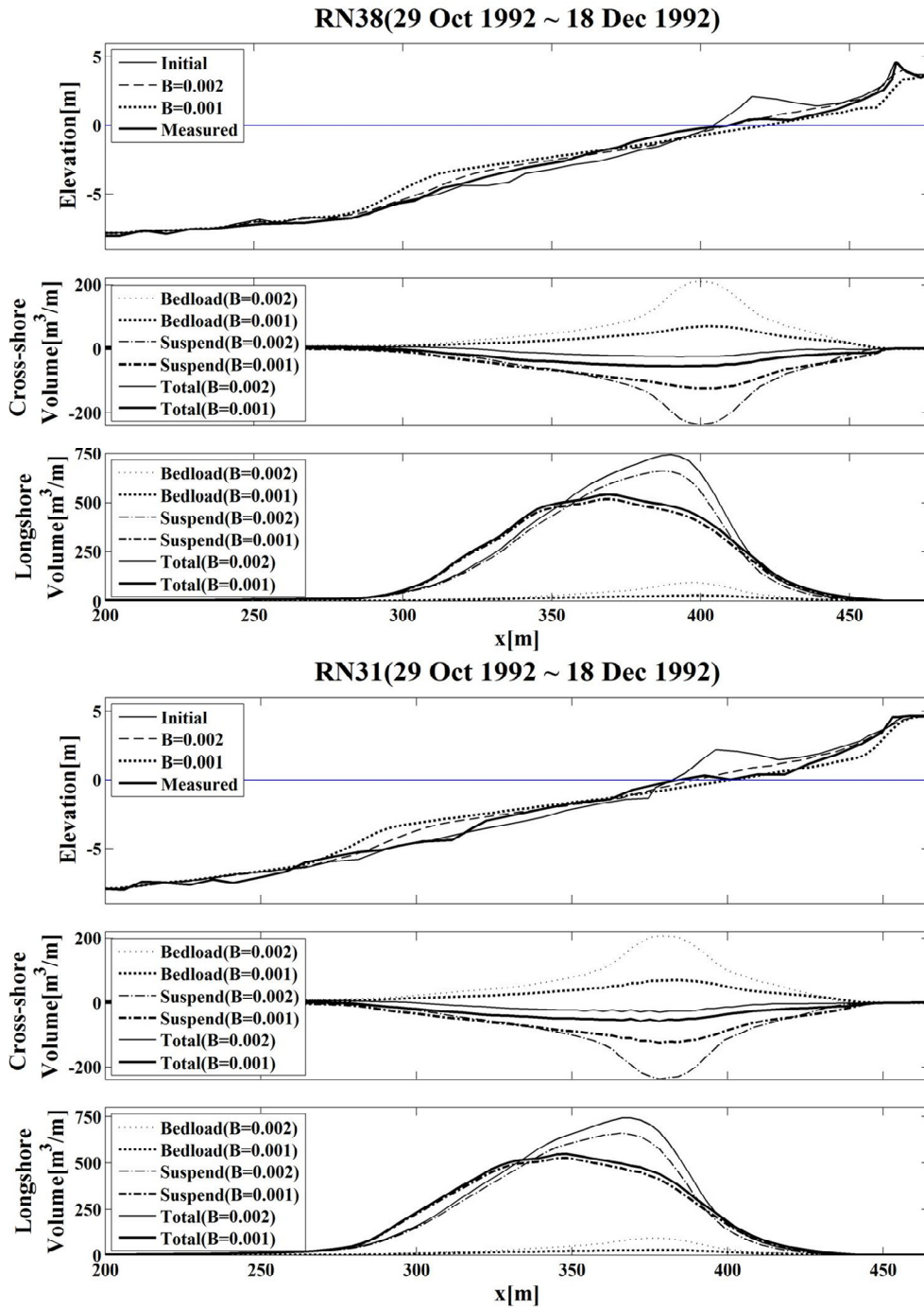


Figure 4.33 Effects of reduced bed load parameter $B = 0.001$ in Figure 4.1 based on $B = 0.002$.

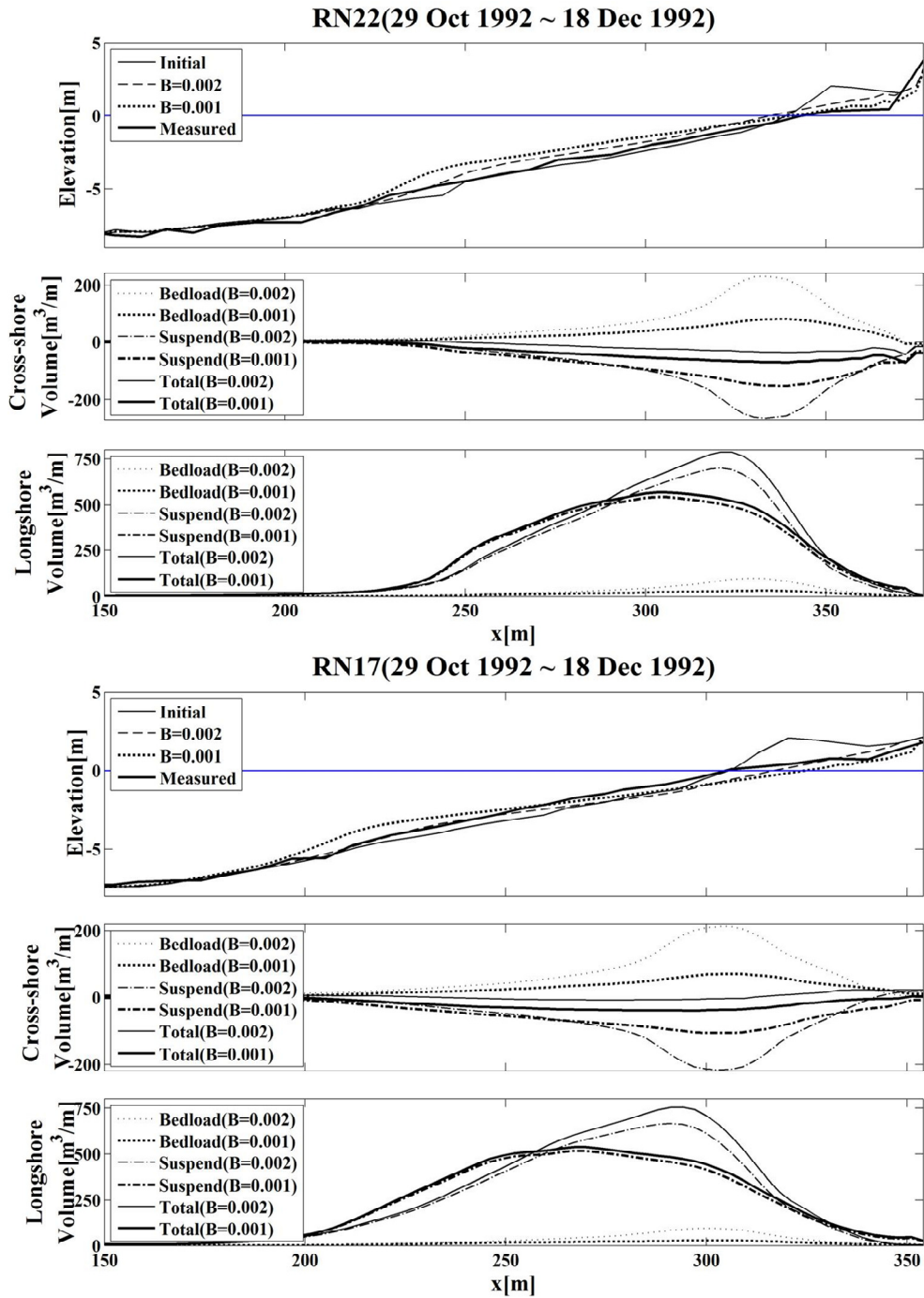


Figure 4.34 Effects of reduced bed load parameter $B = 0.001$ in Figure 4.2 based on $B = 0.002$.

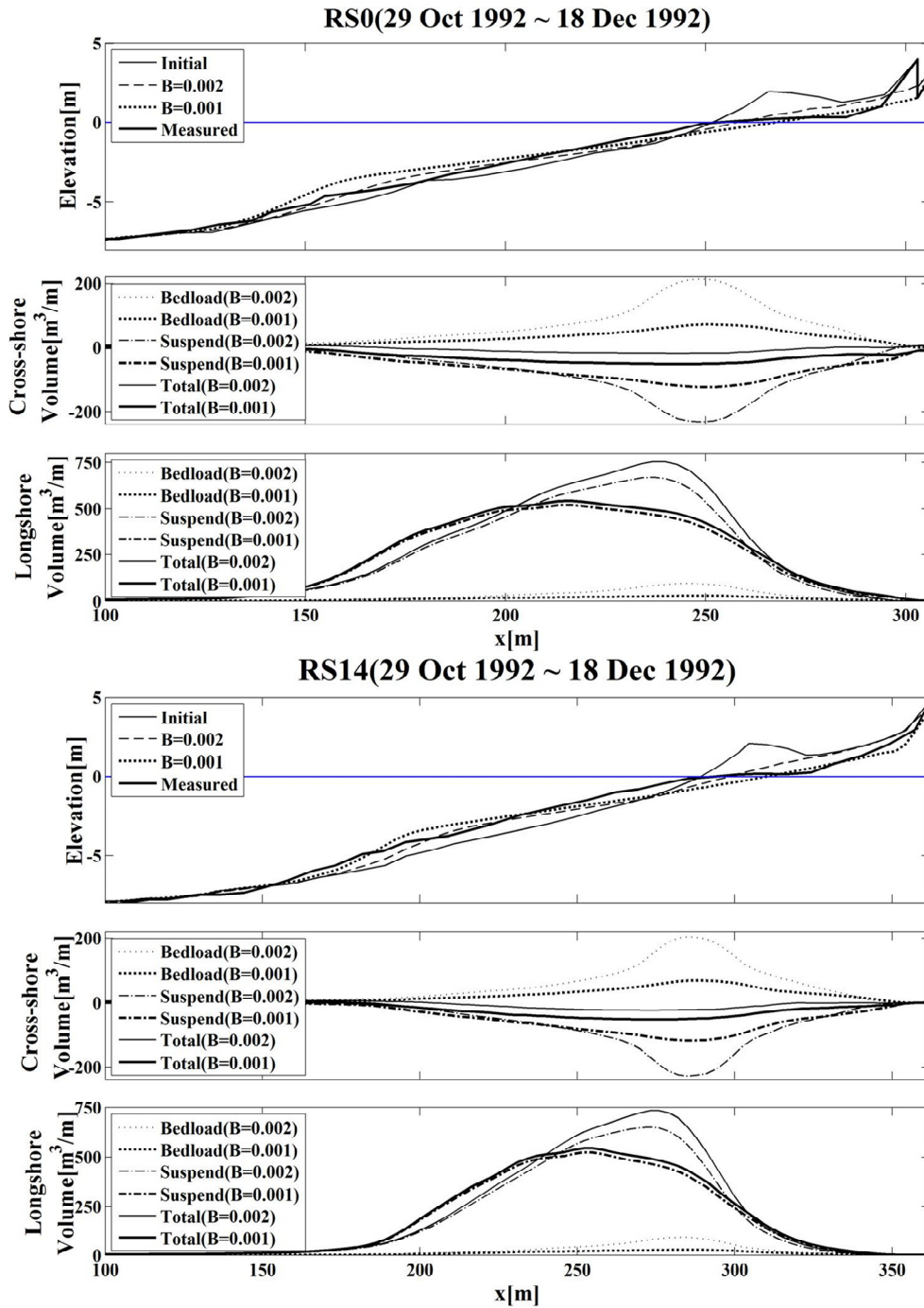


Figure 4.35 Effects of reduced bed load parameter $B = 0.001$ in Figure 4.3 based on $B = 0.002$.

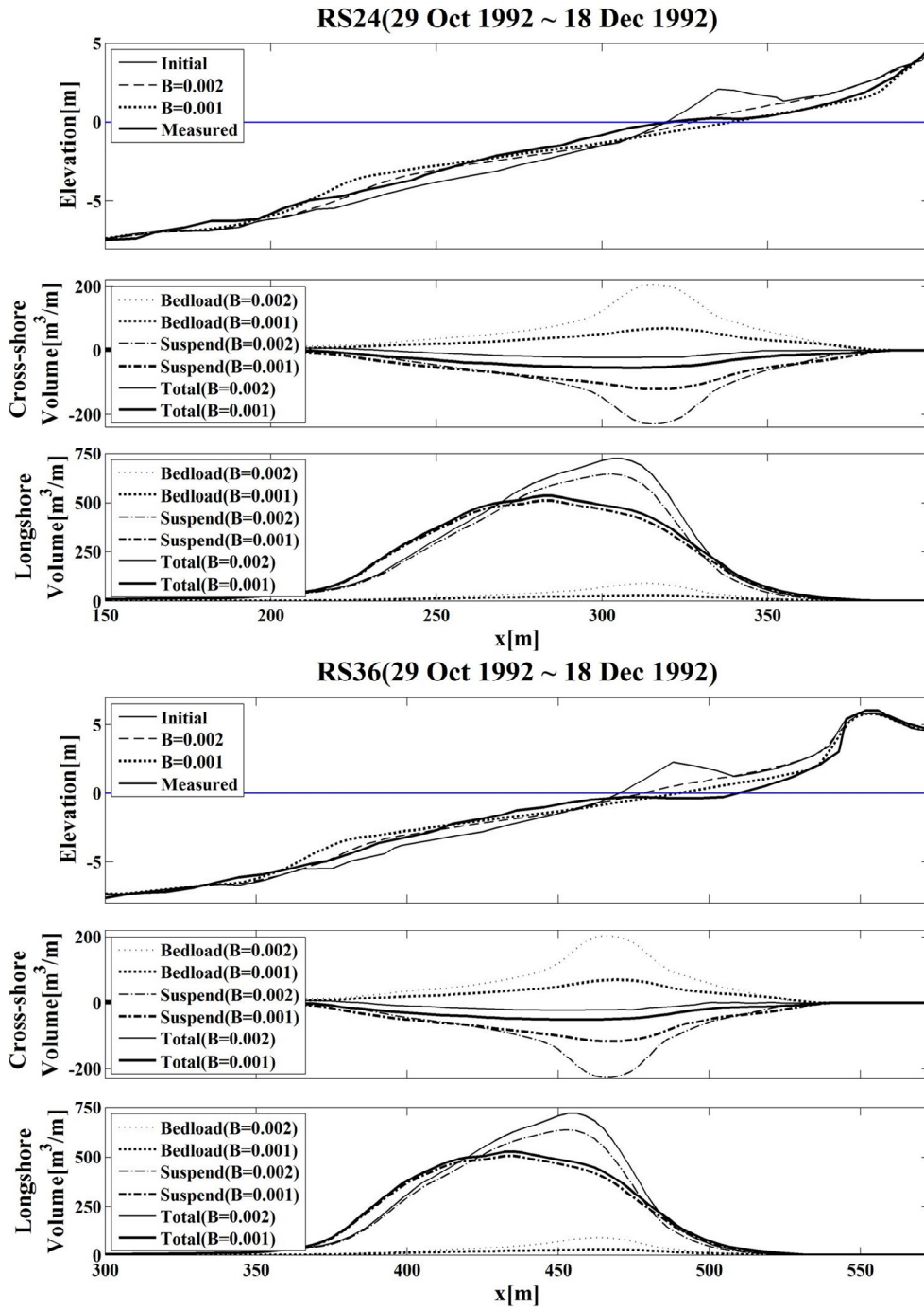


Figure 4.36 Effects of reduced bed load parameter $B = 0.001$ in Figure 4.4 based on $B = 0.002$.

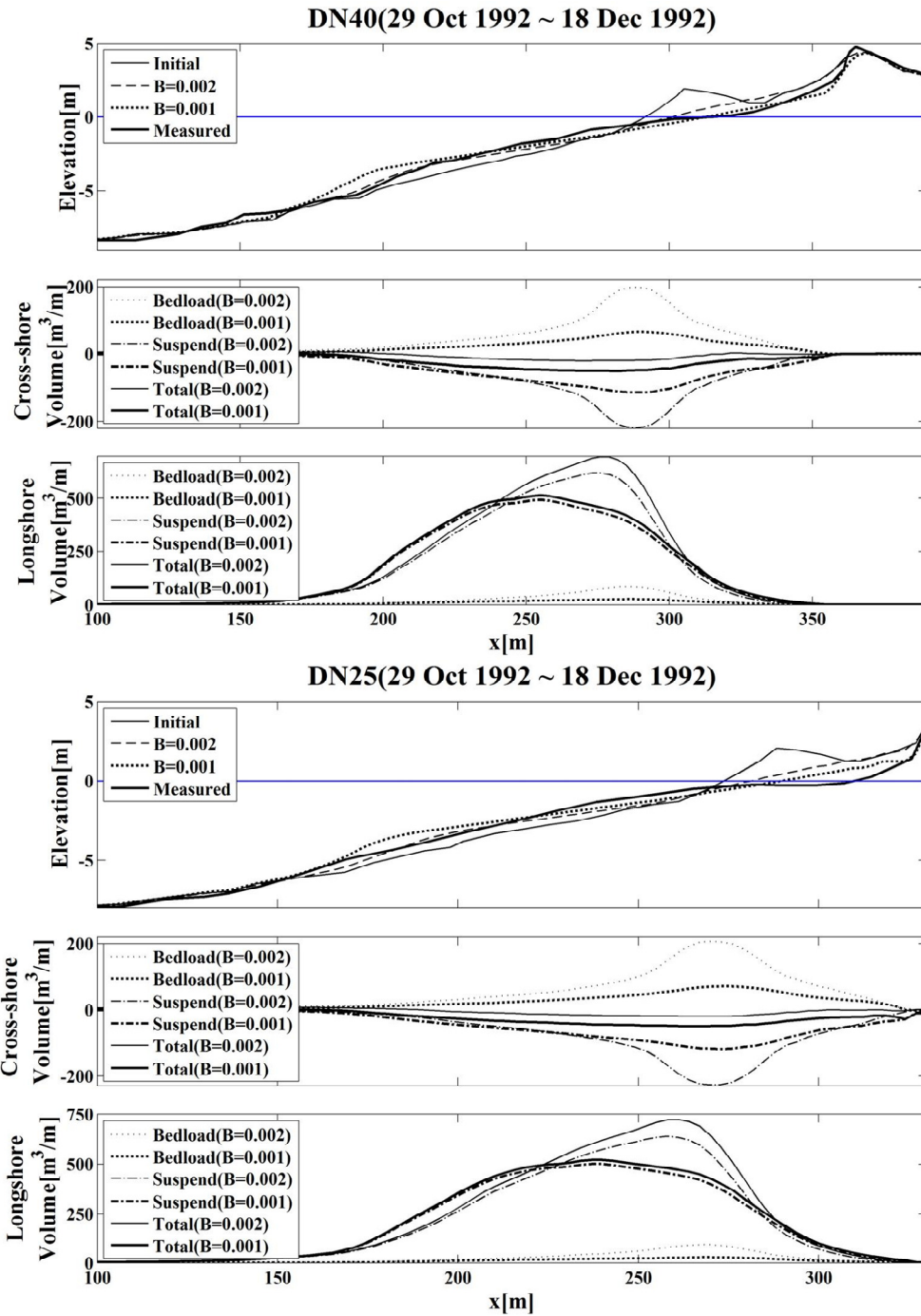


Figure 4.37 Effects of reduced bed load parameter $B = 0.001$ in Figure 4.5 based on $B = 0.002$.

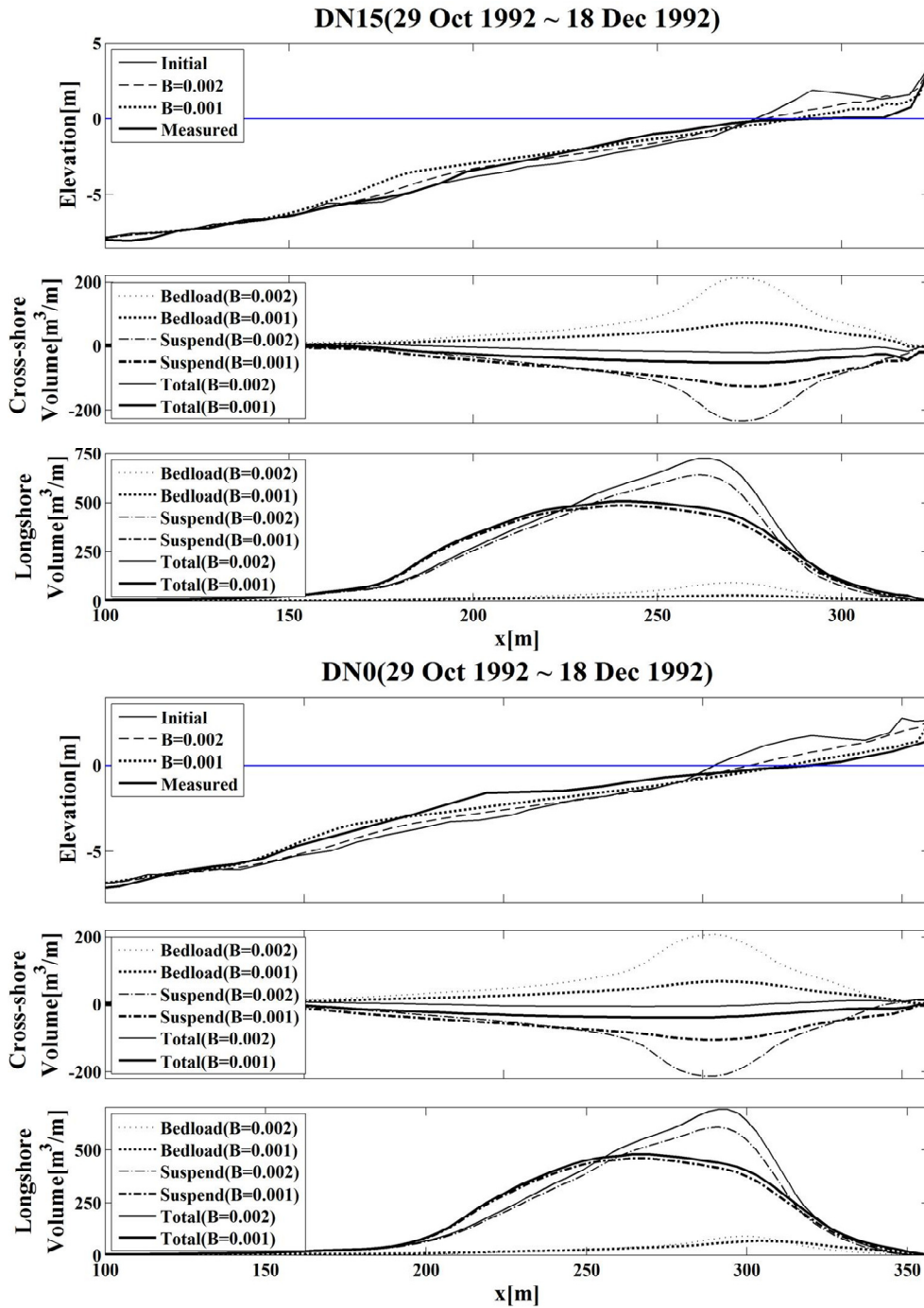


Figure 4.38 Effects of reduced bed load parameter $B = 0.001$ in Figure 4.6 based on $B = 0.002$.

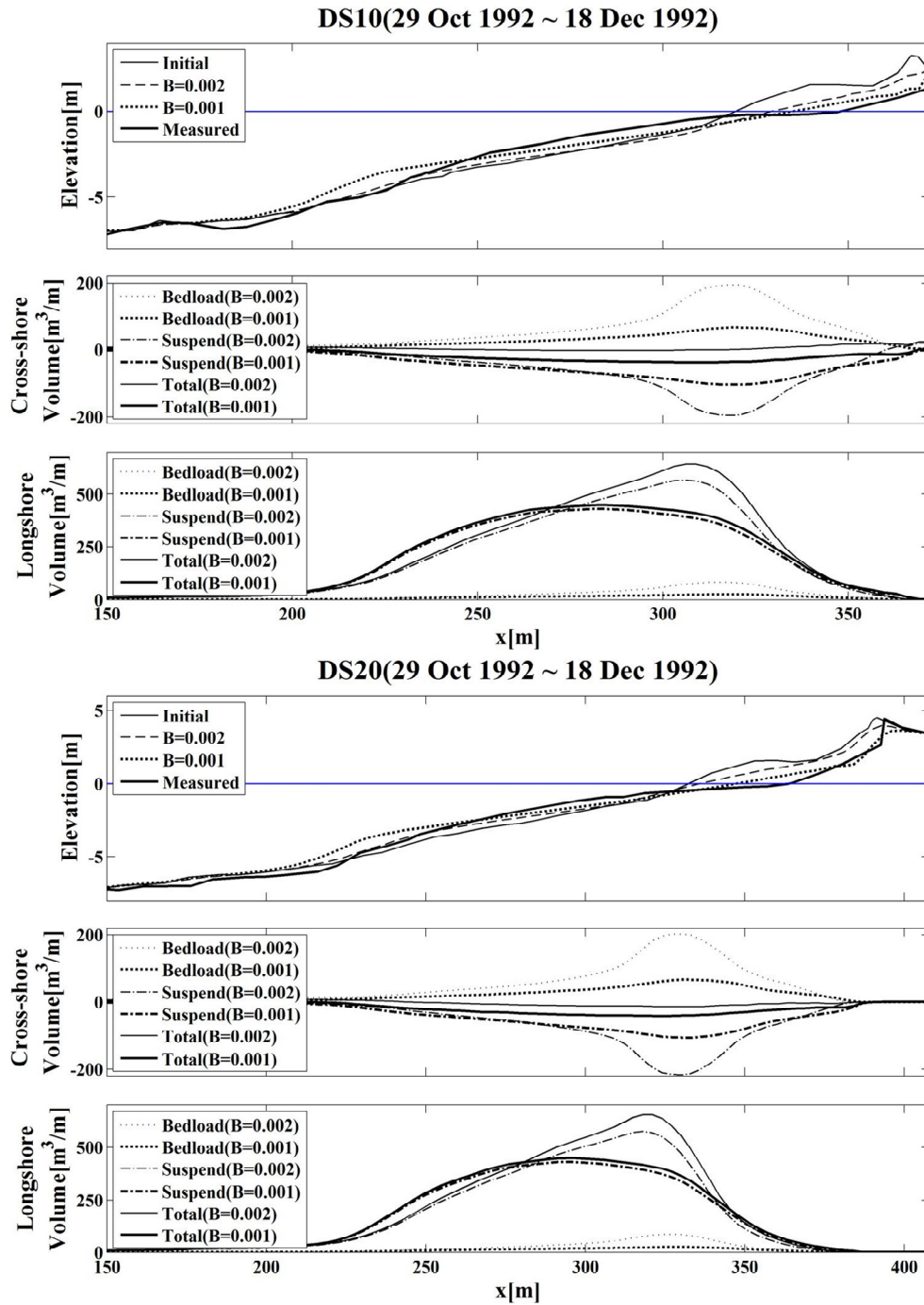


Figure 4.39 Effects of reduced bed load parameter $B = 0.001$ in Figure 4.7 based on $B = 0.002$.

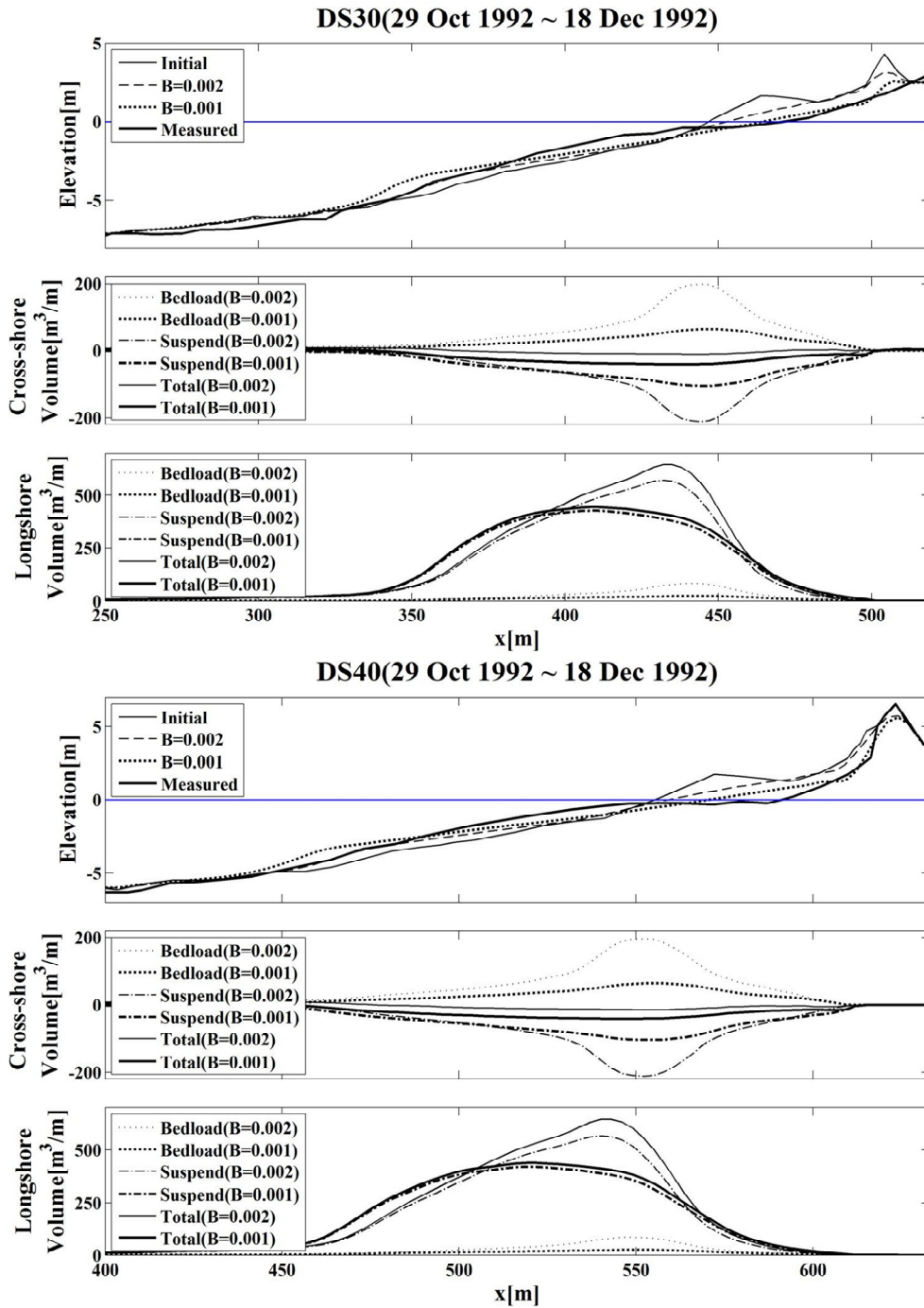


Figure 4.40 Effects of reduced bed load parameter $B = 0.001$ in Figure 4.8 based on $B = 0.002$.

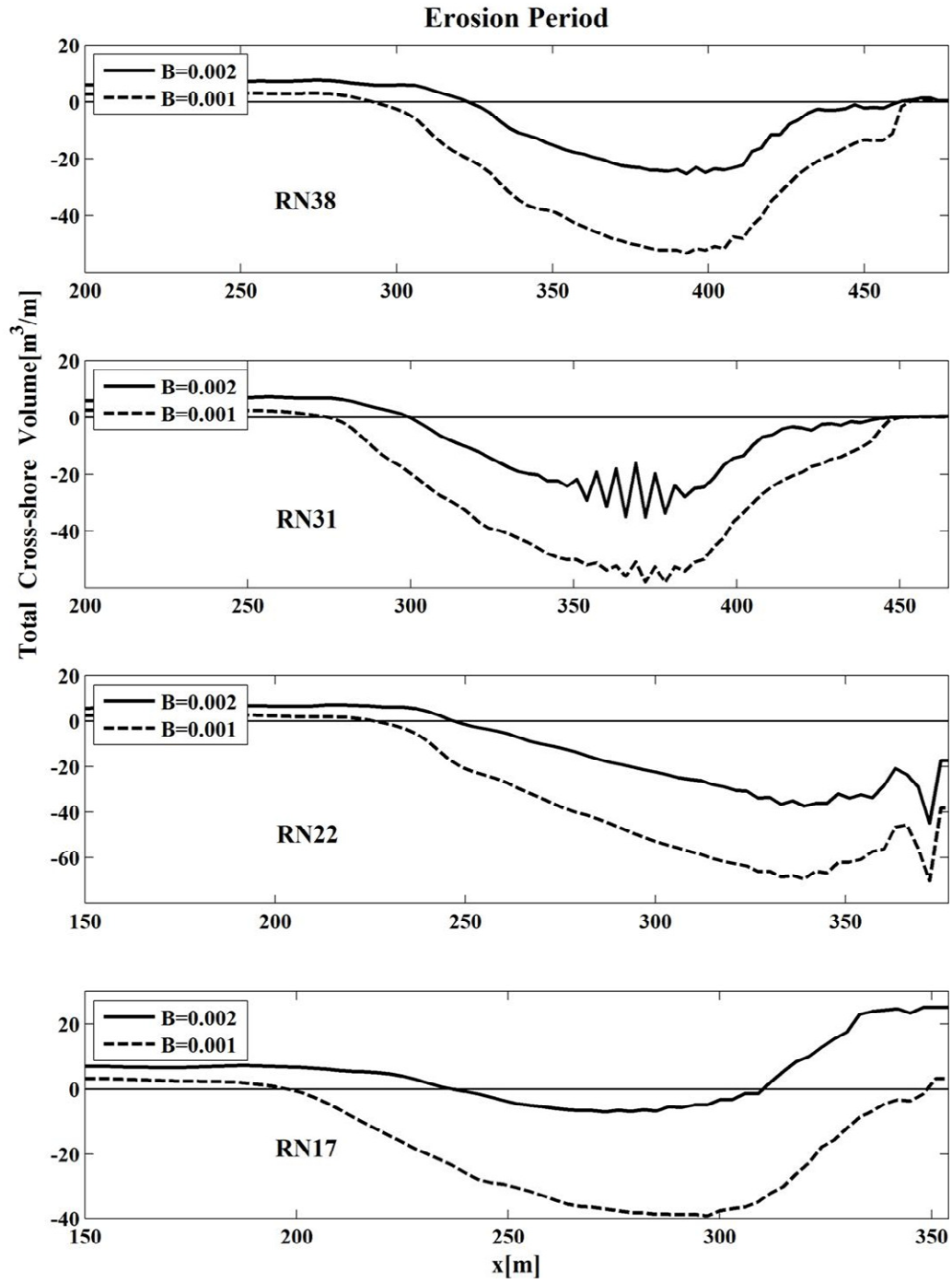


Figure 4.41 Cumulative total cross-shore sand transport volume per unit width during erosion period for RN38, RN31, RN22, and RN17.

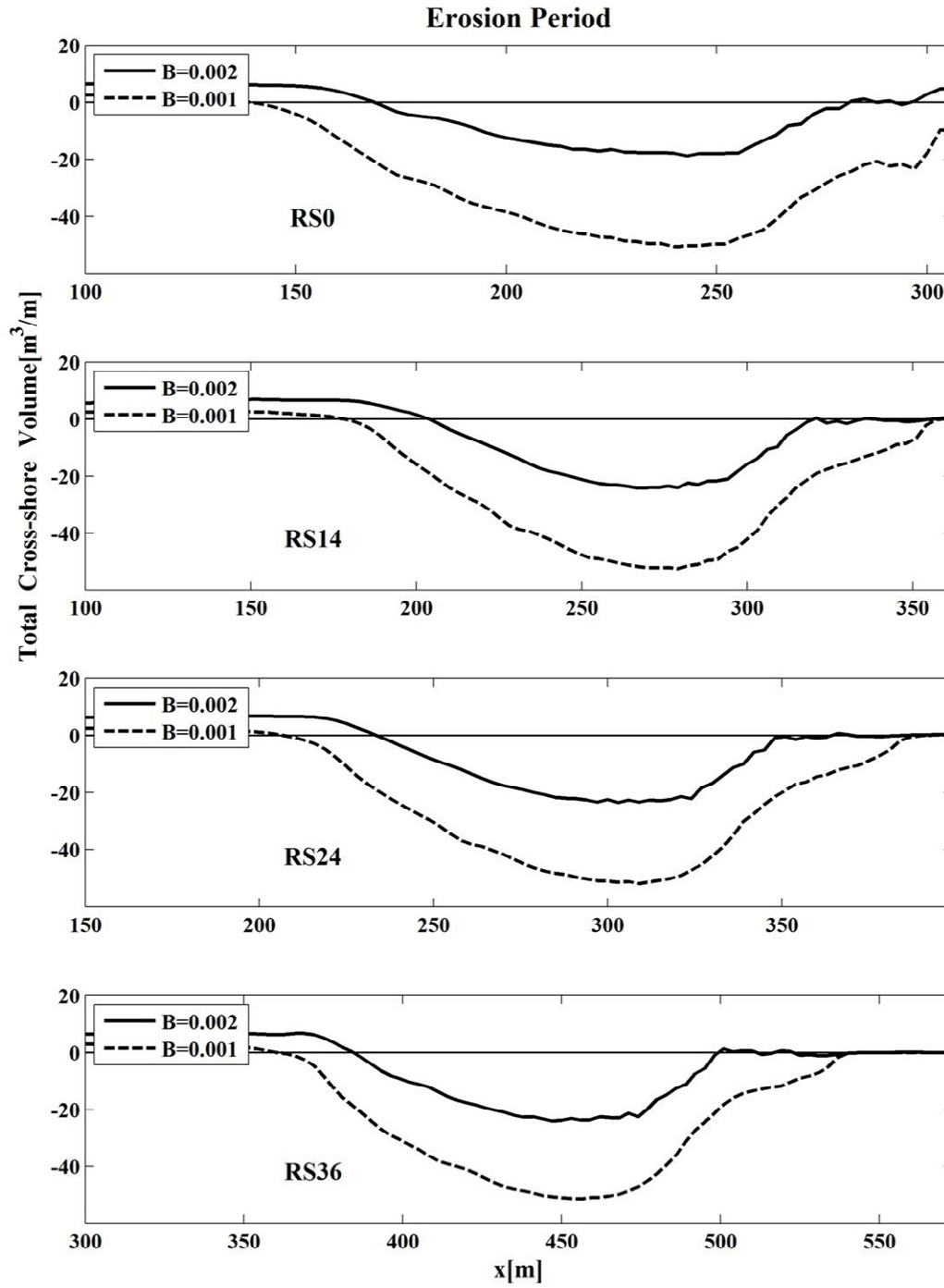


Figure 4.42 Cumulative total cross-shore sand transport volume per unit width during erosion period for RS0, RS14, RS24, and RS36.

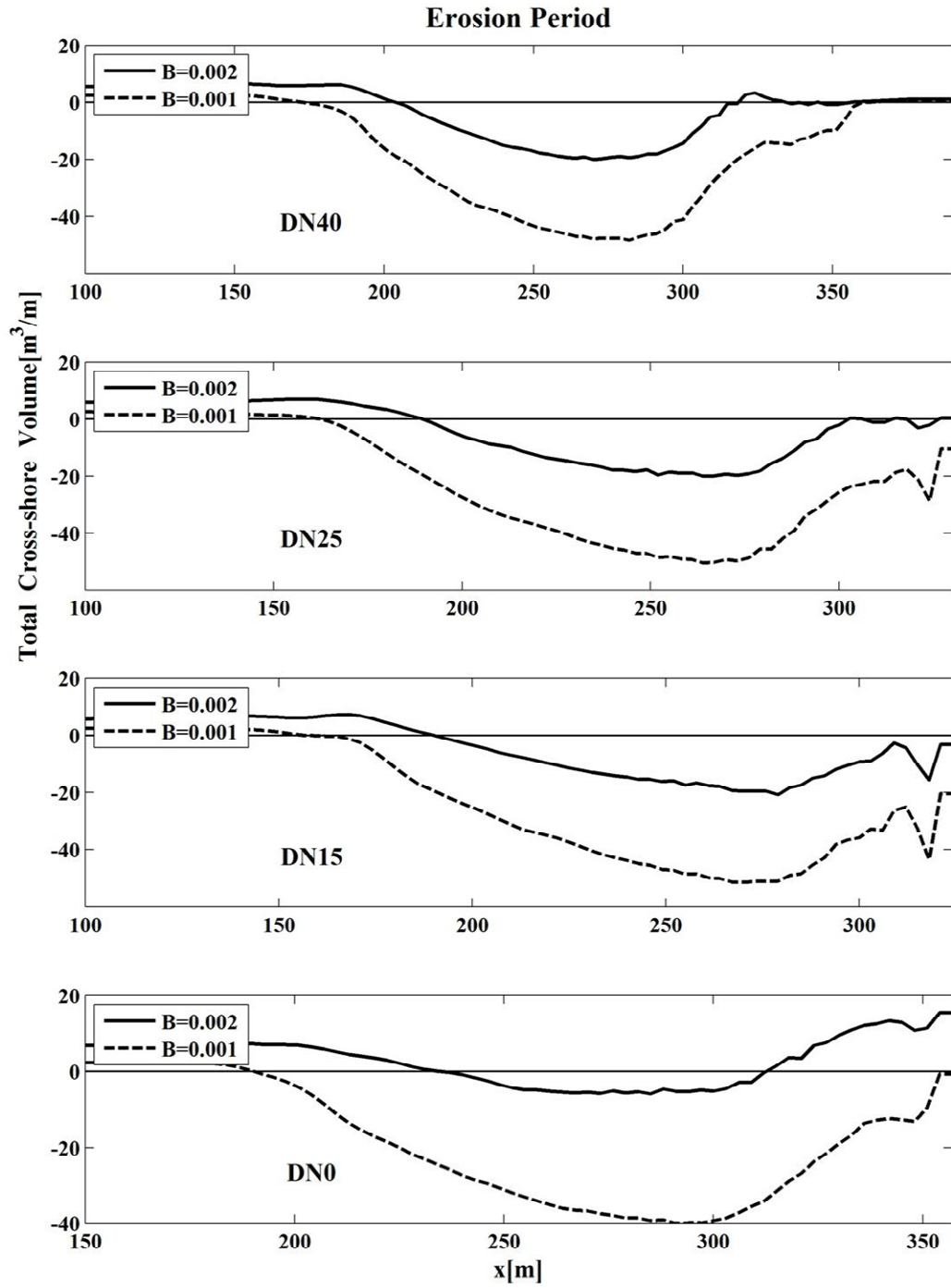


Figure 4.43 Cumulative total cross-shore sand transport volume per unit width during erosion period for DN40, DN25, DN15, and DN0.

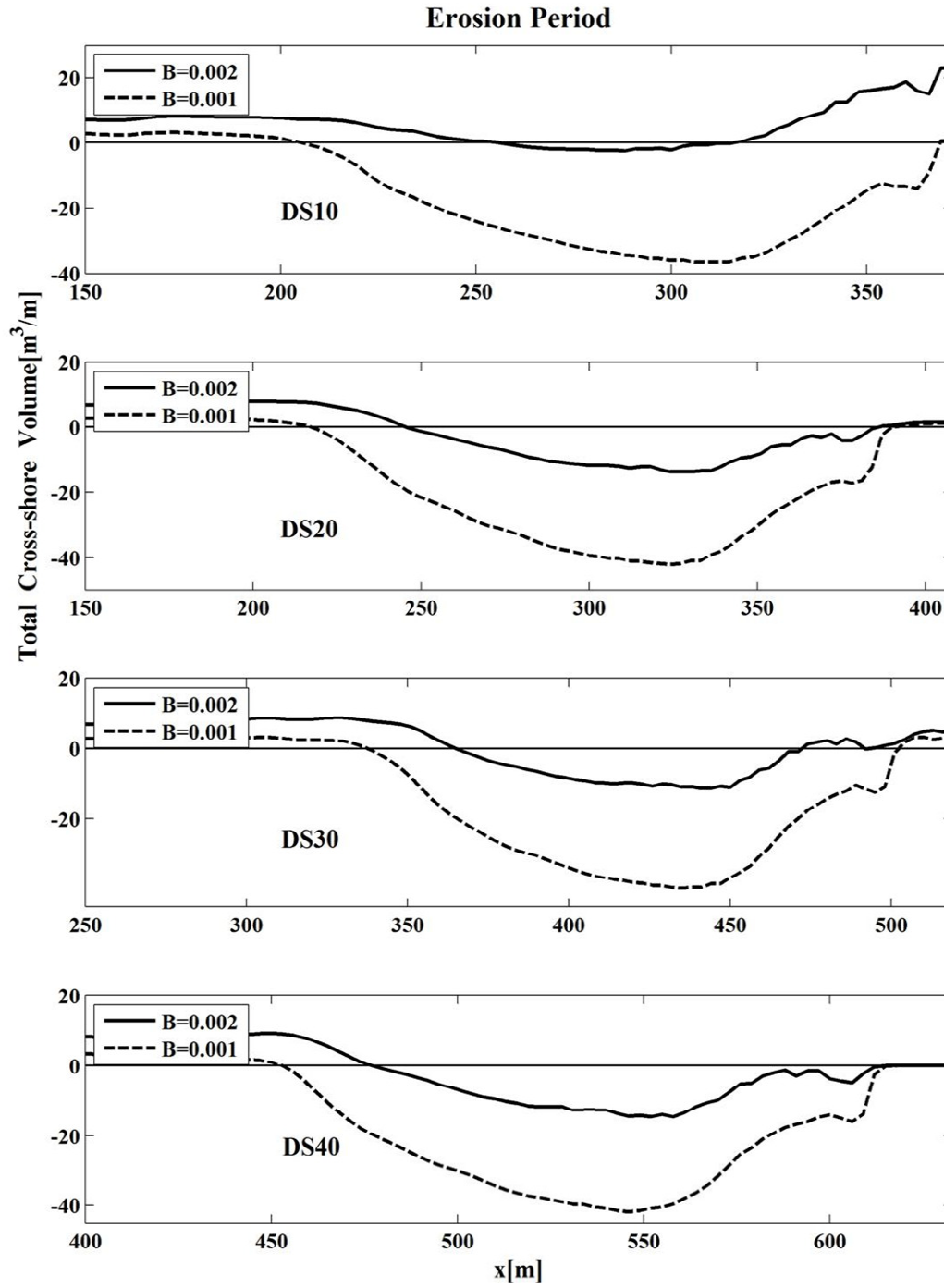


Figure 4.44 Cumulative total cross-shore sand transport volume per unit width during erosion period for DS10, DS20, DS30, and DS40.

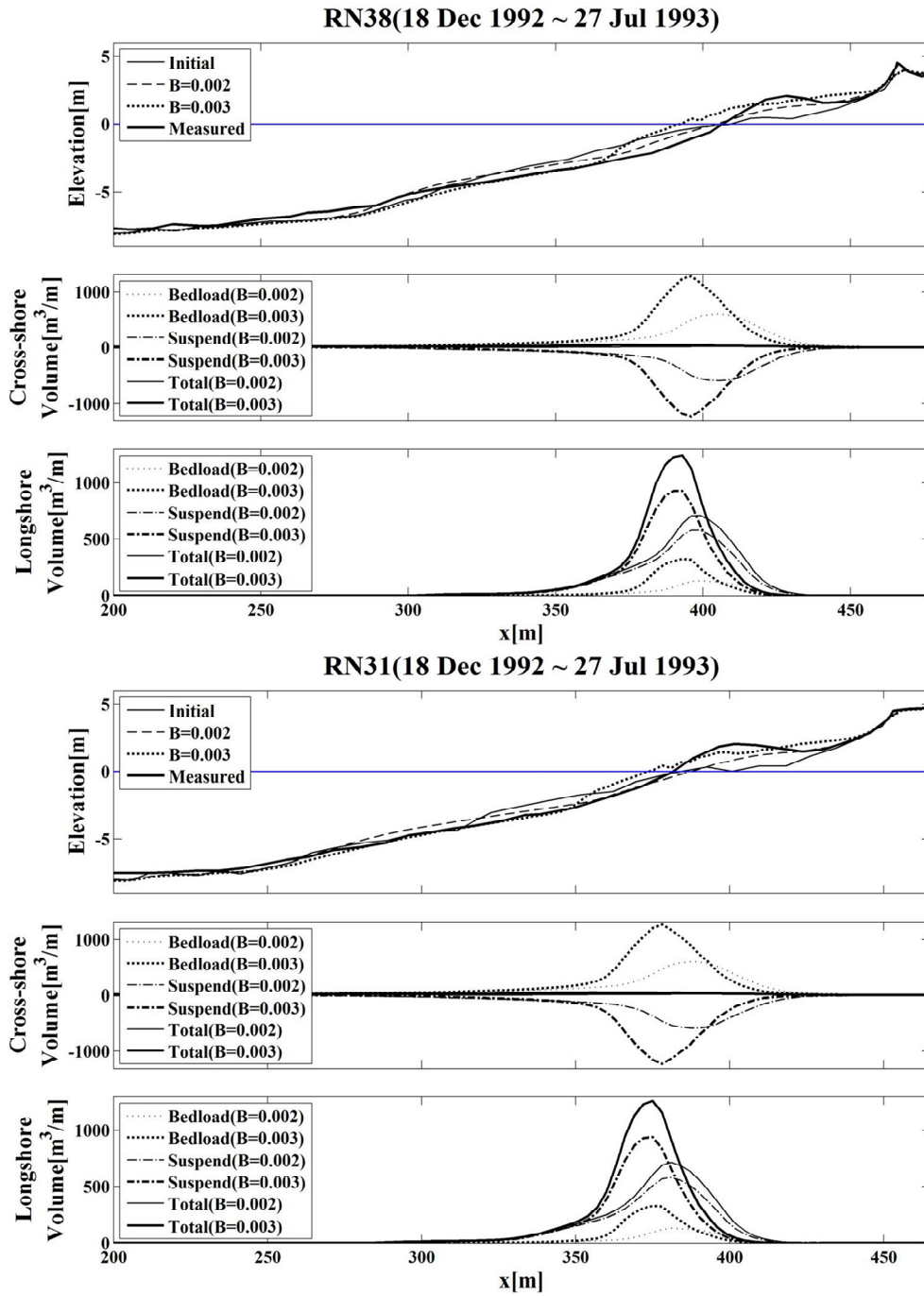


Figure 4.45 Effects of increased bed load parameter $B = 0.003$ in Figure 4.17 based on $B = 0.002$

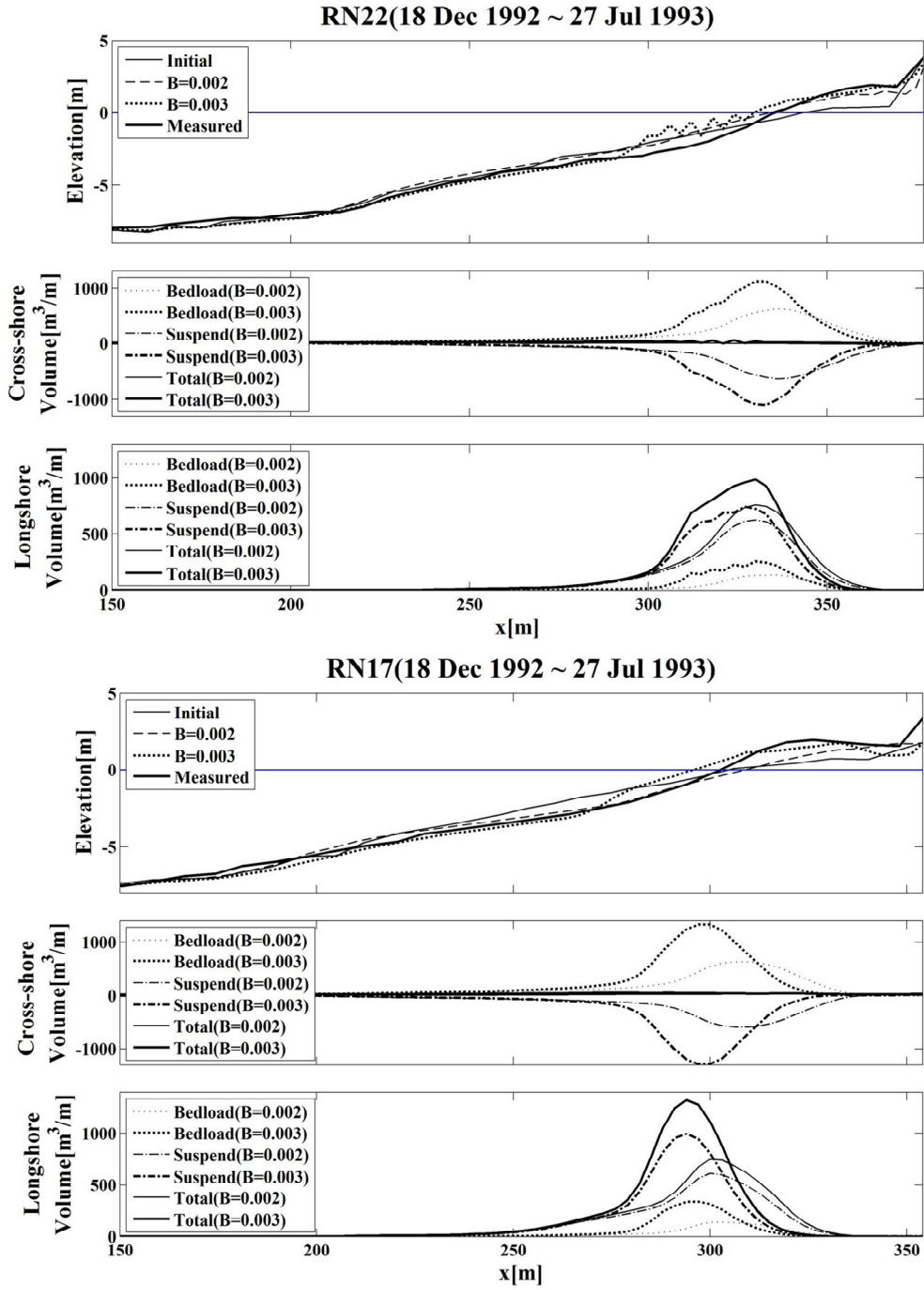


Figure 4.46 Effects of increased bed load parameter $B = 0.003$ in Figure 4.18 based on $B = 0.002$

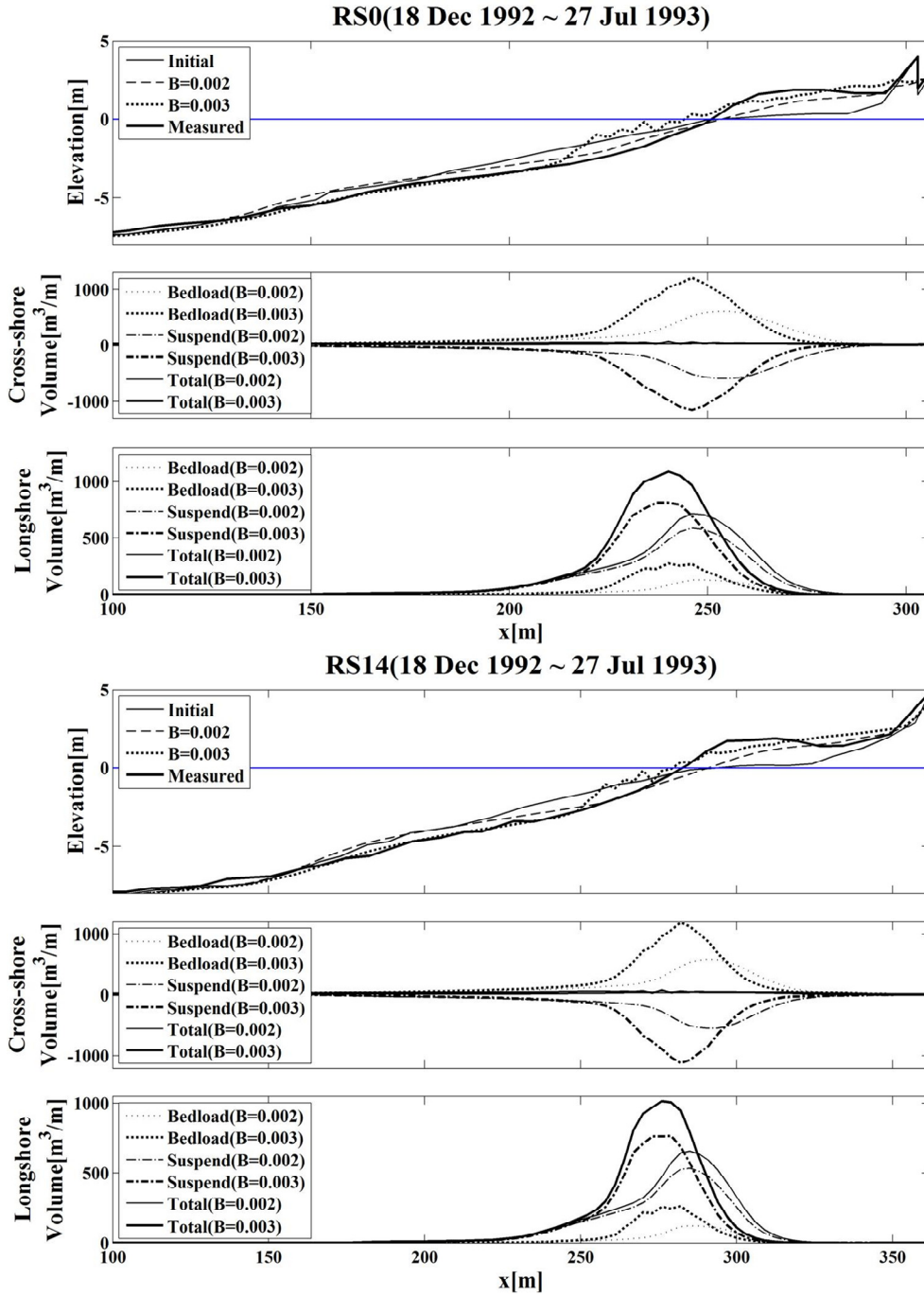


Figure 4.47 Effects of increased bed load parameter $B = 0.003$ in Figure 4.19 based on $B = 0.002$

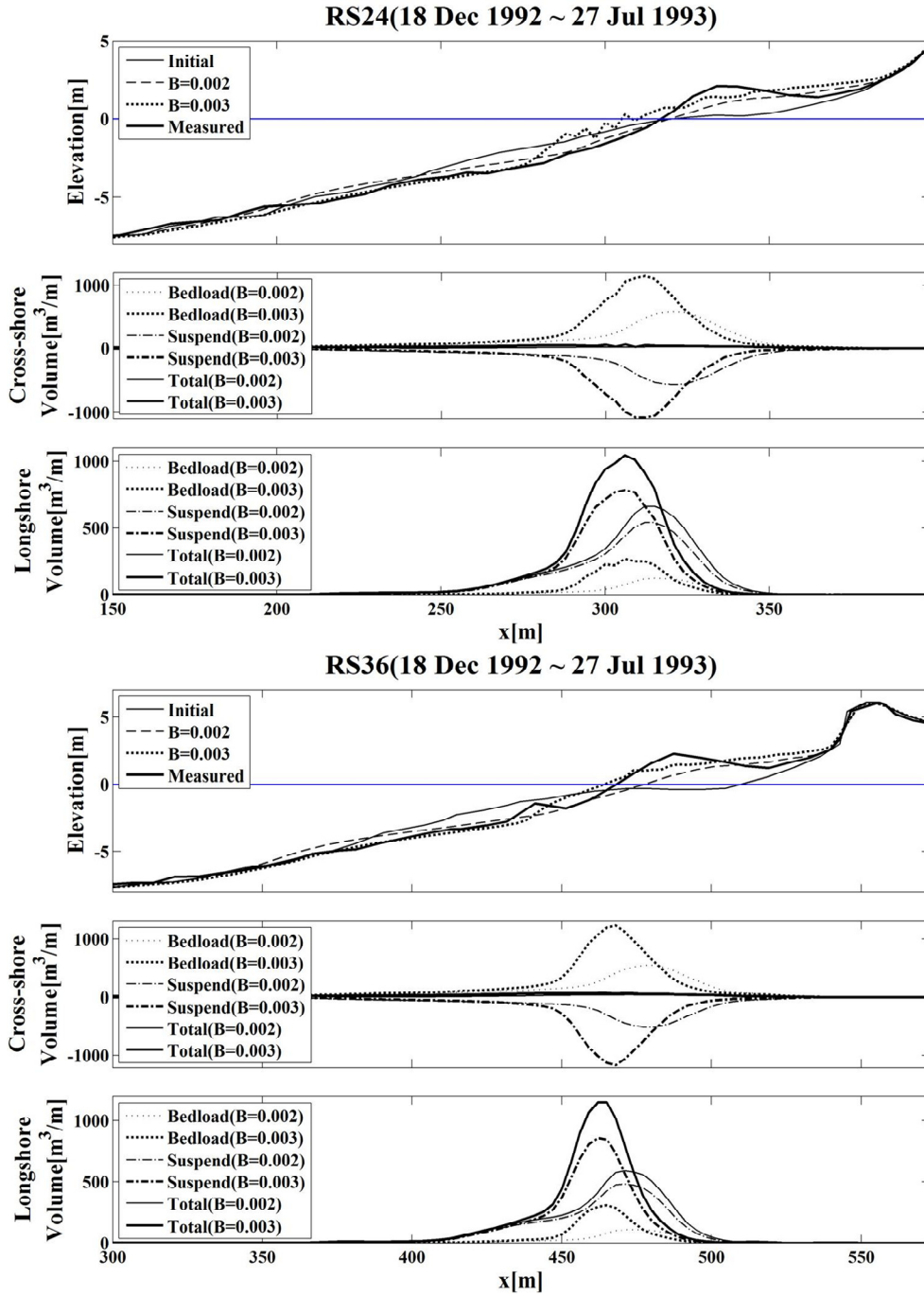


Figure 4.48 Effects of increased bed load parameter $B = 0.003$ in Figure 4.20 based on $B = 0.002$

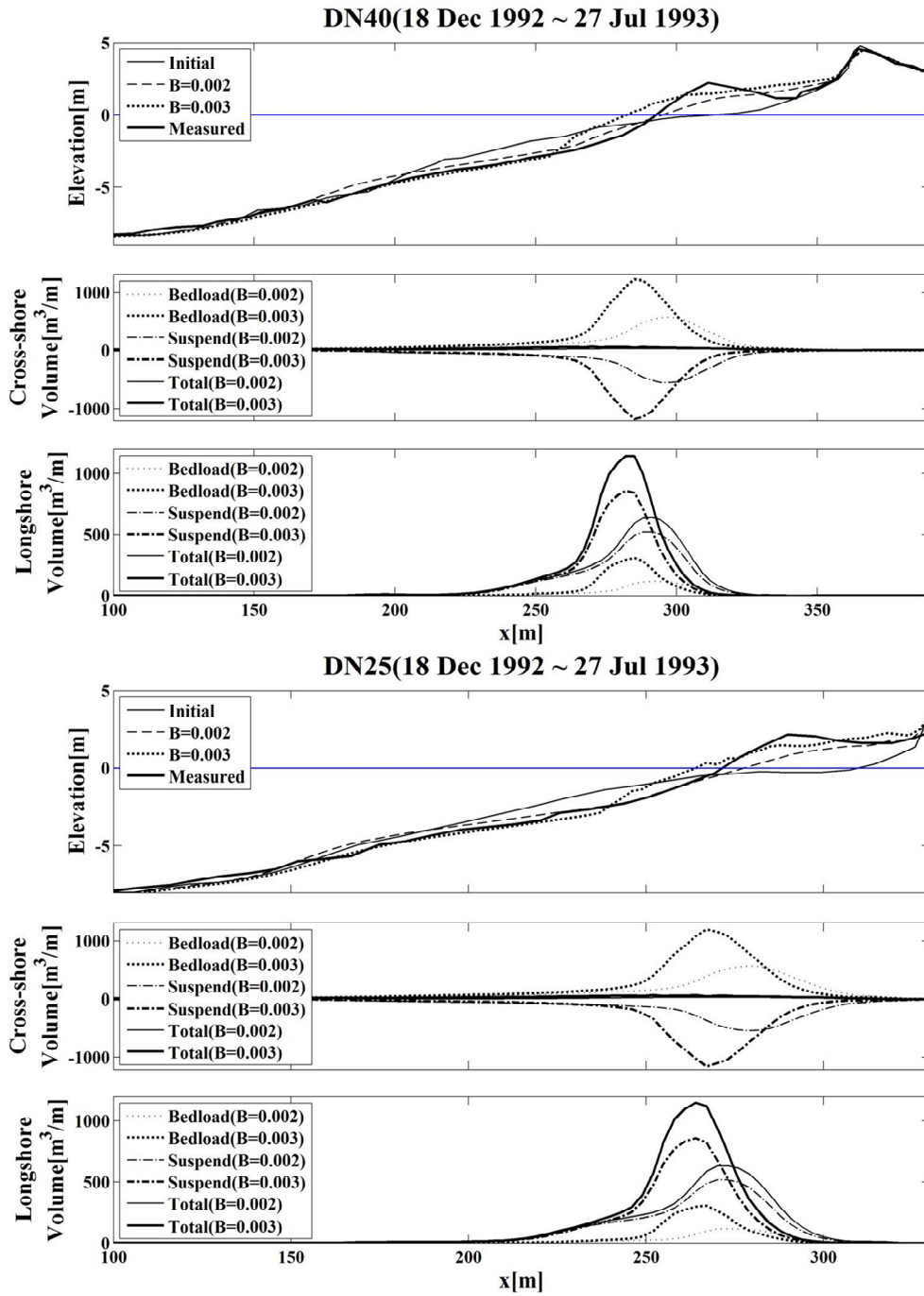


Figure 4.49 Effects of increased bed load parameter $B = 0.003$ in Figure 4.21 based on $B = 0.002$

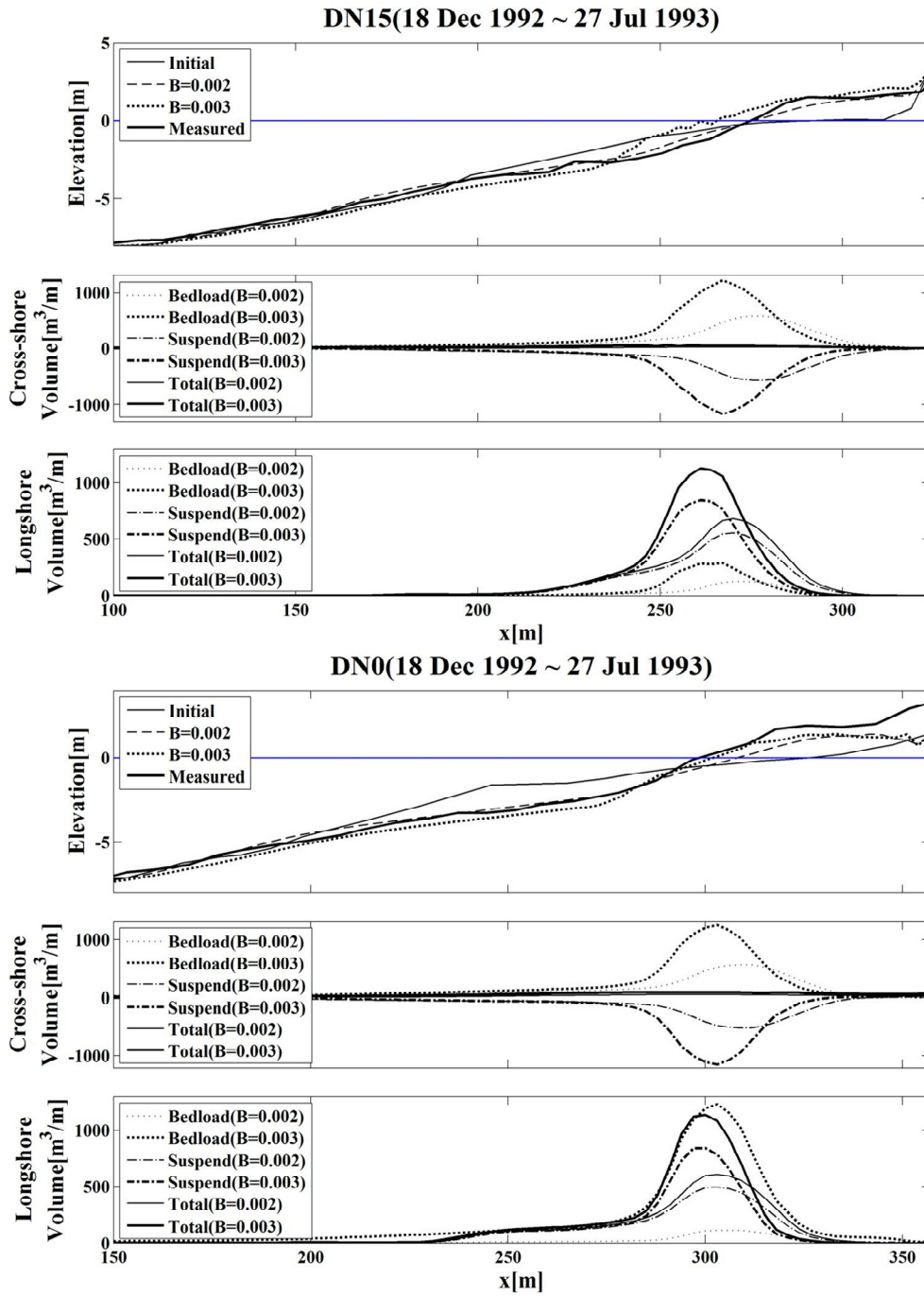


Figure 4.50 Effects of increased bed load parameter $B = 0.003$ in Figure 4.22 based on $B = 0.002$

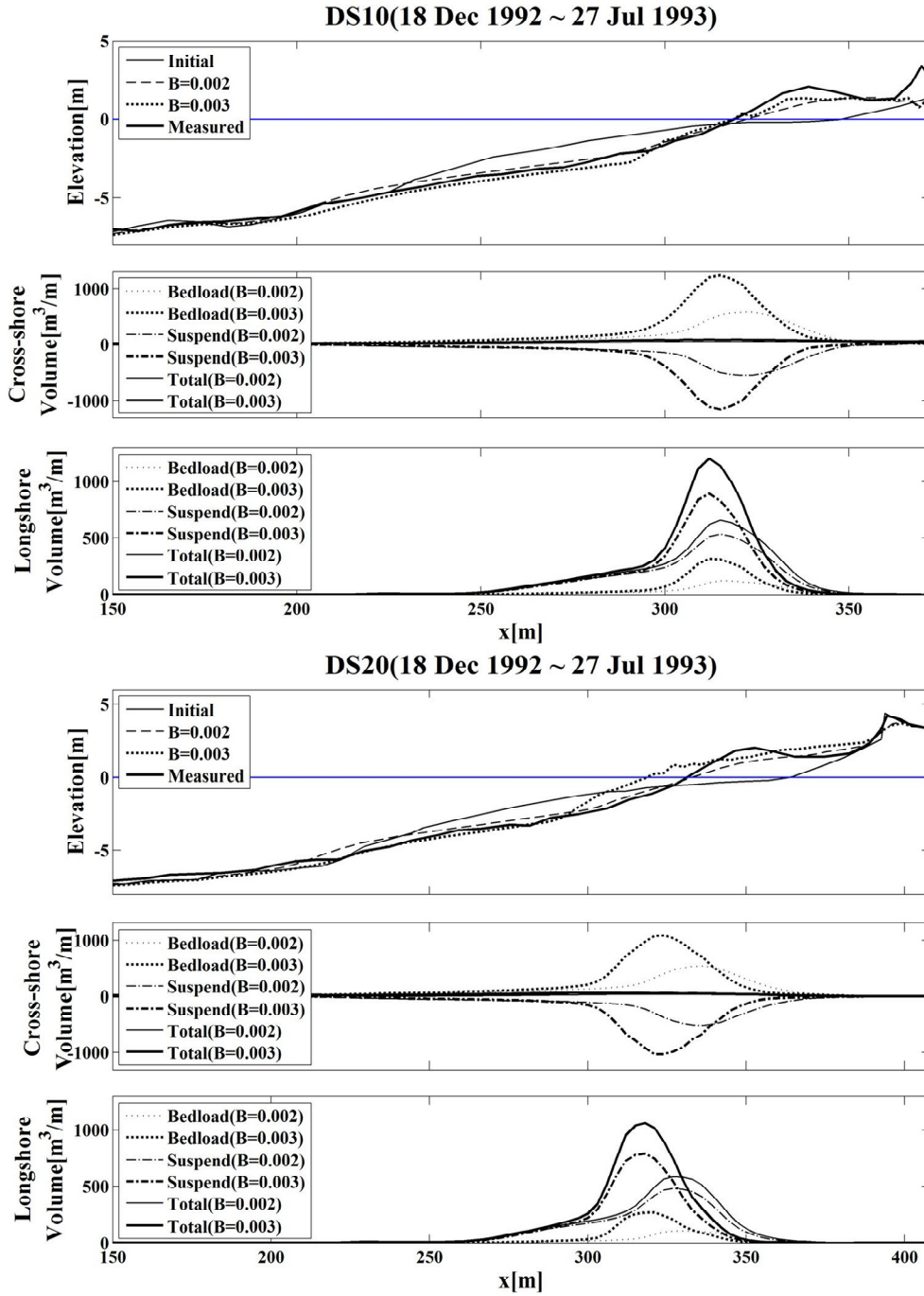


Figure 4.51 Effects of increased bed load parameter $B = 0.003$ in Figure 4.23 based on $B = 0.002$

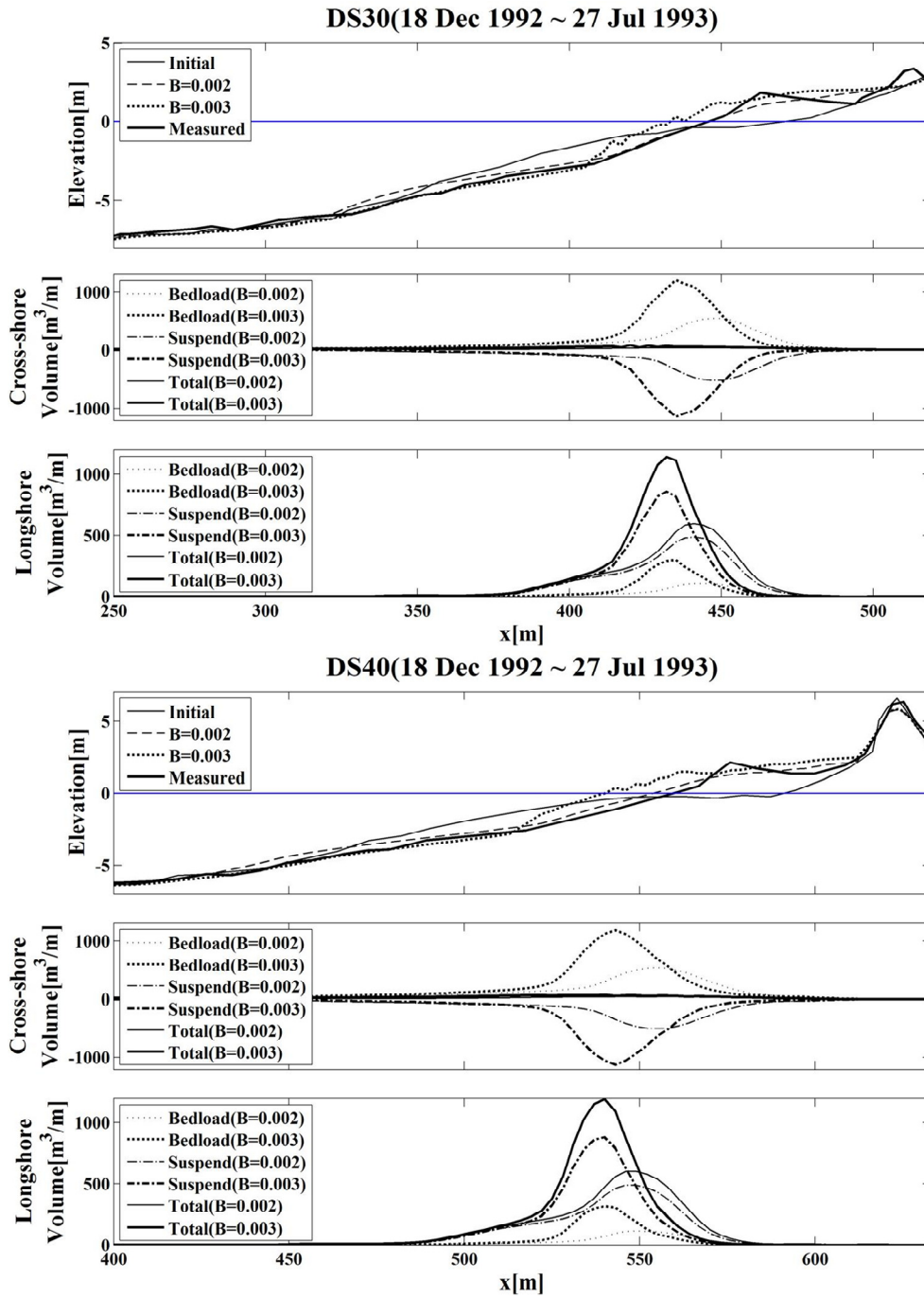


Figure 4.52 Effects of increased bed load parameter $B = 0.003$ in Figure 4.24 based on $B = 0.002$

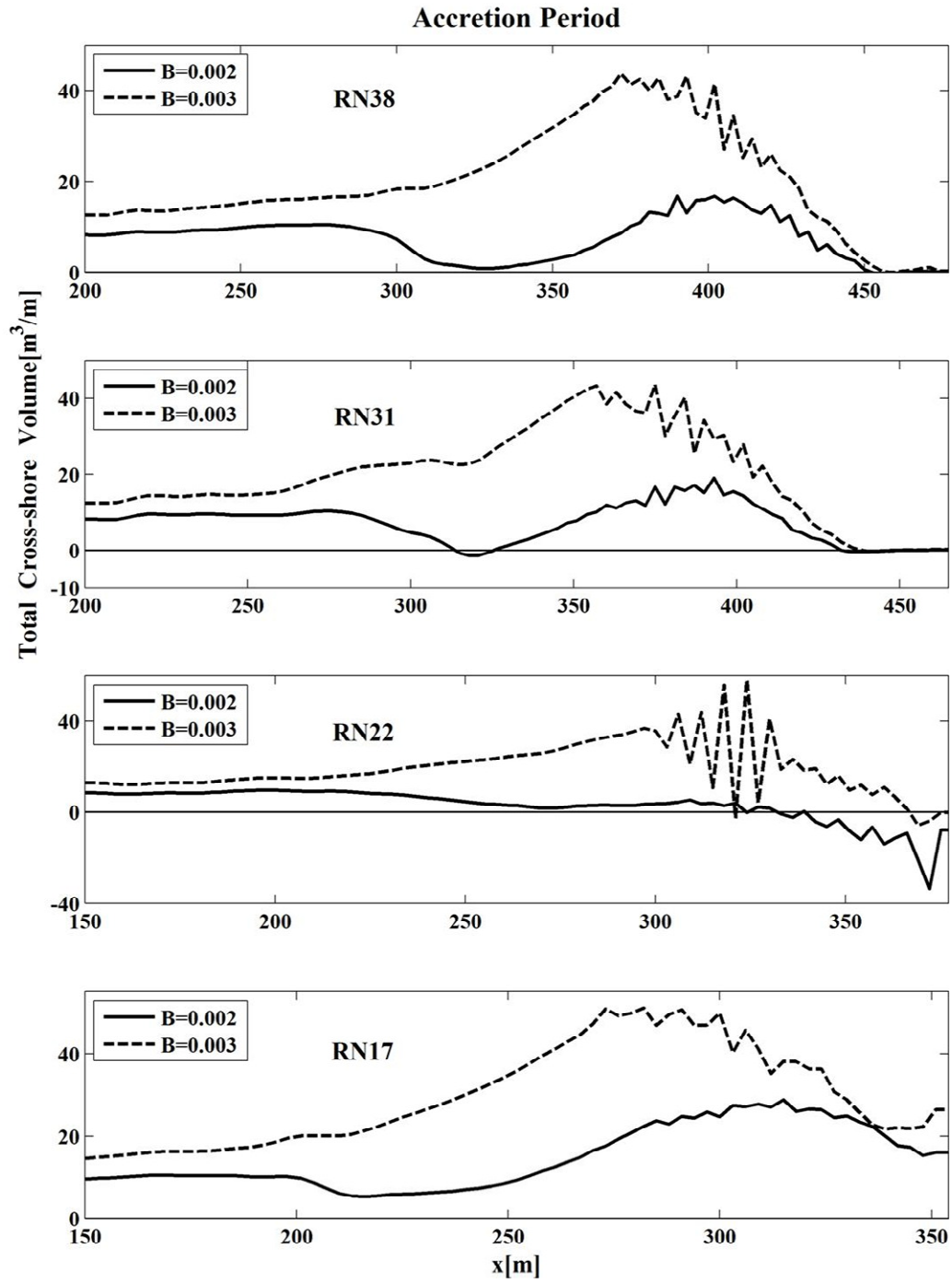


Figure 4.53 Cumulative total cross-shore sand transport volume per unit width during accretion period for RN38, RN31, RN22, and RN17.

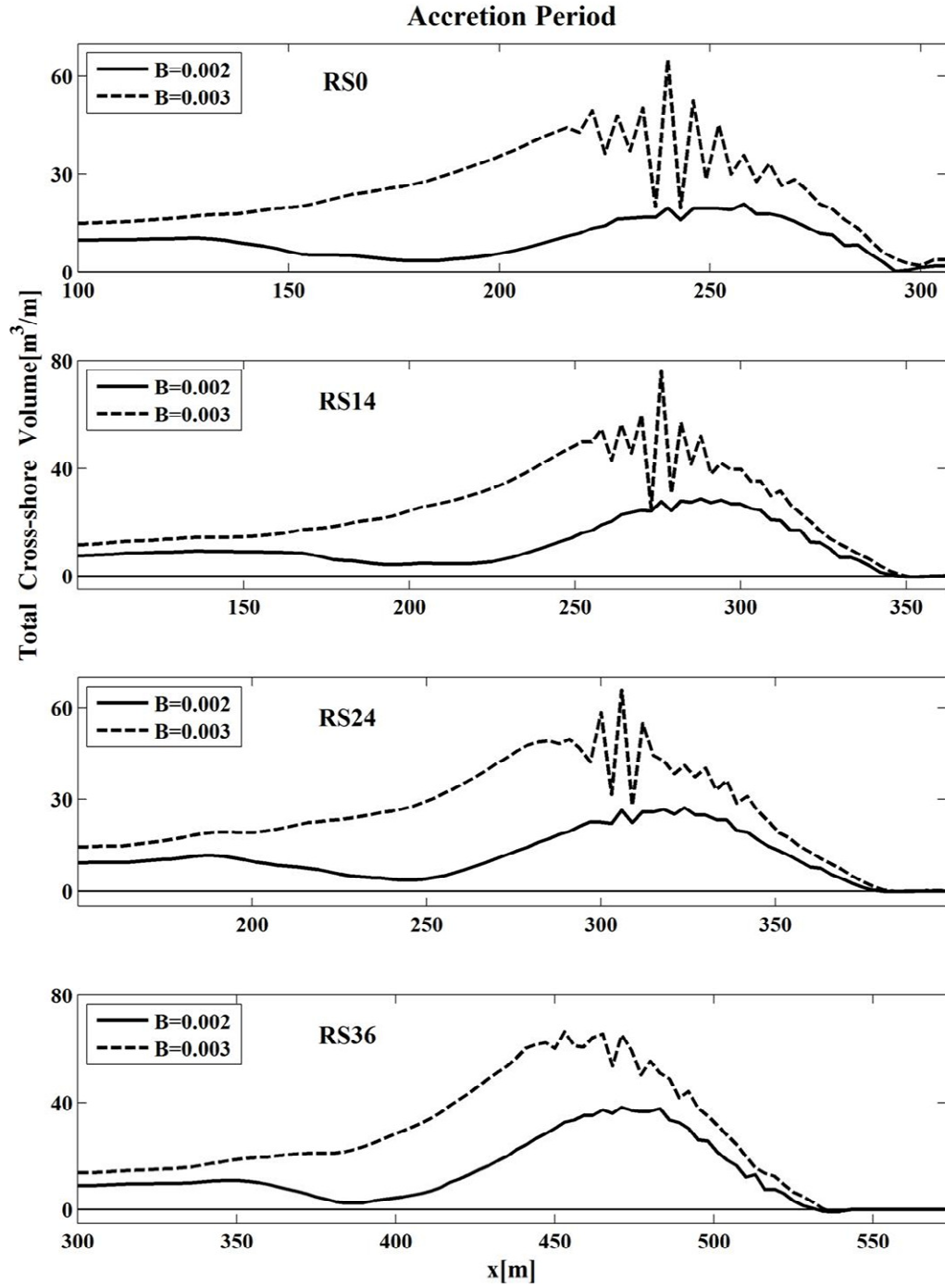


Figure 4.54 Cumulative total cross-shore sand transport volume per unit width during accretion period for RS0, RS14, RS24, and RS36.

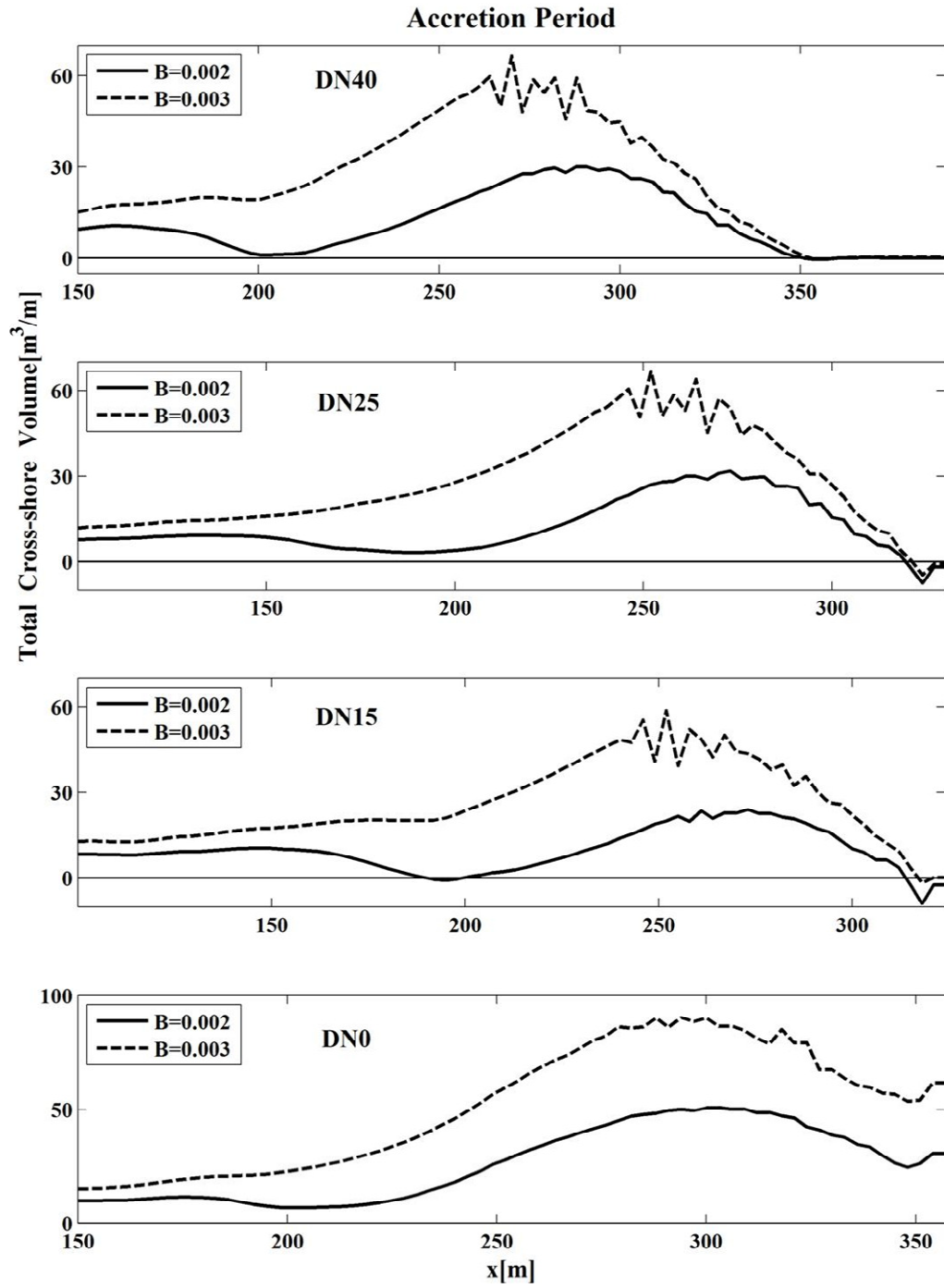


Figure 4.55 Cumulative total cross-shore sand transport volume per unit width during accretion period for DN40, DN25, DN15, and DN0.

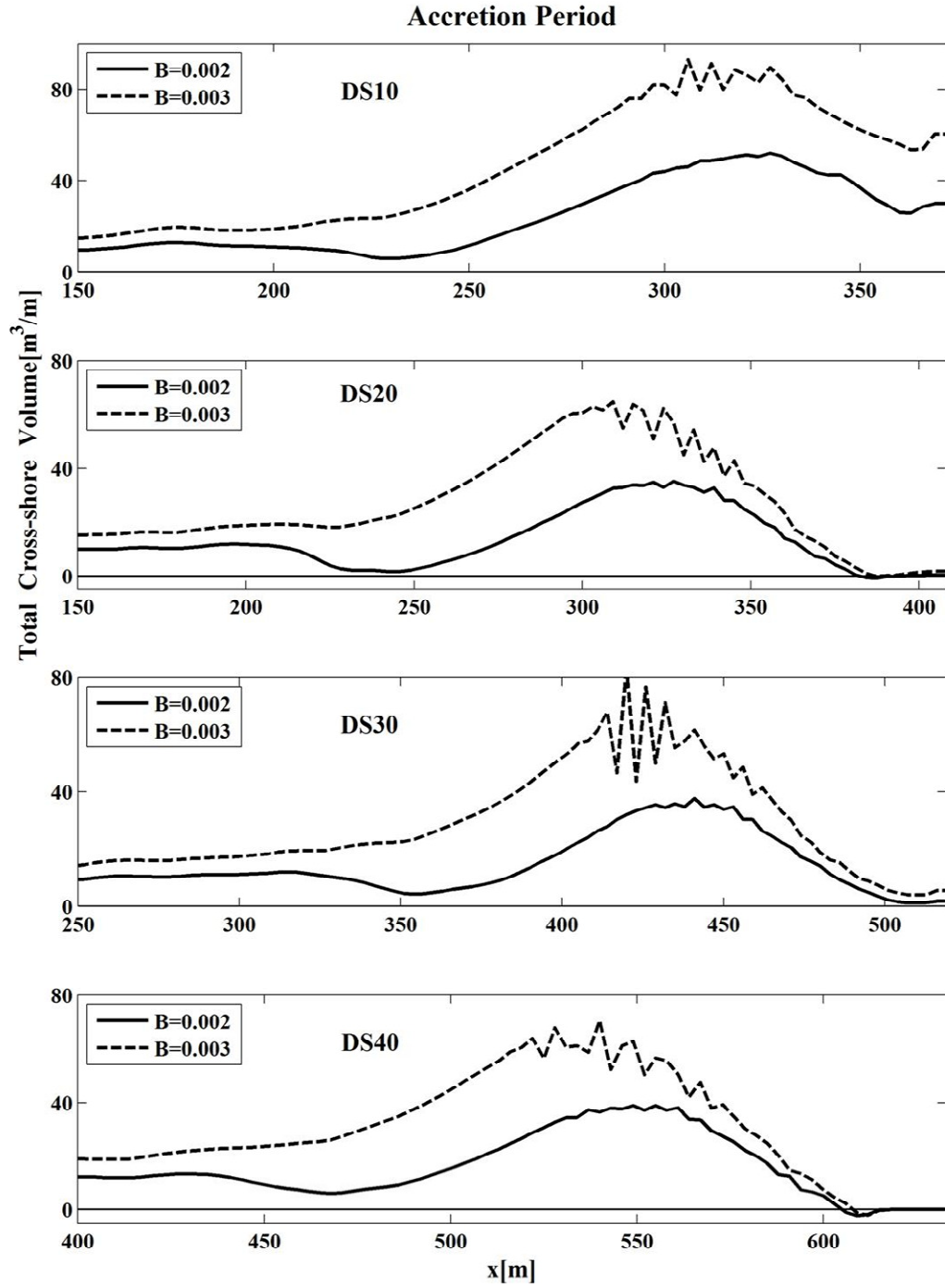


Figure 4.56 Cumulative total cross-shore sand transport volume per unit width during accretion period for DS10, DS20, DS30, and DS40.

4.4 Erosion and Accretion Volumes

Figure 4.57 compares the computed erosion and accretion volumes per unit alongshore length above MSL for the 16 lines with the measured values listed in Table 2.3 where RN38 and DS40 are located at the alongshore coordinate $y = 4975$ m and $y = 0$, respectively. First, the computed volumes for $B = 0.002$ are compared with the measured volumes. The erosion volume is predicted well in the northern (N) segment of Rehoboth Beach. The underprediction of the erosion volume increases southward. On the other hand, the alongshore variation of the agreement for the accretion volume is opposite. The agreement is good at the southern (S) end of Dewey Beach but the underprediction persists northward. The computed results in this study account for the initial profile differences among the 16 lines but the offshore wave conditions at $x = 0$ are assumed to be invariant alongshore. The erosion volume is predicted better for $B = 0.001$ which cannot predict accretion. The accretion volume is predicted better for $B = 0.003$ which cannot predict erosion. The use of $B = 0.002$ predicts the erosion and accretion volumes within a factor of about 2. The accurate prediction of both erosion and accretion is difficult because of the small difference between the onshore bed load transport and the offshore suspended sediment transport.

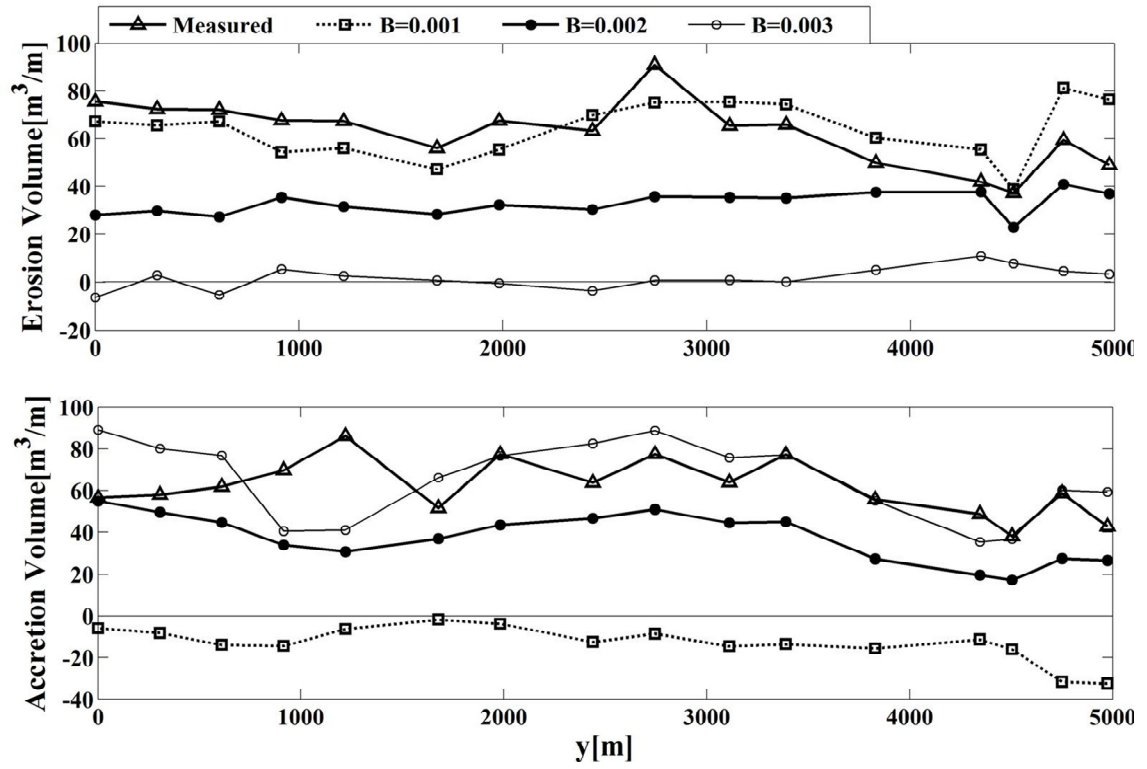


Figure 4.57 Measured and computed erosion (top) and accretion (bottom) volumes above MSL per unit alongshore length

4.5 Longshore Sediment Transport

The cumulative total sediment volume per unit width transported alongshore and northward is integrated from $x = 0$ to $x = x_m$ to obtain the sediment volume (no void) transported during the erosion and accretion periods. Figure 4.58 shows the computed sediment volumes for the 16 lines for $B = 0.001$, 0.002 and 0.003 . The longshore sediment transport is less sensitive to the parameter B for bed load. The computed volume of sediment transported alongshore increases somewhat in the southern segment of Dewey Beach and fluctuates slightly northward during the erosion period. The erosion and accretion in the computed elevation differences in Figures 4.13 to 4.16 are consistent with this alongshore variation. The computed sediment volume is almost constant during the accretion period and the elevation differences plotted in Figures 4.29 to 4.32 are very small.

For $B = 0.002$, the average sediment volume transported alongshore is $5.4 \times 10^4 \text{ m}^3$ during the erosion period of 50.8 days and $2.6 \times 10^4 \text{ m}^3$ during the accretion period of 220.8 days. The annual net longshore sediment (no void) transport rate has been estimated to be of the order of $6 \times 10^4 \text{ m}^3/\text{year}$ to the north (e.g., Puleo 2010) where the sand porosity is assumed to be 0.4 in this study. The longshore sediment transport rate predicted by CHSORE is of the same order as the previous estimate partly because of the use of the bottom friction factor $f_b = 0.02$ calibrated using two data sets obtained in the Large-scale Sediment Transport Facility of the U.S. Army Engineer Research and Development Center (Kobayashi et al. 2007). The bottom friction factor affects longshore current and suspended sediment transport.

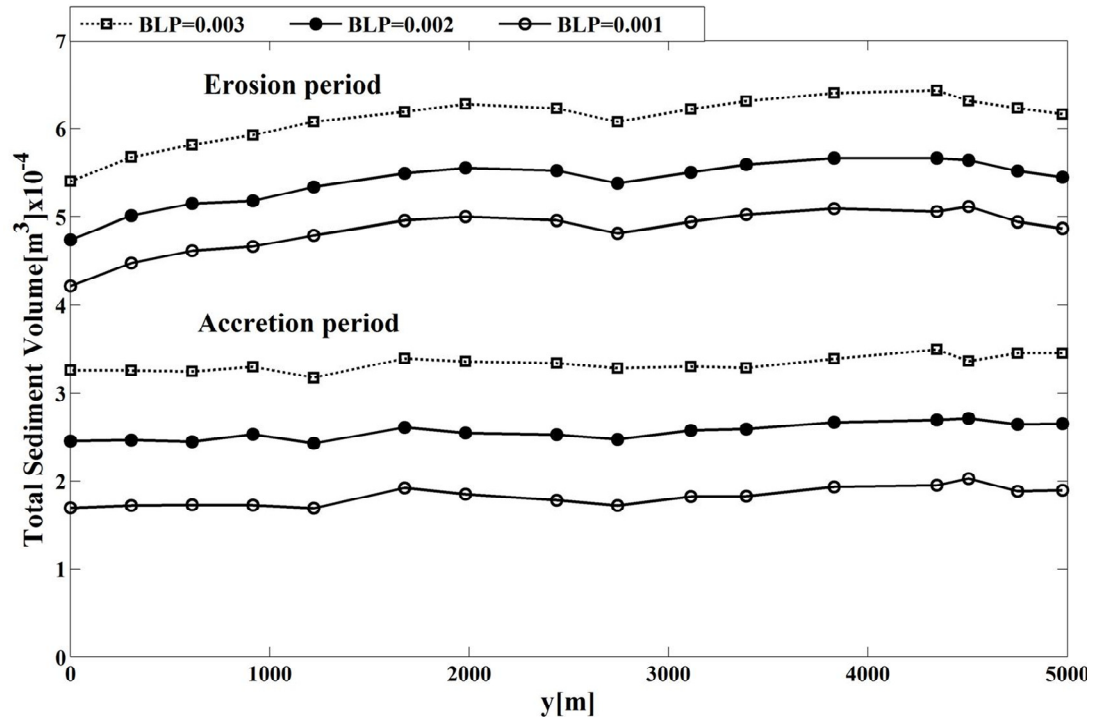


Figure 4.58 Computed sand (no void) volumes transported alongshore for $B = 0.001, 0.002,$ and 0.003 during erosion period (top 3 lines) and accretion period (bottom 3 lines)

Chapter 5

CONCLUSION

Beach profile data from Rehoboth and Dewey beaches are analyzed to examine the cycle of beach erosion and recovery during 1992 to 1993 before major beach nourishment was initiated on these beaches in 1994. The field data are used to assess the capability and limitation of the cross-shore numerical model CSHORE for predicting both beach erosion and accretion. CSHORE has been extended to multiple cross-shore lines so as to include the alongshore gradient of the longshore sediment transport rate in the beach profile evolution. The bed load parameter b in CSHORE is adjusted to increase b with the fraction of irregular breaking waves in order to reproduce the berm reconstruction above MSL during the accretion period. The eroded and accreted profiles at 16 cross-shore lines spanning 5 km alongshore are predicted within a factor of about 2. The computed beach profile evolution is found to be affected little by the alongshore gradient of the longshore sediment transport. The total longshore sediment transport volumes computed during the erosion and accretion periods do not vary much alongshore for the present field data. The extended CSHORE will need to be compared to data with larger alongshore variations in order to assess the accuracy of the approximate method proposed for the alongshore gradient of the longshore sediment transport. Furthermore, CSHORE will need to be verified using nourished beach data before it may be applied to improve the beach nourishment design.

REFERENCES

- Anderson, D.A., Tannehill, J .C., and Pletcher, R.H. (1984). *Fluid mechanics and heat transfer*, Hemisphere Publishing Corp., New York.
- Figlus, J., and Kobayashi, N. (2008). “Inverse estimation of sand transport rates on nourished Delaware beaches.” *J. Waterway, Port, Coastal, Ocean Eng.*, 134(4), 218-225.
- Figlus, J., Kobayashi, N., Gralher, C., and Iranzo, V. (2011). “Wave overtopping and overwash of dunes.” *J. Waterway, Port, Coastal, Ocean Eng.*, 137(1), 26-33.
- Garriga, C.M., and Dalrymple, R.A. (2002). “Development of a long-term costal management plan for the Delaware Atlantic coast.” *Res. Rep. No. CACR-02-04*, Center for Applied Coastal Research, Univ. of Delaware, Newark, Del.
- Hanson, H. (1989). “GENESIS – A generalized shoreline change numerical model.” *J. Coastal Res.*, 5(1), 1-27.
- Kobayashi, N., and Jung, H.(2010). “Beach erosion and recovery.” *J. Waterway, Port, Coastal, Ocean Eng.* (submitted).
- Kobayashi, N., Agarwal, A., and Johnson, B.D. (2007). “Berm and dune erosion during a storm.” *J. Waterway, Port, Coastal, Ocean Eng.*, 133(4), 296-304.
- Kobayashi, N., Payo, A., and Schmied, L. (2008). “Cross-shore suspended sand and bed load transport on beaches.” *J. Geophys. Res.*, 113, C07001.
- Kobayashi, N., Buck, M., Payo, A., and Johnson, B.D. (2009). “Berm and dune erosion during a storm.” *J. Waterway, Port, Coastal, Ocean Eng.*, 135(1), 1-10.

- Kobayashi, N., Farhadzadeh, A., Melby, J., Johnson, B., and Gravens, M. (2010). "Wave overtopping of levees and overwash of dunes." *J. Coastal Res.*, 26(5), 888-900.
- Puleo, J.A. (2010). "Estimating alongshore sediment transport and the nodal point location on the Delaware-Maryland coast." *J. Waterway, Port, Coastal, Ocean Eng.*, 136(3), 135-144.
- Roelvink, D., Reniers, A., van Dongeren, A., van Thiel de Vries, J., McCall, R., and Lescinski, J. (2009). "Modelling storm impacts on beaches, dunes and barrier islands." *Coastal Eng.*, 56, 1133-1152.
- U.S. Army Engineer Research and Development Center. (2002). *Coastal engineering manual, Part III, Coastal Sediment Processes*. Coastal and Hydraulics Lab., Vicksburg, Miss.
- Wise, R.A., Smith, S.J., and Larson, M. (1996). "SBEACH: Numerical model for simulating storm-induced beach changes. Report 4: Cross-shore transport under random waves and model validation with SUPERTANK and field data." *Technical Rep. No. CERC-89-9*, U.S. Army Engineer Waterways Experiment Station, Vicksburg, Miss.
- Yates, M.L., Guza, R.T., and O'Reilly, W.C. (2009). "Equilibrium shoreline response: Observations and modeling." *J. Geophys. Res.*, 114, C09014.